ROLL DAMPING ESTIMATION VIA SWAY-ROLL COUPLED EQUATION AND THE MOIRC (MOST OFTEN INSTANTANEOUS ROTATION CENTER) CONSIDERATION

Peyman Asgari

Tese de Doutorado apresentada ao Programa de Pós-graduação em Engenharia Oceânica, COPPE, da Universidade Federal do Rio de Janeiro, como parte dos requisitos necessários à obtenção do título de Doutor em Engenharia Oceânica.

Orientador: Antonio Carlos Fernandes

Rio de Janeiro
Dezembro de 2018

ROLL DAMPING ESTIMATION VIA SWAY-ROLL COUPLED EQUATION AND THE MOIRC (MOST OFTEN INSTANTANEOUS ROTATION CENTER) CONSIDERATION

Peyman Asgari

TESE SUBMETIDA AO CORPO DOCENTE DO INSTITUTO ALBERTO LUIZ COIMBRA DE PÓS-GRADUAÇÃO E PESQUISA DE ENGENHARIA (COPPE) DA UNIVERSIDADE FEDERAL DO RIO DE JANEIRO COMO PARTE DOS REQUISITOS NECESSÁRIOS PARA A OBTENÇÃO DO GRAU DE DOUTOR EM CIÊNCIAS EM ENGENHARIA OCEÂNICA.

Examinada por:

Prof. Antonio Carlos Fernandes, Ph.D.

Prof. Carlos Antonio Levi da Conceição, Ph.D.

Prof. Joel Sena Sales Junior, D.Sc.

Prof. Luis Volnei Sudati Sagrilo, Ph.D.

Dr. Allan Carré de Oliveira, D.Sc.

Prof. Alexandre Nicolaos Simos, Ph.D.

RIO DE JANEIRO, RJ - BRASIL

DEZEMBRO DE 2018

Asgari, Peyman

Roll Damping Estimation via Sway-Roll Coupled Equation and the MOIRC (Most Often Instantaneous Rotation Center) Consideration / Peyman Asgari. – Rio de Janeiro: UFRJ/COPPE, 2018.

XVI, 146 p.: il.; 29,7 cm.

Orientador: Antonio Carlos Fernandes

Tese (doutorado) – UFRJ/ COPPE/ Programa de Engenharia Oceânica, 2018.

Referências Bibliográficas: p. 129-135.

1. Roll Damping. 2. Nonlinear roll damping. 3. Sway/roll coupling motion. 4. Roll center. I. Fernandes, Antonio Carlos. II. Universidade Federal do Rio de Janeiro, COPPE, Programa de Engenharia Oceânica. III. Título.

To my dear family, who always
picked me up and encourage me
to go on every adventure,
my mother ***Suri*** *and my father* ***Mohsen***
and my wife ***Fernanda Gabriela****.*

Acknowledgement

This thesis has been carried out under supervision of Prof. Antonio Carlos Fernandes at the Program of Ocean Engineering of Federal University of Rio de Janeiro. I would like to thank him not only for his guidance and supervision but also for introducing the world and teaching how look to the world, he was my friend and will have my respect for the rest of my life.

I would like also to appreciate great helps have come from LOC laboratory.

Peyman Asgari

December 2018

Resumo da Tese apresentada à COPPE/UFRJ como parte dos requisitos necessários para a obtenção do grau de Doutor em Ciências (D.Sc.)

ESTIMATIVA DO AMORTECIMENTO DE ROLL ATRAVÉS DE EQUAÇÃO ACOPLADA DE SWAY-ROLL E DE CONSIDERAÇÃO DO MOIRC (MOST OFTEN INSTANTANEOUS ROTATION CENTER - CENTRO INSTANTÂNEO DE ROTAÇÃO MAIS PROVÁVEL)

Peyman Asgari

Dezembro /2018

Orientador: Antonio Caros Fernandes
Programa: Engenharia Oceânica

Este trabalho foca na estimativa do amortecimento de roll de embarcações tipo FPSO, realizado através de decaimento livre e onda regular sobre uma seção 2D do corpo médio paralelo. Dois temas são preocupações deste estudo: a definição do centro de rotação e efeitos do termo de acoplamento sway/roll no amortecimento do roll. O trabalho define um polo único arbitrário na obtenção das equações no caso de decaimento livre de roll e é usado para desenvolver uma abordagem robusta (abordagem de 3ª ordem) que usa técnicas de identificação do sistema para obter propriedades de amortecimento dos testes de decaimento. Do estudo do centro instantâneo de rotação (CIR) nos casos de decaimento livre e em condições ondas regulares experimentalmente e numericamente, observou-se que o lugar geométrico temporal do CIR é uma linha reta dependente da frequência e do amortecimento dominante. O estudo desenvolve uma equação em forma fechada para este lugar geométrico. Através do estudo do CIR, esta pesquisa propõe uma nova definição do MOIRC (*Most Often Instantaneous Rotation Center* – Centro Instantâneo de Rotação Mais Provável)) através da distribuição de Cauchy, que fornece uma visão com claras interpretações físicas do movimento de roll e consequentemente do amortecimento deste modo de moviemnto.

Abstract of Thesis presented to COPPE/UFRJ as a partial fulfillment of the requirements for the degree of Doctor of Science (D.Sc.)

ROLL DAMPING ESTIMATION VIA SWAY-ROLL COUPLED EQUATION AND THE MOIRC (MOST OFTEN INSTANTANEOUS ROTATION CENTER) CONSIDERATION

Peyman Asgari

December /2018

Advisor: Antonio Carlos Fernandes
Department: Ocean Engineering

This work focuses on the roll damping estimation performing free decay roll and regular beam wave for e 2D section of a FPSO in transversal plan. Two terms are concerns of this study, definition of rotation center and sway/roll coupling term effects on the roll damping. A unique pole is defined in condition of free decay roll and is used to develop a robust approach (3rd order approach) that uses system identification techniques to obtain damping properties from the decay tests. The research studies on instantaneous rotation center for free decay test and in regular condition experimentally and numerically, the locus of the IRCs is a frequency dependent straight line and devises a closed form equation for the IRC locus. Surprisingly, the so-called roll center is not a concept well defined for rolling ships or platforms that submitted to a wave field. This research proposes a new definition of MOIRC via Cauchy distribution which provides a deeper and remarkable insight into roll motion and roll damping of FPSO.

S

S

K99 ; Yk Y R; . Y Y

n Yu; wz ; ; ' k k. Wyr Wy 9 r

v ; 'r w ; ; . WY ; TT; ; r ; . k ''

x ; Yk' R; . 'Yu Y

x k k ; k Y) ; ;

–Y; k w' wn Y kr k Y

–Y; k w' w kr k Y

–Y; k ; xr ; YYk Y

T; x k k ; k Y) ; ;

k0; r v ''

; w . Y'k Y ; . WY ; TT; ; r ; . k ''

; Yk' YY Tx k k ; k Y) ; ;

Chapter 1 Introduction

1.1 General

The knowledge of the roll motion is essential in the safe design of FPSOs (Floating Production Storage and Offloading Platforms). Since the start of the use of FPSOs in the 1960's, roll motions have revealed to be a major concern for operators of these units. Even now-a-days very large roll motions, with values above design limits, have been reported for FPSOs. Some observations showed single amplitude of up to seventeen degrees in the presence of swells (Ferreira, 2005). This implies in process plant downtime, uncomfortable conditions for the crew, and degradation of the structural integrity of topside supports, hull, bilge-keels and risers. These observations led FPSO to use unconventional anti-roll system such very large bilge-keel. Seeking in classification's regulations, it can be observed that the old-fashioned methods have been adopted for roll damping estimation even for the FPSOs such as such ITH (Himeno, 1981) in BV and (Tanaka, 1961) in DNV. Waveship software© (Veritas, 2013) would be an example which the non-linear roll damping methods for ship hulls includes those published by (Tanaka, 1961) and Kato (Kato, 1965) (Kato, 1958). Anyway, there is a sense that the field is still open to discuss the adequacy of currently employed methods for roll motion prediction.

1.2 Literature Review

Most roll motion investigations in the literature use one degree of freedom second order ordinary nonlinear differential equation for roll displacement. This can be traceable in Froude's researches (Froude, 1861) (Froude, 1955). Froude proposed the non-linear roll damping to be a linear-plus-quadratic velocity-dependent form to account for dissipation of energy during roll motion (Froude, 1861). Froude's method uses decay tests equating the potential energy lost to damping in each half cycle to the work done by the equivalent linearized damping moment during the same period. It took about a century to other researchers move on this topic and in middle of the 20th century, the first roll damping models in frequency domain had been developed and the individual physical aspects of ship roll damping been performed (Sasajima, 1954) (Tanaka, 1957) (Kato, 1958). (Dalzell, 1978) was on the first to suggest a roll damping that consists of linear-plus-cubic velocity-dependent term as an extension of Froude's method (also used by (Haddara, 1971) and (Lewison, 1973)).

Influence of Rotation Center on Damping - During the past 50 years, more information has become available supporting that roll damping prediction is influenced by the position of the 'roll center' (or equivalently center of roll). The first important arguments emerged in the 1970s when Ikeda conducted series of forced roll experiments to develop his roll damping prediction method (Ikeda, 1977a) (Ikeda, 1977) (Himeno, 1981). Later, (Himeno, 1981) organized Ikeda and Tanaka's researches about the roll damping published it as a state of art (which nowadays is known as Ikeda-Tanaka-Himeno ITH method). He showed that components of roll damping such, eddy, lift,

wave and friction are directly function of distance of fixed rotation center from center of gravity. The ITH method provided a considerable attention on role of the position of the roll center in roll damping. Maybe because of that (Haddara, 1990) and (Bass, 1991) conducted roll decay experiments to determine roll response curve for various imposed roll centers for three fishing boat models. The results for damping graphs showed a very noticeable characteristic for two models, by increasing the position of the imposed roll center the roll damping increased in both linear and nonlinear terms. Likewise, the same conclusion has reached by (Chun, 2001).

Ten years later, (Park, 2000) studied on the same subject but this time for a FPSO. Similarly, his investigation indicate that the roll damping is sensitive to the imposed position of the roll center and it will increase if the rotation axis is placed above the still-water level (increasing distance of roll center from center of gravity), the same conclusion made by (Chun, 2001). Recently, (Ommani, 2015) studied geometrical characteristics such center of rotation influence on roll damping using an efficient hybrid numerical code. In his study again, an imposed center of rotation was adopted. The result of roll damping variation with rotation center showed similar results has the already mentioned (Bass, 1991) and (Park, 2000). In the later the importance of the coupling between draft of ship and vertical position of rotation center has been pointed out.

Definition of Rotation Center - Thus far, previous studies observed and confirmed that importance of the 'roll center'. But tracking the definition of the 'roll center', a clear and unique definition may not be found in the literature, looking in the references following definitions/assumptions may be adopted by authors: center of gravity, center of buoyancy, intersection of center-line with still-water line and so on. Based on

(Roberts, 1985a), only the sway motion is significantly coupled with roll and that the influence of the sway-into-roll damping term is small. Robert suggests that it is possible to inertially decouple roll from sway equation by moving the origin of the coordinate system to a new position that he called 'roll center' (sic), where mass-inertia matrix is diagonal; he did not mention the damping coupling. In the Principles of Naval Architecture (Lewis, 1989), the 'roll center' (sic) refer to the origin of a coordinate system where sway and roll equations of motion are inertialy decoupled from each other. In (Lewis, 1989) one can find a questionable statement, "a very rough estimate for the location of the roll center (sic) is half way between the center of gravity and the center of buoyancy".

(Standing, 1991) investigates the form of the viscous roll damping term and possible effects of sway and heave on roll response. In the most cases, the roll center is assumed to be at the body's center of gravity, this being the appropriate point for decoupling motion of a rigid body in air. According to (Standing, 1991), the roll center can be calculated at least in two distinct way: (i) through coupling terms in the equation of motion with the off-diagonal component of the inertia when there is no significant roll damping, in this situation, the 'roll center' (sic) is placed where sway and roll equations may be fully decoupled. (ii) because the vortex damping depends on the relative velocity at bilge-keels, where there is a significant roll damping, the roll center may be defined as the point of minimum sway response (sic) in a free roll decay or forced oscillation type of experiment or simulation (Standing, 1988).

On the other hand, there are many evidences which show that the body does not have a symmetric roll motion in condition of beam seas or in the other word, the rotation

center is out of the symmetry-plan. (Esperança, 2008) reports experiments with FPSO model with soft moorings lines in regular waves with different amplitudes in beam seas with bilge-keels. The main observation of this research is that the bilge-keel loads on the incident wave side of the model were much higher than the loads on the opposite side. Recently, (Ferreira, 2012) studied the asymmetric FPSO roll response with attached lines and they observed that the roll response at the bilge-keel for a wave incidence of 270° (through the side where the risers were connected) is substantially lower than for the one progressing with a 90° incident angle. Based on the shape of the response, they suggested that the riser system might act as a vibration absorber for the FPSO roll motion (Ferreira et al., 2012). These two examples and many others are witness of asymmetric rotation center in condition of beam seas.

The confusion and mismatch of roll center definitions would be the reason of (Molin, 2002) to call it "mystérieux center du roulis" (mysterious roll center, in French) in his recent book. Later, Faltinsen mentioned in his book (Faltinsen, 2005) that since there is a strong sway component in the rolling of ships, among other couplings, a ship does not actually roll about a single roll axis.

Sway/Roll coupling effects into the roll damping - Several lines of evidence emphasis that the rotation center or better explained MOIRC is should be assessed by roll coupling with other modes, mainly sway. However, traditionally, probably for the sake of a practical method, the roll motion mostly has been studied via one degree of freedom equation in roll, where coupling effects between roll and sway damping were assumed negligible (principal works: (Ikeda, 1978b), (Himeno, 1981), (Cardo, 1982), (Roberts, 1985b), (Chakrabarti, 2001) and etc). (Vugts, 1968) calculate experimentally coupling coefficients of sway-into-roll and roll-into-sway for three types of bodies (box,

triangle and u-type) with different beam/draft ratios. Both types of coupling damping terms showed influence of viscosity.

(Ikeda, 1981) studied on the viscous effects on forces and moments acting on a ship in sway and roll motion at zero forward speed. He observed that coupling terms sway-into-roll and roll-into-sway are affected considerably by viscosity of fluid, one year later, (Ikeda, 1982) showed that the sway-into-roll coupling is also significant. In the same vein, (Bass, 1991) performed an extensive series of experiments to determine roll and coupling damping characteristics for several small fishing vessels. He was expecting significant value for sway-into-roll coupling term, nevertheless, the sway-into-roll damping coefficient measured was a great deal larger than that predicted from potential theory. Also, he clearly observed that there is an influence of sway-into-roll coupling on position of the so called 'roll center'.

These studies provide important insights into the importance of coupling terms effects on roll damping towards the investigation of the instantaneous rotation center (IRC) of a FPSO hull in during free roll decay test. Hence, the present work aims to clarify how IRC behave during and its effect on damping estimation in a free roll decay with different nonlinearity levels.

In what follows, first subsequent session presents and analyzes the results of the experiments. The surprising results what includes the level of the damping for each half cycle and its relation with the IRC position motivated a linear theoretical analysis. The explanation of the data where confirmed in an innovative statistical analysis. The next session discusses the non-linear aspects. Finally, in the end a conclusion session summarizes the achievements probably seen for the first time in the literature.

1.3 Scope of Present Study

1.3.1 Statement of Problems

Several techniques have been introduced by researchers such free roll decay, forced oscillation and so on, but each method resulting different (one example in shown in Figure 1.1 from (Ikeda, 1993)). Two main questions may come to your mind, why they are generating different results? and which one is more trustable? Responding to these questions would improve our understanding about roll damping and leads to more accurate roll damping estimation.

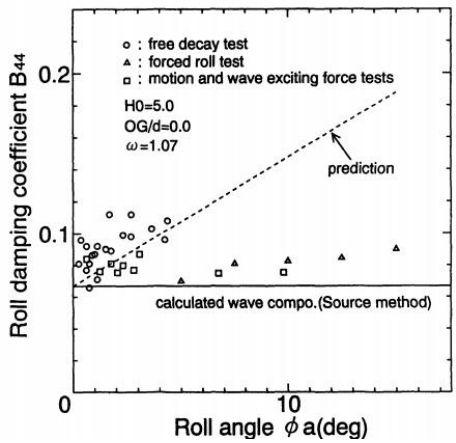

Figure 1.1 – Comparison among three kinds of methods to obtain the roll damping model (Ikeda, 1993).

In fact, numerous works related to the estimation of roll damping in oil tankers have been published during the last decades. Nevertheless, most have two fundamental issues which may propagate errors to damping estimation. The first is related to the lack of a unique definition of the pole necessary for rotational equations, despite the fact that the importance of this definition for damping estimation has been shown by

some researchers. This pole is in principle arbitrary, as known from theory, and is known as either the 'roll center' or the 'center of roll'. However, these names prove to be meaningless, as they have no clear definition. A better understanding of the pole would definitely improve roll estimation procedures. The second fundamental issue is related to the understanding of the coupling of roll with other degrees of freedom.

The fact is that the accurate estimation of roll motions is not an easy task while roll damping nonlinearity of unconventional anti-roll system involved several sources which still need more investigations.

1.3.2 Limitation and Objective

The study is limited to the two-dimensional body in the still water for free decay test and regular gravity waves in case of the wave test, without forward speed, wind and current. The motivation of using two-dimensional case is for having detailed and controlled observation of physics and the possibility to extend the study into three-dimensional case in the future. The information obtained of this study will be valuable as a reference regarding the using of a typical FPSO (box shape) section performance in roll motion. Based on the challenges described 1.3.1, the objectives objective of the study would be listed as below:

- This work presents an innovative, robust approach to assess roll damping of FPSOs, taking into account a correct definition of the pole on which to center the motion equations as well as the influence of the unavoidable coupled damping for sway and roll damping estimation, using both numerical and experimental techniques.

- This work tries to present a concrete definition of rotation center (or better defined MOIRC) for a typical FPSO in conditions such: free roll damping, in regular waves, experimentally and analytically.
- This study tries to distinguish the techniques and interpret the physics of roll through the instantaneous rotation center.

1.3.3 Structure of the Thesis

After a literature review of the topic in Chapter1, the structure of the thesis is as follows:

Chapter2: theory and mathematics of the problem, the chapter presents the 3rd Order equation (linear and nonlinear) of roll/sway.

Chapter3: the 3rd order approach to estimate the roll damping is presented and results of the free decay roll experiments are discussed.

Chapter4: the same experiments of the Chapter 3 reanalysed but this time in aspect of the instantaneous center of rotation to study behaviour of IRCs during the decay, experimentally and analytically.

Chapter5: investigates behaviour of the IRCs and MOIRC for the FPSO exposed to the regular beam-wave and discusses the experimental results.

Chapter6: is the conclusion.

The thesis's contributions also have been presented briefly in following papers: (Fernandes, 2015), (Fernandes, 2016), (Fernandes, 2018) and (Asgari, 2019).

Chapter 2 Sway/Roll 3rd Order Equation

Prediction of FPSO's motions is important because it is directly related to the safe and economic operation of platforms. The motion of a FPSO exposed to external forces such as wind, waves, currents, mooring lines and risers. In order to derive the FPSO equations of motion, it is necessary to study the motion of rigid bodies, hydrodynamics and hydrostatics. The overall goal of Chapter 2 is to drive 3-DoF fully nonlinear and linear equations of motion and finally the propose 3rd order equation of motion in 2-DoF (sway/roll).

2.1 Fully Non-Linear Equation of Motion (3-DoF)

Maybe after Clayton & Bishop (Clayton, 1982) which published their classical book about marine vehicle's motion, the earlier studies of nonlinear equation of motion for floating bodies could be traced back in Fossen et al works ((Fossen, 1994), (Fossen, 2011) and (Fossen, 2005)). According to (Fossen, 1991), general rigid-body kinetics can be expressed in vectorial setting as equation (2.1) where M_{RB} is rigid body mass matrix, C_{RB} is rigid body Coriolis and centripetal matrix and also involving hydrodynamic and hydrostatics forces.

$$\underbrace{M_{RB}\dot{\boldsymbol{\nu}} + C_{RB}\boldsymbol{\nu}}_{\text{rigid-body forces}} = \underbrace{\underbrace{M_A\dot{\boldsymbol{\nu}}_r + C_A(\boldsymbol{\nu}_r)\boldsymbol{\nu}_r + D(\boldsymbol{\nu}_r)\boldsymbol{\nu}_r}_{\text{hydrodynamic forces}} + \underbrace{g(\eta) + g_0}_{\text{hydrostatic forces}} + \tau_{\mathrm{p}} + \tau_{m,r}}_{\tau_{RB}} \tag{2.1}$$

The study focuses on 2D problem in vertical plane, hence, to simplify the problem, equation of motion reduced from 6-DoF into 3-DoF, which represents the mid-ship section of FPSO. Coordinate system is illustrated in Figure 2.1 in earth inertial frame. For the midship section of FPSO, generalized velocity vector $\boldsymbol{\nu}$ and generalized external force vector τ_{RB} would be reduced as equations (2.2) and (2.3), where $\boldsymbol{v}$, $\boldsymbol{w}$ and $\boldsymbol{p}$ are sway, heave and roll velocities, respectively and *Y, Z* and *K* sway, heave and roll external forces respectively.

$$\boldsymbol{\nu} = [\dot{\eta}_2, \dot{\eta}_3, \dot{\eta}_4]^T \tag{2.2}$$

$$\tau_{RB} = [Y, Z, K]^T \tag{2.3}$$

The rigid body equations of motion could be derived using the *Newton-Euler formulation* and *vectorial mechanics*. The equation will be represented in two body-fixed reference point: (i) C_{ar} – origin o_b of *{b}*; (ii) C_{cg} – center of gravity, these points coincide if the vector $\vec{r}_g = \vec{0}$ (see Figure 2.1), meanwhile, it is advantageous to use an arbitrary reference point C_{ar} since the C_{cg} depends on the load conditions.

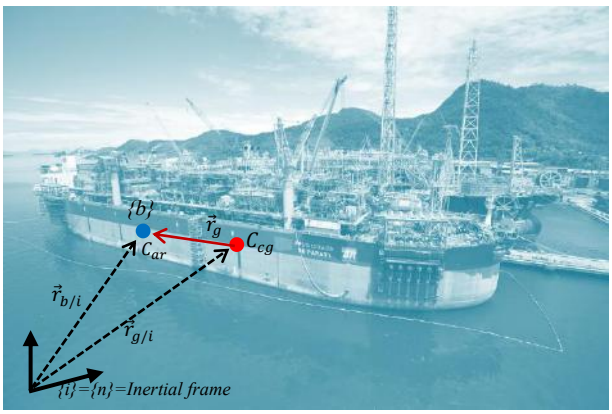

Figure 2.1 – Definition of the coordinate origins C_{ar} and C_{cg} for 2D section of FPSO.

2.1.1 Newton-Euler Equation of Motion about C_{cg}

The *Newton-Euler formulation* is based on *Newton's second law*, which is mass m multiplied by acceleration $\dot{\vec{v}}_{g/i}$ (where $\vec{v}_{g/i}$ is velocity of the center of gravity with respect to the *inertial frame* $\{i\}$) equal to force $\vec{f}_g$.

$$m\dot{\vec{v}}_{g/i} = \vec{f}_g \tag{2.4}$$

Newton's laws were published in 1687 be Isaac Newton (1643-1727), but later, Leonhard Euler (1707-1783) showed that Newton's second law can be expressed in terms of conservation of both linear momentum $\vec{p}_g$ and angular momentum $\vec{h}_g$.

$$\frac{{}^{i}d}{dt}\vec{p}_g = \vec{f}_g \qquad \vec{p}_g = m\vec{v}_{g/i} \tag{2.5}$$

$$\frac{{}^{i}d}{dt}\vec{h}_g = \vec{m}_g \qquad \vec{h}_g = I_g\vec{\omega}_{b/i} \tag{2.6}$$

The application of these equations is often referred to as *vectorial mechanics* since both conservation laws are expressed in terms of vectors. Where $\vec{f}_g$ and $\vec{m}_g$ are the forces and moments acting on center of gravity of the body, $\vec{\omega}_{b/i}$ is the angular velocity of $\{b\}$ with respect to $\{i\}$ and I_g is the inertia dyadic about center of gravity of the body. Time differentiation in the inertial frame $\{i\}$ is denote by $\frac{{}^{i}d}{dt}$. According to (Fossen, 2011), the Newton-Euler equation with respect to the center of gravity can be represented in matrix form according to

$$M_{RB}^{CG}\begin{bmatrix}\dot{v}_{g/n}^{b}\\ \dot{\omega}_{g/n}^{b}\end{bmatrix}+C_{RB}^{CG}\begin{bmatrix}v_{g/n}^{b}\\ \omega_{g/n}^{b}\end{bmatrix}=\begin{bmatrix}f_g^b\\ m_g^b\end{bmatrix} \tag{2.7}$$

or

$$\underbrace{\begin{bmatrix}mI_{2\times2} & 0_{2\times1}\\ 0_{1\times2} & I_{g(1\times1)}\end{bmatrix}}_{M_{RB}^{CG}}\begin{bmatrix}\dot{v}_{g/n(2\times1)}^{b}\\ \dot{\omega}_{g/n(1\times1)}^{b}\end{bmatrix} + \underbrace{\begin{bmatrix}mS(\omega_{g/n}^{b})_{\,2\times2} & 0_{2\times1}\\ 0_{1\times2} & -S(\omega_{g/n}^{b}I_g)_{\,(1\times1)}\end{bmatrix}}_{C_{RB}^{CG}}\begin{bmatrix}v_{g/n}^{b}\\ \omega_{g/n}^{b}\end{bmatrix}=\begin{bmatrix}f_g^b\\ m_g^b\end{bmatrix} \tag{2.8}$$

Where the cross-product is written in matrix form using the skew-symmetric matrix, where $S \in SS(3)$ is defined as:

$$S(\lambda)=-S^T(\lambda)=\begin{bmatrix}0 & -\lambda_3 & \lambda_2\\ \lambda_3 & 0 & -\lambda_1\\ \lambda_2 & \lambda_1 & 0\end{bmatrix},\quad \lambda=\begin{bmatrix}\lambda_1\\ \lambda_2\\ \lambda_3\end{bmatrix} \tag{2.9}$$

2.1.2 Newton-Euler Equation of Motion about C_{ar}

For any floating body it is desirable to drive the equations of motion for an arbitrary origin to take advantage of body's geometric properties. In order to do this the equations of motion about C_{cg} are transformed to C_{ar} using a coordinate transformation. The equations of motion in body inertial coordinate are shown in (2.10) and (2.11) where the translational and rotational transformation are explained by detail in (Fossen, 2011).

$$m\left[\dot{v}_{b/n}^{b} + \dot{\omega}_{b/n}^{b} \times r_{g}^{b} + \omega_{b/n}^{b} \times v_{b/n}^{b} + \omega_{b/n}^{b} \times (\omega_{b/n}^{b} \times r_{g}^{b})\right] = f_{b}^{b} \tag{2.10}$$

$$I_{b}\dot{\omega}_{b/n}^{b} + \omega_{b/n}^{b} \times I_{b}\omega_{b/n}^{b} + m r_{g}^{b} \times (\dot{v}_{b/n}^{b} + \omega_{b/n}^{b} \times v_{b/n}^{b}) = m_{b}^{b} \tag{2.11}$$

f_{b}^{b} is the force through o_{b}, since translational motion is independent of the attack point then $f_{b}^{b} = f_{g}^{b}$, but for rotational motion, the moment about o_{b} shown in (2.11) can be expresses mathematically as (2.12).

$$m_{b}^{b} = m_{g}^{b} + r_{g}^{b} \times f_{g}^{b} = m_{g}^{b} + S(r_{g}^{b}) f_{g}^{b} \tag{2.12}$$

2.2 Linearization of Equation of Motions

Fully nonlinear involving too many parameters such as damping, wave forces, control and propulsion forces, hydrodynamic added mass and many other parameters. It is very difficult and time consuming to solve the fully non-linear equation formulated in (2.1), especially when the a FPSO has unconventional antiroll system. Commonly, it is simplified by linear approximation, that is, there are recast in a form that is linear in

the mathematical sense. Equations (2.10) and (2.11) presented in 2.1.2 could be derived linearly in 3-DoF for vertical plane yz in below:

$f_b^b = [Y, Z]^T$ Force through o_b expressed in $\{b\}$

$m_b^b = [K]^T$ Moment about o_b expressed in $\{b\}$

$v_{b/n}^b = [\dot{\eta}_2, \dot{\eta}_3]^T$ Linear velocity of o_b relative to o_n expressed in $\{b\}$

$\omega_{b/n}^b = [\dot{\eta}_4]^T$ Angular velocity of $\{b\}$

$r_g^b = [x_g, y_g, z_g]^T$ Vector from o_b to C_{cg} expressed in $\{b\}$

Applying these notations, the equations (2.10) and (2.11) become,

$$m\left[\ddot{\eta}_2 - \dot{\eta}_3\dot{\eta}_4 - y_g\dot{\eta}_4^2 - z_g\ddot{\eta}_4\right] = Y \tag{2.13}$$

$$m\left[\ddot{\eta}_3 + \dot{\eta}_2\dot{\eta}_4 - z_g\dot{\eta}_4^2 - y_g\ddot{\eta}_4\right] = Z \tag{2.14}$$

$$I_x\ddot{\eta}_4 + m\left[y_g(\ddot{\eta}_3 + \dot{\eta}_2\dot{\eta}_4) - z_g(\ddot{\eta}_2 - \dot{\eta}_3\dot{\eta}_4)\right] = K \tag{2.15}$$

2.2.1 Theory of Small Disturbances (Perturbation theory)

Perturbation theory or small disturbances can be found in literatures such (Dalgarno, 1956), (Hayes, 1959), (Bishop, 1974), (Bishop, 1977) and (Clayton, 1982). The equations developed in 2.2 can be linearized using the small disturbance theory, eessentially, the idea of mathematical linearization the equations of motion of the

FPSO consists of small deviations about a steady condition. All variables in the equations of motion are replaced by a reference value plus a perturbation or disturbance:

$$\dot{\eta}_2 = \dot{\bar{\eta}}_2 + \Delta\dot{\eta}_2 \qquad \dot{\eta}_3 = \dot{\bar{\eta}}_3 + \Delta\dot{\eta}_3 \qquad \dot{\eta}_4 = \dot{\bar{\eta}}_4 + \Delta\dot{\eta}_4$$

$$Y = \bar{Y} + \Delta Y \qquad Z = \bar{Z} + \Delta Z \qquad K = \bar{K} + \Delta K$$

To summarize, the all detail expressions are not included in the text. One of the main problems in ship dynamics arises from the need to reduce expression like this to mathematical form which is both simple and reasonable approximation to reality. Several techniques are available for this purpose. The conventional method, which has been used for many years, is to express increments like ΔY in terms of the instantaneous motion of the body by means of *slow motion derivatives*.

Slow Motion Derivatives - The easiest and most common method of simplifying the infinite representation is simply to curtail it. Thus, for the system with 6-DoF, the Forces and moment can be written as:

$$\Delta X = X_{\dot{\eta}_1}\dot{\eta}_1 + X_{\dot{\eta}_2}\dot{\eta}_2 + X_{\dot{\eta}_3}\dot{\eta}_3 + X_{\dot{\eta}_4}\dot{\eta}_4 + X_{\dot{\eta}_5}\dot{\eta}_5 + X_{\dot{\eta}_6}\dot{\eta}_6 + X_{\ddot{\eta}_1}\ddot{\eta}_1 + X_{\ddot{\eta}_2}\ddot{\eta}_2 + X_{\ddot{\eta}_3}\ddot{\eta}_3 + X_{\ddot{\eta}_4}\ddot{\eta}_4 + X_{\ddot{\eta}_5}\ddot{\eta}_5 + X_{\ddot{\eta}_6}\ddot{\eta}_6 + X(t)$$

$$\dots \tag{2.16}$$

$$\dots$$

$$\Delta \mathrm{N} = N_{\dot{\eta}_1}\dot{\eta}_1 + N_{\dot{\eta}_2}\dot{\eta}_2 + N_{\dot{\eta}_3}\dot{\eta}_3 + N_{\dot{\eta}_4}\dot{\eta}_4 + N_{\dot{\eta}_5}\dot{\eta}_5 + N_{\dot{\eta}_6}\dot{\eta}_6 + N_{\ddot{\eta}_1}\ddot{\eta}_1 + N_{\ddot{\eta}_2}\ddot{\eta}_2 + N_{\ddot{\eta}_3}\ddot{\eta}_3 + N_{\ddot{\eta}_4}\ddot{\eta}_4 + N_{\ddot{\eta}_5}\ddot{\eta}_5 + N_{\ddot{\eta}_6}\ddot{\eta}_6 + \mathrm{N}(t)$$

Where $X_{\dot{\eta}_1}, \dots, X_{\ddot{\eta}_6}$ are called '*slow motion derivate*' or in other definition $X_{\dot{\eta}_1}, X_{\dot{\eta}_2}, \dots, X_{\dot{\eta}_6}$ are the linear damping coefficients and $X_{\ddot{\eta}_1}, X_{\ddot{\eta}_2}, \dots, X_{\ddot{\eta}_6}$ represent hydrodynamic added mass. For a 6-DoF system, there will be a total of 36 mass and 36 damping elements proportional to velocity and acceleration, but for this study which is 3-DoF system number of the elements reduce to 9. Therefore, the (2.16) can be written for vertical plane motion including sway, heave and roll.

$$\Delta Y = Y_{\dot{\eta}_2}\dot{\eta}_2 + Y_{\dot{\eta}_3}\dot{\eta}_3 + Y_{\dot{\eta}_4}\dot{\eta}_4 + Y_{\ddot{\eta}_2}\ddot{\eta}_2 + Y_{\ddot{\eta}_3}\ddot{\eta}_3 + Y_{\ddot{\eta}_4}\ddot{\eta}_4 + Y(t) \tag{2.17}$$

$$\Delta Z = Z_{\dot{\eta}_2}\dot{\eta}_2 + Z_{\dot{\eta}_3}\dot{\eta}_3 + Z_{\dot{\eta}_4}\dot{\eta}_4 + Z_{\ddot{\eta}_2}\ddot{\eta}_2 + Z_{\ddot{\eta}_3}\ddot{\eta}_3 + Z_{\ddot{\eta}_4}\ddot{\eta}_4 + Z(t) \tag{2.18}$$

$$\Delta K = K_{\dot{\eta}_2}\dot{\eta}_2 + K_{\dot{\eta}_3}\dot{\eta}_3 + K_{\dot{\eta}_4}\dot{\eta}_4 + K_{\ddot{\eta}_2}\ddot{\eta}_2 + K_{\ddot{\eta}_3}\ddot{\eta}_3 + K_{\ddot{\eta}_4}\ddot{\eta}_4 + K(t) \tag{2.19}$$

Consequently,

$$Y_{\ddot{\eta}_2}\ddot{\eta}_2 + Y_{\dot{\eta}_2}\dot{\eta}_2 + Y_{\ddot{\eta}_3}\ddot{\eta}_3 + Y_{\dot{\eta}_3}\dot{\eta}_3 + Y_{\ddot{\eta}_4}\ddot{\eta}_4 + Y_{\dot{\eta}_4}\dot{\eta}_4 = m\ddot{\eta}_2 - Y(t) \tag{2.20}$$

$$Z_{\ddot{\eta}_2}\ddot{\eta}_2 + Z_{\dot{\eta}_2}\dot{\eta}_2 + Z_{\ddot{\eta}_3}\ddot{\eta}_3 + Z_{\dot{\eta}_3}\dot{\eta}_3 + Z_{\ddot{\eta}_4}\ddot{\eta}_4 + Z_{\dot{\eta}_4}\dot{\eta}_4 = m\ddot{\eta}_3 - Z(t) \tag{2.21}$$

$$K_{\ddot{\eta}_2}\ddot{\eta}_2 + K_{\dot{\eta}_2}\dot{\eta}_2 + K_{\ddot{\eta}_3}\ddot{\eta}_3 + K_{\dot{\eta}_3}\dot{\eta}_3 + K_{\ddot{\eta}_4}\ddot{\eta}_4 + K_{\dot{\eta}_4}\dot{\eta}_4 = I_x\ddot{\eta}_4 - K(t) \tag{2.22}$$

2.2.2 Equation of Vertical Plane Motion

In order to construct the governing equations of motion, the following assumptions are made:

- The floating body is slender and rigid with symmetric distribution of mass.
- Motion amplitude is small so that equations can be linearized.
- Except in roll motion, the effect of viscosity is neglected.

Considering restoring forces mentioned in (2.1), the equations (2.20) to (2.22) can be expressed as below,

$$\begin{aligned}(M + A_{22})\ddot{\eta}_2 + B_{22}\dot{\eta}_2 + C_{22}\eta_2 + A_{23}\ddot{\eta}_3 + B_{23}\dot{\eta}_3 + C_{23}\eta_3 \\ + (A_{24} - Mz_c)\ddot{\eta}_4 + B_{24}\dot{\eta}_4 + C_{24}\eta_4 = F_2\end{aligned} \tag{2.23}$$

$$\begin{aligned}(M + A_{33})\ddot{\eta}_3 + B_{33}\dot{\eta}_3 + C_{33}\eta_3 + A_{34}\ddot{\eta}_4 + B_{34}\dot{\eta}_4 + C_{34}\eta_4 \\ + A_{32}\ddot{\eta}_2 + B_{32}\dot{\eta}_2 + C_{32}\eta_2 = F_3\end{aligned} \tag{2.24}$$

$$\begin{aligned}(I_4 + A_{44})\ddot{\eta}_4 + B_{44}\dot{\eta}_4 + C_{44}\eta_4 + A_{43}\ddot{\eta}_3 + B_{43}\dot{\eta}_3 + C_{43}\eta_3 \\ + (A_{42}\ddot{\eta}_2 - Mz_c) + B_{42}\dot{\eta}_2 + C_{42}\eta_2 = F_4\end{aligned} \tag{2.25}$$

By simple reasoning the equations (2.23) to (2.25) can be simplified greatly. The horizontal displacement is not opposed by any restoring forces, so $C_{22} = C_{32} = C_{42} = 0$. The coefficients C_{33} and C_{44} can be determined by pure hydrostatics. The vertical motion is symmetric with respect to the z-axis and cannot produce any lateral forces or moment; therefore $A_{23} = B_{23} = C_{23} = A_{43} = B_{43} = C_{43} = 0$. A static heel η_4 does

not generate a horizontal force, or $c_{24} = 0$. But due to differences in the immersed and emerged wedge when heeling about a fixed axis in space, in general $c_{24} \neq 0$. Under the above assumptions, the governing equations can be expressed in below matrix set as a formal notation of equations (2.23) to (2.25):

$$\sum_{i=2}^{4}\sum_{j=2}^{4}\{[M_{ij}] + [A_{ij}]\}[\ddot{\eta}_i] + [B_{ij}][\dot{\eta}_i] + [C_{ij}][\eta_i] = [F_i] \tag{2.26}$$

$$[M_{ij}] = \begin{bmatrix} M & 0 & -Mz_c \\ 0 & M & 0 \\ -Mz_c & 0 & I_{44} \end{bmatrix} \qquad [A_{ij}] = \begin{bmatrix} A_{22} & 0 & A_{24} \\ 0 & A_{33} & 0 \\ A_{42} & 0 & A_{44} \end{bmatrix}$$

$$[B_{ij}] = \begin{bmatrix} B_{22} & 0 & B_{24} \\ 0 & B_{33} & 0 \\ B_{42} & 0 & B_{44} \end{bmatrix} \qquad [C_{ij}] = \begin{bmatrix} 0 & 0 & 0 \\ 0 & C_{33} & 0 \\ 0 & 0 & C_{44} \end{bmatrix}$$

$[M_{ij}]$ are the components of the generalized mass matrix of the FPSO, this item can be easily calculated in theory, in many cases, it is estimated based on very simple formulae for the gyration radius in proportion to the beam.

$[A_{ij}]$ is the frequency-dependent added-mass/added inertia, the linear assumption to compute the vessel added mass coefficients due to the complexity is considered in solving the complete non-linear problem. Comparisons between results from linear theory and experiments (Vugts, 1968) already demonstrated noticeable discrepancy between roll motions added mass coefficients, while for the other motions a reasonable agreement was found. However, we shall remark that those added mass coefficients are small and that measurement errors may justify part of the differences encountered.

$[B_{ij}]$ are damping coefficients which is the critical parameter in equation of motion. Among damping coefficient in the matrix, the roll damping is considered the most critical in the prediction of roll and has been an object of research for more than 150 years. It is generally accepted that the energy dissipation for a rolling vessel is not governed by the wave generation mechanism as for the other motions, but by viscous effects which are not accounted for in the potential theory employed for the assessment of seakeeping behaviour of floating units. Furthermore, it is well known that those viscous effects governing the roll damping are not linearly evolving with the roll amplitude, which makes the predictions of motions in real sea conditions even more complicated.

$[C_{ij}]$ are the hydrostatic restoring coefficients, the linear restoring moment and forces can be easily checked after hull construction by measuring the initial metacentric height during the inclining test, which is mandatory. On the other hand, the nonlinearity of restoring moments is responsible for parametric instability problems in container ships, for instance. But the conditions for this instability to occur are met only when the vessel has a forward speed. Also, the shape of such vessels varies significantly along their length, which is not the case for FPSOs.

$[F_i]$ is exciting force and moments, this term comes from the environmental loads acting on the hull of the unit. The main uncertainties associated with it are directly related to the amount and quality of the environmental data obtained for the location of the unit and their treatment. For the model test in laboratory environment it could be assumed in linear condition, but further uncertainties are associated with the linear theory employed to compute the loads; for large amplitudes of motions, this linear

assumption is obviously inaccurate. As it showed in (2.26), heave does not influence the coupled sway-roll in vertical plane motion; but the reverse may not be true.

2.3 3rd Order Equation (Linear)

This part goal is to drive a 3rd order equation sway/roll motion in condition of the free roll decay. part 2.2.2 showed that the roll/sway coupling in vertical plane (2D) while heave has no influence on roll-sway. Equation (2.27) expresses the coupling sway/roll for any arbitrary pole in free roll decay.

$$\begin{bmatrix} M + A_{22}^{pole} & A_{24}^{pole} - Mz_c \\ A_{42}^{pole} - Mz_c & I_4^{pole} + A_{44}^{pole} \end{bmatrix} \begin{bmatrix} \ddot{\eta}_2^{pole} \\ \ddot{\eta}_4^{pole} \end{bmatrix} + \begin{bmatrix} B_{22}^{pole} & B_{24}^{pole} \\ B_{42}^{pole} & B_{44}^{pole} \end{bmatrix} \begin{bmatrix} \dot{\eta}_2^{pole} \\ \dot{\eta}_4^{pole} \end{bmatrix} + \begin{bmatrix} 0 & 0 \\ 0 & C_{44} \end{bmatrix} \begin{bmatrix} \eta_2^{pole} \\ \eta_4^{pole} \end{bmatrix} = \begin{bmatrix} 0 \\ 0 \end{bmatrix}$$

(2.27)

It is easy to inertially decouple the roll and sway equations by moving the origin of the coordinate system to a position at which the mass matrix is diagonal (zero off-diagonal elements). This position of the origin is referred to here as the Inertial Decoupling Point - C_{idp}. A new set of sway and roll equations can then be written for the C_{idp} coordinate system as (2.28) generalized by the mass-inertia matrix:

$$\begin{bmatrix} 1 & 0 \\ 0 & 1 \end{bmatrix} \begin{bmatrix} \ddot{\eta}_2^{idp} \\ \ddot{\eta}_4^{idp} \end{bmatrix} + \begin{bmatrix} b_{22}^{idp} & b_{24}^{idp} \\ b_{42}^{idp} & b_{44}^{idp} \end{bmatrix} \begin{bmatrix} \dot{\eta}_2^{idp} \\ \dot{\eta}_4^{idp} \end{bmatrix} + \begin{bmatrix} 0 & 0 \\ 0 & c_{44} \end{bmatrix} \begin{bmatrix} \eta_2^{idp} \\ \eta_4^{idp} \end{bmatrix} = \begin{bmatrix} 0 \\ 0 \end{bmatrix}$$

(2.28)

Where,

$$b_{22} = \frac{B_{22}}{(\mathrm{M} + A_{22})} \qquad c_{44} = \frac{C_{44}}{(I_4^{idp} + A_{44}^{idp})}$$

$$b_{44}^{idp} = \frac{B_{44}^{idp}}{(I_4^{idp} + A_{44}^{idp})} \qquad b_{24}^{idp} b_{42}^{idp} = \frac{B_{24}^{idp} B_{42}^{idp}}{(I_4^{idp} + A_{44}^{idp})(\mathrm{M} + A_{22})}$$

The vertical position of the *idp* (z_{idp}) which is related to the vertical position of the center of gravity (z_{cg}) and the coupling added mass (A_{42}^{cg}) can be easily obtained by the Formula (2.29) where the off-diagonal terms of inertia matrix (2.27) are equal to zero.

$$z_{idp} = z_{cg} - \left(\frac{A_{42}^{cg}}{M + A_{22}} \right) \tag{2.29}$$

Thus far, several studies have demonstrated that the C_{idp} could be interpreted as a 'roll center' where the roll is fully-decoupled from other modes of motion and could be studied as 1-DoF. Note that, despite the roll being inertially decoupled in (2.28), non-zero coupled damping terms, b_{24}^{idp} and b_{42}^{idp}, remain. Indeed, these terms are numerically large, having the same order of magnitude as $b_{22}$and b_{44}^{idp}. Sway and roll equations can be showed as (2.30) and (2.31) from matrix (2.28).

$$\ddot{\eta}_2^{idp} + b_{22}^{idp} \dot{\eta}_2^{idp} + b_{24}^{idp} \dot{\eta}_4^{idp} = 0 \tag{2.30}$$

$$\ddot{\eta}_4^{idp} + b_{42}^{idp} \dot{\eta}_2^{idp} + b_{44}^{idp} \dot{\eta}_4^{idp} + c_{44} \eta_4^{idp} = 0 \tag{2.31}$$

The equation (2.31) is the roll equation, and clearly includes a term depending on sway velocity and a damping coupling term. However, evidences reviewed in the literature reveal that for decades the equation for one degree of freedom (2.32) has been used in the literature. The quote from the PNA (Lewis, 1989) stating that "roll is still coupled

to the sway equation, but only through the coefficient B42, and this coupling is not strong (…) (therefore) we ignore the coupling terms ” does not seem to be correct.

$$\ddot{\eta}_4 + b(\dot{\eta}_4)\dot{\eta}_4 + c(\eta_4)\eta_4 = 0 \tag{2.32}$$

Note that equation (2.32) has no theoretical basis unless $b_{42}^{idp}\dot{\eta}_2^{idp} = 0$ for some reason. In fact, during decay tests (especially for the pure moment method) the sway velocity might be small, but the coupling damping term is not. Even if this were the case, the pole of the equation with one degree of freedom (defined according to Equation (2.29)) can only be the C_{idp} - it cannot be the C_{cg} or another point. One can find in the literature studies that place the pole at the C_{cg}, then use the parallel axis theorem to get the damping with respect to the C_{idp}, which is conceptually wrong.

Now, note that the sway-roll problem is semi-definite, since the sway mode has no restoring force. Hence, the system is initially of fourth order, as seen in (2.27), but it may become third order if the pole is positioned on the C_{idp}. The roll equation can be rearranged from (2.31) as following:

$$\dot{\eta}_2^{idp} = \frac{-1}{b_{42}^{idp}}\{\ddot{\eta}_4^{idp} + b_{44}^{idp}\dot{\eta}_4^{idp} + c_{44}\eta_4^{idp}\} \tag{2.33}$$

Calculating derivative of (2.33),

$$\ddot{\eta}_2^{idp} = \frac{-1}{b_{42}^{idp}}\{\dddot{\eta}_4^{idp} + b_{44}^{idp}\ddot{\eta}_4^{idp} + c_{44}\dot{\eta}_4^{idp}\} \tag{2.34}$$

The $\dot{\eta}_2^{idp}$ obtained from (2.33) can be substituted in (2.30),

$$\ddot{\eta}_2^{idp} = \frac{1}{b_{42}^{idp}}\{b_{22}\ddot{\eta}_4^{idp} + (b_{22}b_{44}^{idp} - b_{24}^{idp}b_{42}^{idp})\dot{\eta}_4^{idp} + b_{22}c_{44}\eta_4^{idp}\} \tag{2.35}$$

Both equations (2.34) and (2.35) show acceleration of sway as function of roll, therefore, a 3rd order ordinary differential homogenous roll equation can be obtained by (2.34)=(2.35) as following:

$$\dddot{\eta}_4^{idp} + \{b_{22} + b_{44}^{idp}\}\ddot{\eta}_4^{idp} + \{b_{44}^{idp}b_{22} - b_{24}^{idp}b_{42}^{idp} + c_{44}\}\dot{\eta}_4^{idp} + \{b_{22}c_{44}\}\eta_4^{idp} = 0 \tag{2.36}$$

The 3rd order ordinary differential non-homogenous equation for sway motion forced by roll can be obtained following the same procedure described above.

$$\dddot{\eta}_2^{idp} + \{b_{22} + b_{44}^{idp}\}\ddot{\eta}_2^{idp} + \{b_{44}^{idp}b_{22} - b_{24}^{idp}b_{42}^{idp}\}\dot{\eta}_2^{idp} = \{b_{24}^{idp}c_{44}\}\eta_4^{idp} \tag{2.37}$$

Note that Equation (2.36) is homogeneous, involving only roll. The coupling terms add to the roll restoring term, which multiplies $\dot{\eta}_4^{idp}$. Hence, the remainder of this work will deal with Equation (2.36) to address the roll problem on an innovative, robust basis. Also note that, in principle, once η_4^{idp} is know it can be used to obtain $\dot{\eta}_2^{idp}$ and plug it into (2.37), allowing η_2^{idp} to be obtained after integration.

2.4 3rd Order Equation of Roll (Linear-plus-Quadratic)

It is well known that linear roll damping cannot represent well real damping coefficient of a FPSO with attached bilge-keel, the damping is nonlinear with the damping moment mostly represented by linear-plus-quadratic velocity dependent terms (see (2.38)).

$$b_{44}^{pole}(\dot{\eta}_4^{pole}) = b_1^{pole}\dot{\eta}_4^{pole} + b_2^{pole}\dot{\eta}_4^{pole}\left|\dot{\eta}_4^{pole}\right| \tag{2.38}$$

Remembering equation (2.33), the derivate of $b_{44}^{pole}(\dot{\eta}_4^{pole})$ should be known to obtain the 3rd order equation for non-linear damping.

$$\dot{b}_{44}^{pole}(\dot{\eta}_4^{pole}) = \frac{\partial \dot{b}_{44}^{pole}(\dot{\eta}_4^{pole})}{\partial \dot{\eta}_4^{pole}}\ddot{\eta}_4^{pole} \tag{2.39}$$

According to Figure 2.2, derivative of the $\dot{\eta}_4^{pole}\left|\dot{\eta}_4^{pole}\right|$ will be as $2\left|\dot{\eta}_4^{pole}\right|$, thus the equation (2.39) can be expressed as (2.40) for C_{idp} pole.

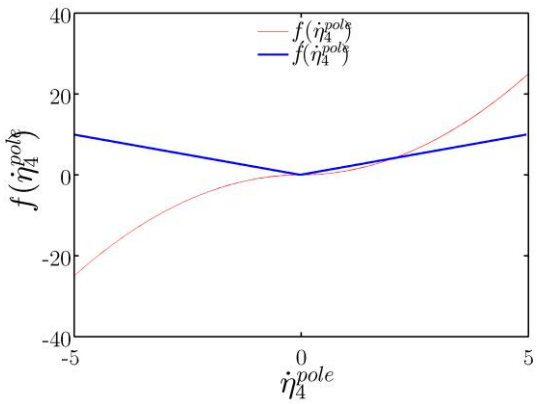

Figure 2.2 – Comparison of function $f(\dot{\eta}_4^{pole}) = \dot{\eta}_4^{pole}\left|\dot{\eta}_4^{pole}\right|$ with its derivative $f'(\dot{\eta}_4^{pole})$.

$$\dot{b}_{44}^{idp}(\dot{\eta}_4^{idp}) = b_1^{idp}\ddot{\eta}_4^{idp} + 2b_2^{idp}\ddot{\eta}_4^{idp}\left|\dot{\eta}_4^{idp}\right| \tag{2.40}$$

The 3rd order roll equation including linear-plus-quadratic damping terms can be obtained from equation as:

$$\dddot{\eta}_4 + \left\{b_{22} + b_1^{idp}\right\}\ddot{\eta}_4^{idp} + \left\{2.\, b_2^{idp}\right\}\left|\dot{\eta}_4^{idp}\right|.\,\ddot{\eta}_4^{idp} + \left\{b_{22} b_2^{idp}\right\}\dot{\eta}_4^{idp}\left|\dot{\eta}_4^{idp}\right| + \left\{b_{22} b_1^{idp} - b_{24}^{idp} b_{42}^{idp} + c_{44}\right\}\dot{\eta}_4^{idp} + \{b_{22} c_{44}\}\eta_4^{idp} = 0 \tag{2.41}$$

Chapter 3 Free Decay Roll: Roll Damping Estimation via 3rd Order System Identification

Free decay test is a common practice for identifying nonlinear roll damping of a ship, this test is almost always part of a model test campaign applied for industrial either academic purposes. This chapter presents innovative 3rd order system identification to estimate roll damping accurately considering coupling effects from free roll decay test. Results are showed numerically, experimentally and compared with Faltinsen and Froude's approaches.

3.1 Non-Linear Roll Damping Models

Generally, the method practiced by the industry is physically linked to the local effects of viscosity over the hull and bilge-keels. Most roll motion studies in the literature use a second order ordinary nonlinear differential equation that is traceable to the works of Froude. the damping moments is nonlinear with the damping moment represented by linear-plus-quadratic velocity dependent terms (See (2.38)). In order to obtain linear (b_1^{idp}) and quadratic (b_2^{idp}) two approaches were raised by Froud and Faltinsen.

One common way to analyse the data consists of tabulating the peak values and plotting the change in the roll amplitude divided by the mean of the successive peak values, against the mean of the successive peak values for each cycle. If the roll damping is a quadratic function of roll angular velocity, this plot will be a straight line, the intercept and slope of which are proportional to the linear and second-order damping coefficients, respectively.

3.1.1 Froude's Approach

In this approach, considering a small variation of the angle during a cycle, the damping dissipation (considering harmonic solution) can be estimated by the loss of potential energy observed during a half-cycle. Where the amplitude of the harmonic function (shown in (3.1)) is approximated by the average/arithmetic mean of the peak amplitudes of the cycle (considering half cycle for the analysis).

$$\theta(t) = \theta_m \cos(\omega_n t) \tag{3.1}$$

Calculating the energy dissipated in a half-cycle for this formulation, we have that:

$$E_D = \int_0^{T/2} (b_1\dot{\theta} + b_1\dot{\theta}\,|\,\dot{\theta}\,| + \ldots)\dot{\theta}dt = \frac{1}{2}\pi b_1 \omega \theta_m + \frac{4}{3} b_2 \omega^2 \theta_m^2 + \ldots \tag{3.2}$$

On the other hand, the loss of energy during a half-cycle of a decay test can be calculated by the potential energy difference in each peak:

$$E_R = \int_{\theta_i}^{\theta_{i+1}} \omega^2 \theta d\theta = -\frac{\omega^2}{2}(\theta_i + \theta_{i+1})(\theta_i - \theta_{i+1}) = -\omega^2 \theta_m \delta\theta \tag{3.3}$$

Equating the (3.2) and (3.3),

$$E_R + E_D = 0 \rightarrow \delta\theta = \left(\frac{\pi b_1}{2\omega}\theta_m + \frac{b_2}{3}\theta_m^2 + ... \right) \tag{3.4}$$

The approach to obtain linear and quadratic coefficients from a decay test using Froude methodology is discussed by (Roberts, 1985b) and more recently (Neves, 2004), according to these study, the coefficients b_1 and b_2 can be obtained by adjusting a parabola curve on plotting of $\delta\theta$ versus mean amplitude (θ_m) as shown in Figure 3.1. Note that, the method the first cycle has been neglected for free roll decay.

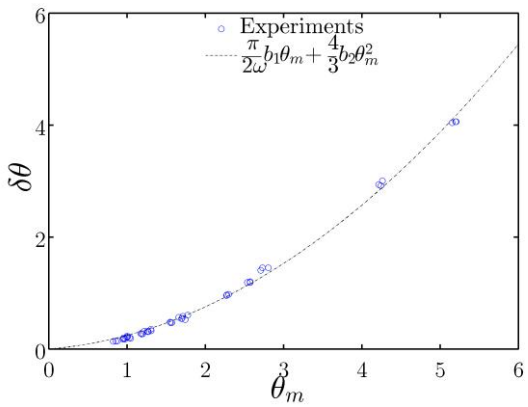

Figure 3.1– Example Froude's approach for estimation of b_1 and b_2.

3.1.2 Faltinsen's Approach

The approach described by Faltinsen (Faltinsen, 1990) is like the Froud approach, presented in 3.1.1. In this approach, the loss of energy is evaluated in terms of a linear equivalent damping coefficient, equalling this to the energy dissipation (3.2) from the quadratic equation. It leads to the result shown in (3.5).

$$P_e = \frac{2\ln\left(\frac{\theta_i}{\theta_{i+1}}\right)}{T} = b_1 + \frac{8\omega}{3} b_2 \theta_m \tag{3.5}$$

In this case, the coefficients b_1 and b_2 can be obtained via a linear adjusting based on least square method as it shown in Figure 3.2.

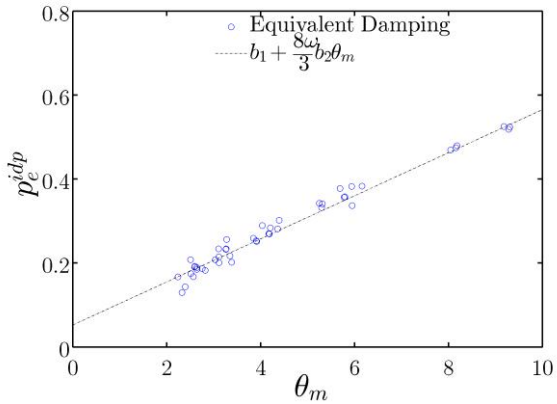

Figure 3.2– Example of Faltinsen's approach for estimation of b_1 and b_2.

Comprehensive study on Froud and Faltinsen approaches can be found in (Fernandes, 2009), (Oliveira, 2011) and (Oliveira, 2014).

3.2 Proposed Approach

A comprehensive 3rd order roll equation including the coupling terms is presented in 2.3. The 3rd order equation could be used in a robust method to assess roll damping in the non-linear quadratic case, including the influence of coupling terms. The method is described in 3.2.1 linearly and final nonlinear form in 3.2.3.

3.2.1 Linear 3rd System Identification

According to part 2.3, the linear equation of motion can be presented as 3rd order ordinary differential homogenous equation (2.36), looking for a particular solution of the form $\eta_4 = ke^{\lambda t}$, substituting η_4 and its derivatives into (2.36), one obtains,

$$(b_{22}+b_{44}^{idp})\lambda_i^2+(b_{22}b_{44}^{idp}-b_{24}^{idp}b_{42}^{idp})\lambda_i+b_{22}c_{44}=-\lambda_i(\lambda_i^2+c_{44}) \tag{3.6}$$

particular solution of λ_i for i=1, 2 and 3 can be obtained from (3.6), taking into account the initial conditions k_1, k_2 and k_3. Considering free roll decay, the general solution for the linear roll response can be represented in exponential form, as seen below:

$$\eta_4(t)=k_1e^{\lambda_1 t}+k_2e^{\lambda_2 t}+k_3e^{\lambda_3 t} \tag{3.7}$$

Supposed that a response of roll displacement of free decay is available from a perfectly linear system with unknown coefficients, in order to identify the linear coefficients of (2.36) a linear system identification technique can be used on the roll time series. In this technique, the linear system identification assumes that the roll response has a form (3rd order) such as (3.7) and proceeds by applying non-linear least squares using the Levenberg-Marquardt method ((Levenberg, 1944), (Marquardt, 1963) and (Moré, 1978)) to the above equation in order to obtain λ_i and k_i, consequently, the coefficients of the 3rd order (2.36) can be obtained from the linear system identification for the following initial conditions:

$$\begin{aligned}\eta_4(0)&=\theta_0\\ \dot{\eta}_4(0)&=0\\ \ddot{\eta}_4(0)&=-c_{44}^{idp}\theta_0\end{aligned} \tag{3.8}$$

The following system of equations can be written based on equation (3.6), for known λ_i and k_i .

$$\begin{pmatrix} 1 & \lambda_1^2 & \lambda_1 \\ 1 & \lambda_2^2 & \lambda_2 \\ 1 & \lambda_3^2 & \lambda_3 \end{pmatrix} \begin{pmatrix} b_{22}c_{44} \\ b_{22}+b_{44}^{idp} \\ b_{22}b_{44}^{idp}-b_{24}^{idp}b_{42}^{idp} \end{pmatrix} = \begin{pmatrix} -\lambda_1(\lambda_1^2+c_{44}) \\ -\lambda_2(\lambda_2^2+c_{44}) \\ -\lambda_3(\lambda_3^2+c_{44}) \end{pmatrix} \tag{3.9}$$

Back to (3.8), the c_{44} could be easily obtained from initial conditions by dividing $\ddot{\eta}_4(0)$ by $\eta_4(0)$, as it shown in (3.10).

$$c_{44} = -\left(\frac{\lambda_1^2 k_1 + \lambda_2^2 k_2 + \lambda_3^2 k_3}{k_1 + k_2 + k_3}\right) \tag{3.10}$$

Therefore, b_{22}, b_{44}^{idp} and $b_{24}^{idp}b_{42}^{idp}$ (product of coupling terms) can be obtained from (3.9). Note that this is a procedure that gets all the information available from the decay test, unlike the Froude and Faltinsen methods, which use global properties: the potential energy difference in the former, and the equivalent harmonic energy dissipation in the latter.

3.2.2 Validation of Linear 3rd System Identification

A numerical model with 3703 panels has been used for the representation of the FPSO's hull - see Figure 3.3 where the radiation/diffraction program – WAMIT® is used to provide hydrostatic coefficients, added mass and potential damping coefficients. Since the calculates are based on potential theory, as a common practice an extra damping (5~6 %) considered for roll damping to represent the viscous effects. The matrices of (2.27) for the numerical dimensional properties for cg coordinate are

shown in (3.11). it is important that roll time history is independent of coordinate system.

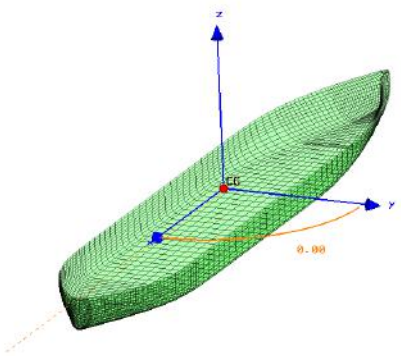

Figure 3.3– Numerical panel/model of the FPSO for draft 14.7m.

$$[M_{ij}^{CG}] = \begin{bmatrix} 211873.79 & 0 \\ 0 & 8.9181e+07 \end{bmatrix} \qquad [A_{ij}^{CG}] = \begin{bmatrix} 1.9220e+05 & -5.6556e+05 \\ -5.6229e+05 & 2.3542e+07 \end{bmatrix}$$

$$[C_{ij}] = \begin{bmatrix} 0 & 0 \\ 0 & 1.8803e+07 \end{bmatrix} \qquad [B_{ij}^{CG}] = \begin{bmatrix} 3.4802e+04 & -1.6878e+05 \\ -1.6830e+05 & 6.3560e+06 \end{bmatrix}$$

(3.11)

or for the same system but in C_{idp} coordinate,

$$[M_{ij}^{idp}] = \begin{bmatrix} 211873.79 & 2.9818e+05 \\ 2.9818e+05 & 8.9591e+07 \end{bmatrix} \qquad [A_{ij}^{idp}] = \begin{bmatrix} 1.9220e+05 & -2.9818e+05 \\ -2.9818e+05 & 2.2337e+07 \end{bmatrix}$$

$$[C_{ij}] = \begin{bmatrix} 0 & 0 \\ 0 & 1.8803e+07 \end{bmatrix} \qquad [B_{ij}^{idp}] = \begin{bmatrix} 3.4802e+04 & -1.2068e+05 \\ -1.1986e+05 & 5.9354e+06 \end{bmatrix}$$

(3.12)

To validate the 3rd system identification method explained in 3.2.1, several time series were generated based on the numerical model's coefficients for different initial angles (θ_0) and linear damping coefficients provided by the general solution of equations with the C_{idp} as the origin. Linear dampings are extracted from the time series by applying the SI and compared with exact numerical solution in Figure 3.4.

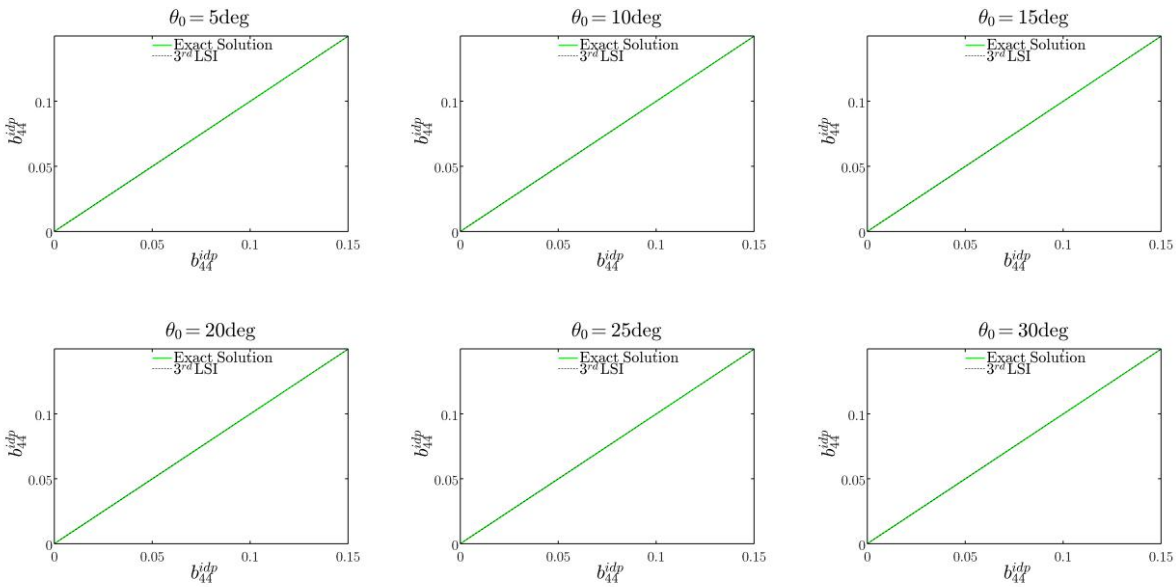

Figure 3.4– Linear roll damping estimation through 3rd Order system Identification approach for different initial angles 5, 15 and 25 degree.

It has been observed that the non-dimensional order of magnitude of $b_{24}^{idp} b_{42}^{idp}$ is much smaller than those of b_{22} and b_{44}^{idp}, consequently, SI estimates of this value suffer from unavoidable numerical errors. For instance, in the case studied here, $b_{24}^{idp} b_{42}^{idp}$ equals 0.0018, while the value estimated with SI is 0.0016. By identifying the role of $b_{24}^{idp} b_{42}^{idp}$ on

the roll equation, it has been concluded that this numerical error 0.0002 may be negligible. Indeed, Figure 3.5 illustrates that the roll time series obtained by linear system identification is very close to the direct numerical result.

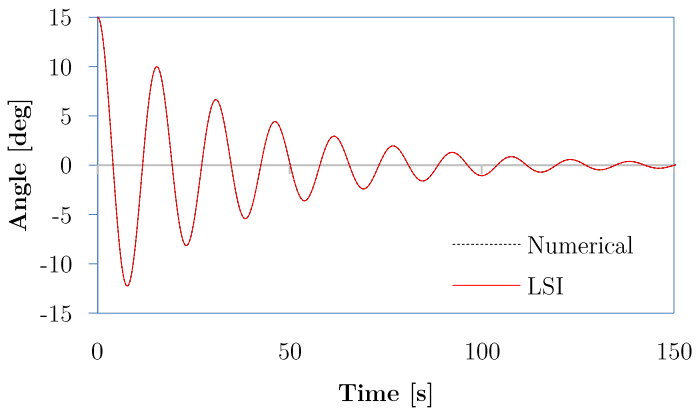

Figure 3.5– Comparison of the roll time series from the numerical model and the results obtained from *Linear 3rd Order System Identification* – LSI.

3.2.3 Pole's Position Error

During the investigation the author observed that there is an old mistake (or maybe not a mistake, just neglecting it!) among the researchers. Many studies of roll damping have considering roll as single degree of freedom as it discussed in 1.2, but there is not clear explanation to which pole the roll damping ratio refers to. There is a common interpretation has: it does not matter where is position of pole since the roll damping ratio definition is $b(\dot{\eta}_4) = (B_{44}^{pole} / I_4^{pole} + A_{44}^{pole})$; it means if you are looking for roll

damping coefficient on center of rotation is enough to substituted I_4^{cg} and A_{44}^{cg} into the formula.

A very simple verification may explain it better. Assuming roll motion in one degree of freedom (see (2.32)), where damping $b(\dot{\eta}_4)$ and restoring coefficients $c(\eta_4)$ are linear and known numerically for any poles (here C_{cg} and C_{idp}) according to (3.11) and (3.12). The roll decay time history can be obtained by solving the (2.32), obviously, for both coordinate system the responses will be the same. As next step, the roll damping and restoring ratio can be estimated by linear 3rd order system identification and Faltinsen approaches, results are shown in Table 3.1.

Table 3.1 – Linear roll damping and restoring ratios obtained from different approaches.

	Numerical coefficient referring to pole		**Obtained from roll time history**	
Ratio	C_{idp}	C_{cg}	*3rd S.I.*	*Faltinsen*
b_{44}^{pole}	0.053029	0.05638	0.05303	0.05302
c_{44}^{pole}	0.16799	0.1668	0.1679	0.1678

Results showed that the roll damping ratio obtained from free roll decay is a unique value which belongs to a specific pole and cannot be generalized to any other pole.

3.2.4 Non-Linear 3rd approach

By applying 3rd order system identification, the linear equivalent dampings and restoring coefficients could be obtained for each cycle (with their corresponding mean angles). This study assumed that the nonlinearity of roll damping can be represented

by a linear-plus-quadratic form (since the focus here is not efficiency of the non-linear models), as (2.38) but in dimensionless form with respect to the C_{idp} .

$$b_{44}^{idp}(\dot{\eta}_4^{idp}) = (b_1^{idp} + b_2^{idp}|\dot{\eta}_4^{idp}|)\dot{\eta}_4^{idp} \tag{3.13}$$

To determine the linear b_1^{idp} and quadratic b_2^{idp} parts of roll damping, conventional damping plot methods such as those described by Froude, Faltinsen and others can be employed. See for example Figure 3.6.

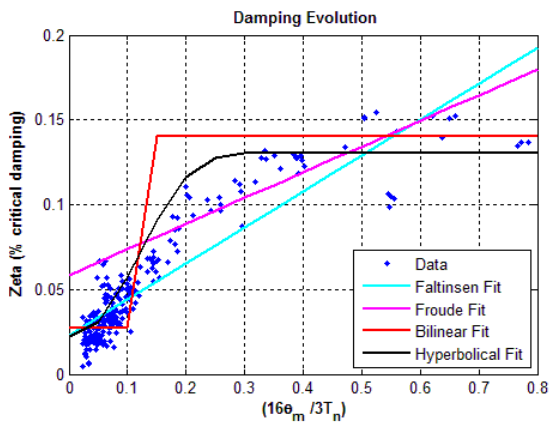

Figure 3.6– Typical damping plot methods to obtain linear and quadratic terms of roll damping, where zeta is $\frac{B_{44}^{idp}}{B_{44}^{critical}}$; (Oliveira, 2014).

Once the linear and quadratic parts are determined the time history of the free roll decay can be plotted using equation (2.41). Figure 3.7 illustrates steps of the nonlinear 3rd order system identification.

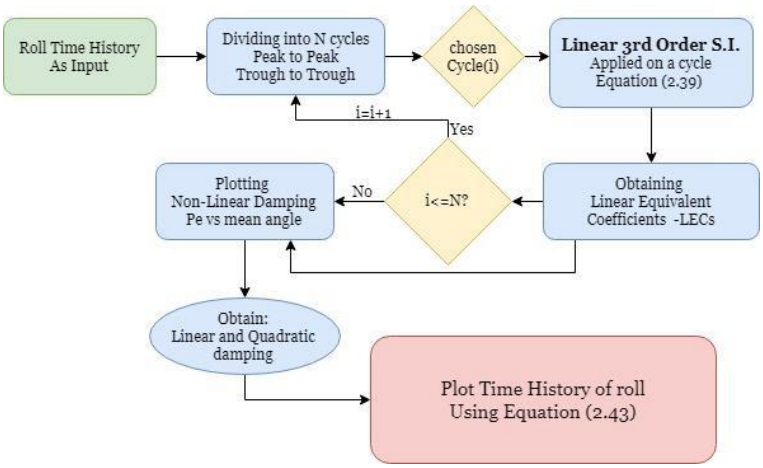

Figure 3.7– 3rd order system identification flowchart.

3.3 Consequences of Applying the 3rd Order Equation

This study now proceeds with an application of the 3rd order equation, from which it is possible to extract several consequences that have been previously overlooked. What is interesting about new approach is that the 3rd order SI can sense coupling terms and taking account into roll damping estimation and consequently increasing accuracy. 3.3.1 investigates influence of coupling terms on nonlinear damping via 3rd order SI and following 3.3.2 compares the results with conventional methods.

3.3.1 Influence of Coupling Terms on Nonlinear Damping Estimation

Numerical study investigate model with variation of nonlinearities and initial angles θ_0, the nonlinearity defined as b_2^{idp}/b_1^{idp} , which is quadratic/linear ratio terms. Based on

possible conditions listed in Table 3.2, numbers of roll decay time histories have provided by the general solution of the equation (2.41) using the C_{idp} as a pole.

Table 3.2 – Conditions for numerical model.

$\frac{b_2^{idp}}{b_1^{idp}}$ - *Nonlinearity ratio* [-]							
0.00	0.10	0.25	0.50	1.00	2.00	3.00	5.00
θ_0 - *Initial angle* [deg]							
5		10	15	20	25	30	

Quadratic Term – in order to study influence of the $b_{24}^{idp} b_{42}^{idp}$ on roll damping, two different 3rd order system identifications are proposed: the first system identification which used equation (3.6) for $b_{24}^{idp} b_{42}^{idp} \neq 0$, and second system identification is when $b_{24}^{idp} b_{42}^{idp} = 0$ as shown in (3.14).

$$(b_{22} + b_{44}^{idp})\lambda_i^2 + b_{22} b_{44}^{idp} \lambda_i + b_{22} c_{44} = -\lambda_i (\lambda_i^2 + c_{44}) \tag{3.14}$$

Both system identifications were applied in order to extract quadratic term b_2^{idp} from different conditions of free decay roll. Figure 3.8 shows the consequences of neglecting $b_{24}^{idp} b_{42}^{idp}$ in the calculation of the quadratic term for different initial angles. The horizontal axes in the figure are the known values defined in the numerical model, while the vertical axes are the values obtained from the 3rd SI.

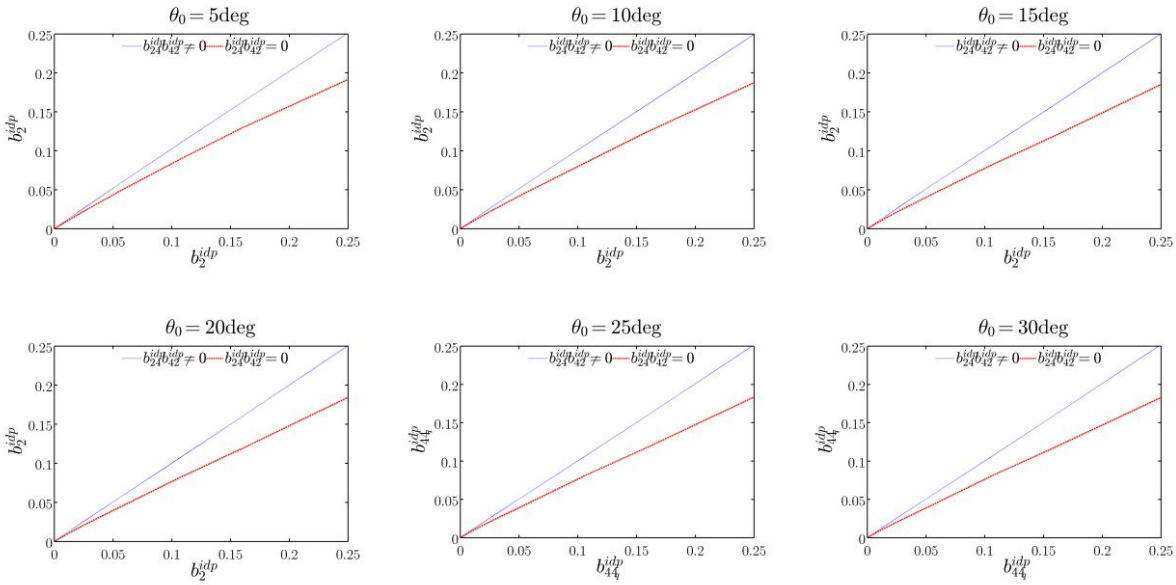

Figure 3.8– Quadratic damping term b_2^{idp} estimation by S.I. with and Without influence of $b_{24}^{idp} b_{42}^{idp}$.

There was a significant positive correlation between coupling term and nonlinear roll damping (quadratic). This sensitivity study reveals a gradual decrease in the precision (about 30% error) of the estimation of the quadratic part of roll damping b_2^{idp} when coupling terms are ignored (see Figure 3.8).

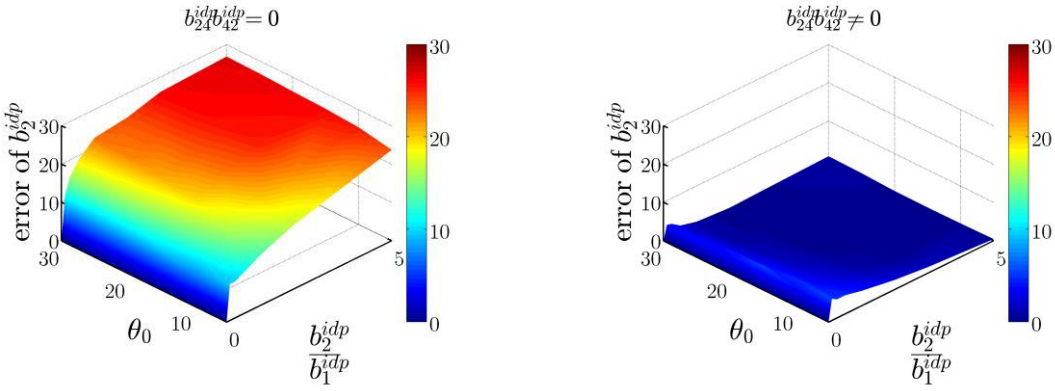

(a) (b)

Figure 3.9– Quadratic damping term b_2^{idp} estimation's error (a) $b_{24}^{idp} b_{42}^{idp} = 0$, (b) $b_{24}^{idp} b_{42}^{idp} \neq 0$.

Note also that Figure 3.9 shows no significant change in the error with variation of the initial angle, especially when coupling terms are taken into account.

Linear Term - The numerical errors of calculating the linear damping part b_1^{idp} for the same cases above are compared in Figure 3.10.

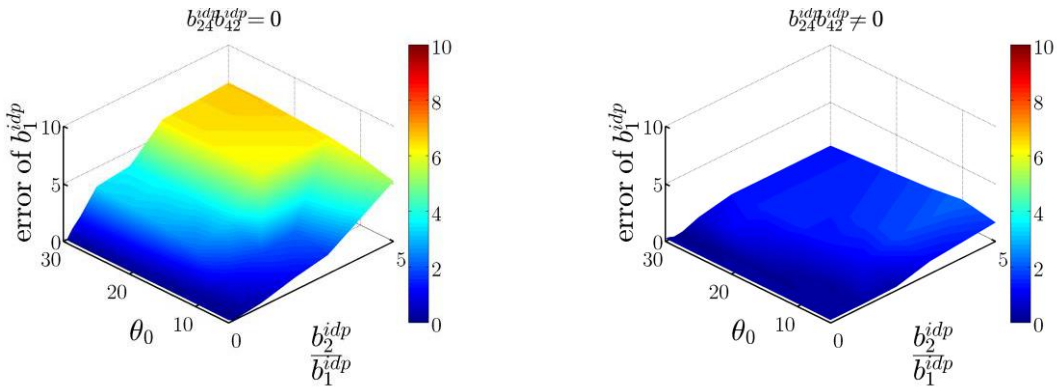

(a) (b)

Figure 3.10– Linear damping term b_1^{idp} estimation's error (a) $b_{24}^{idp}b_{42}^{idp}=0$, (b) $b_{24}^{idp}b_{42}^{idp}\neq 0$.

Generally, 3rd order SI results showed good agreement with exact numerical solutions when predicting the linear term of roll damping. For small nonlinearity ratios b_2^{idp}/b_1^{idp}, the value obtained for b_1^{idp} when including coupling terms in the SI is almost identical to the exact numerical solution; for larger ratios, the error may be up to 1%; however, if coupling terms are ignored in the LSI $(b_{24}^{idp}b_{42}^{idp}=0)$ the error may increase by up to sevenfold (Figure 3.10).

The comparisons between the SI $b_{24}^{idp}b_{42}^{idp}\neq 0$ and SI $b_{24}^{idp}b_{42}^{idp}=0$, show a high accuracy of roll damping prediction by 3rd order System Identification when taking coupling terms into account. Therefore, it can be concluded that neglecting the coupling term is a potential source of error for the estimation of roll damping. This is considered an unexpected result given the guidelines given in (Lewis, 1989).

3.3.2 Comparison of Faltinsen and Froude's results and 3rd Order System Identification

Previous studies evaluating the nonlinearity of roll damping used Froude's and Faltinsen's approaches for comparisons. This part of the study compares these approaches with the 3rd order SI; considering the results above, coupling terms are included for these simulations. Figure 3.11 shows a comparison of the error of roll damping estimation (both linear and quadratic damping terms) between the three approaches.

Froude's approach is very sensitive to both the initial angle and nonlinearity, and leads to larger errors. The errors with Faltinsen's approach are constant for different initial angles but raise quickly with nonlinearity ratios. As shown in Figure 3.11(a), Froude's approach is unfavourable for estimating linear damping, while Faltinsen's approach is unfavourable for predicting the quadratic roll damping term for systems with high nonlinearity. However, Faltinsen's approach showed reasonable results for predicting linear roll damping with low nonlinearity.

Table 3.3 – Comparison between the approaches.

	3rd S.I.	*Faltinsen*	*Froude*
Initial Angle sensitivity	*	**	***
Nonlinear Ratio sensitivity	*	**	***
Precision of linear term estimation	***	**	*
Precision of quadratic term estimation	***	*	**
Calculation time	***	**	**

(low/ *** high)*

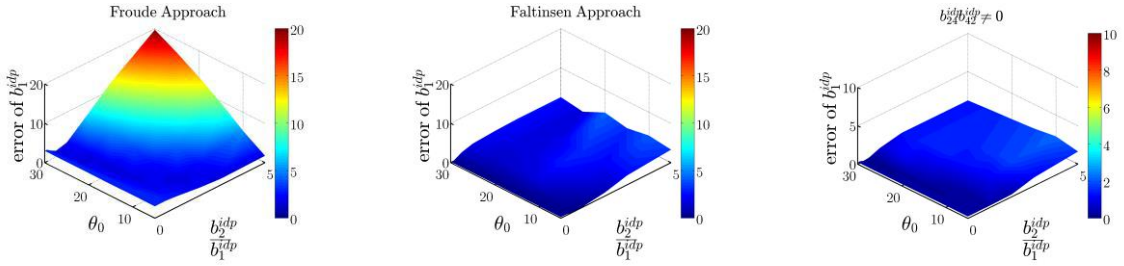

(a) b_1^{idp}

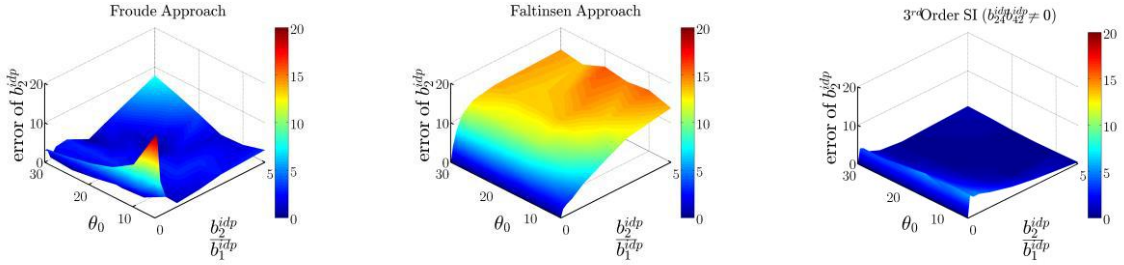

(b) b_2^{idp}

Figure 3.11– Comparison of the errors of Froude and Faltinsen's approaches and errors of the 3rd order SI for (a) Linear damping term and (b) quadratic damping term.

In summary, compared to typical roll damping estimation methods, the 3rd order S.I performed better, showing excellent results for the vast majority of nonlinearity ratios and initial angles. Table 3.3 provides a brief summary of the comparisons.

3.4 Experimental Study

Series of the free roll decay are conducted to estimate the roll dampings. In order to simplify the problem, a 2D model is proposed. The 3D effect is studied by comparing damping ratios obtained from 3D and 2D models and the results illustrates in Figure

3.12. The results from the 2D model shows pretty good agreement with the 3D model and can be representative.

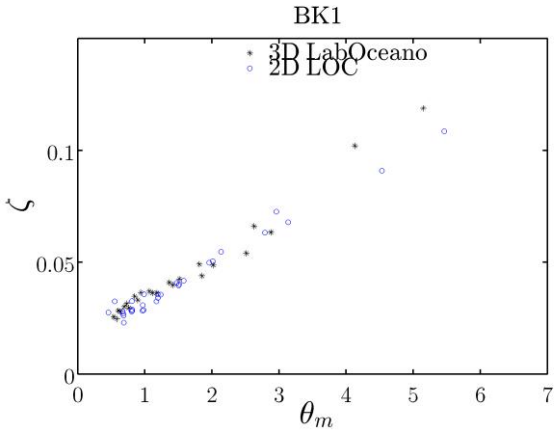

Figure 3.12– Comparison of roll damping ratio obtained from 3D model tests in the *LabOceano* and 2D model tests in the LOC; Draft 21m, BK1.

3.4.1 Test Set-up

The experiments were conducted in the Laboratory of Waves and Currents at COPPE-Federal University of Rio de Janeiro (Laboratório de Ondas e Correntes COPPE-UFRJ). The tank has length of 30m, 1m width and 1m height. The tank is filled with fresh water to a depth of 0.86m. Two wave-absorber beaches are laid on both sides of the tank (See Figure 3.13) which is very convenient for decay tests. The FPSO model is made of the main internal aluminum structure and the external part is covered by fiberglass. The model represents a 1:75 slice of the parallel mid body of a typical FPSO, which has a length to cover 90% of the tank's width to assure two-dimensional flow. The position of the center of gravity, the roll moment of inertia and

the draft floating condition of the model have been properly adjusted. Dynamic similarity is based on Froude number equality. Model test specifications for intermediate draft of 14.7m and full-load draft of 21m are shown in Table 3.4 in the model scale. The parameters for the free decay experiments were the bilge-keel width, the model drafts and initial angles (5, 10 and 15 degrees). The bilge-keels were made of steel flat plate with thickness of 1mm.

Table 3.4 – Model specification for different drafts (scale factor 1:75)

		FPSO		Model Tests	
	Particulars	**Intermediate Draft** (14.7m)	**Full-load Draft (21m)**	**Intermediate Draft** (0.196m)	**Full-load Draft (0.28m)**
Length Overall	$L_{OA}(m)$	337.359		0.90	
Breadth Overall	$B(m)$	54.5		0.726	
Molded Depth	$D(m)$	27.8		0.450	
Mid-ship Coefficient	C_M	0.99		0.99	
Bilge-keel Length Naked Hull - NH	(m)	0.0		0.000	
Bilge-keel Length (Medium) – BK1	(m)	1.2		0.016	
Bilge-keel Length (Large) – BK2	(m)	1.8		0.024	
Displacement	$M(ton, kg)$	211874	310996	127.5	182.6
Center of gravity height (from BL)	$KG(m)$	14.31	14.70	0.191	0.196
Inertial Decoupling Point height (from BL)	$IDP(m)$	15.710	16.387	0.209	0.218
Inertia Moment of roll (respect to *cg)*	$I_4^{cg}(tm^2, kgm^2)$	89181696	104390352	8.235	9.947

**from the BL*

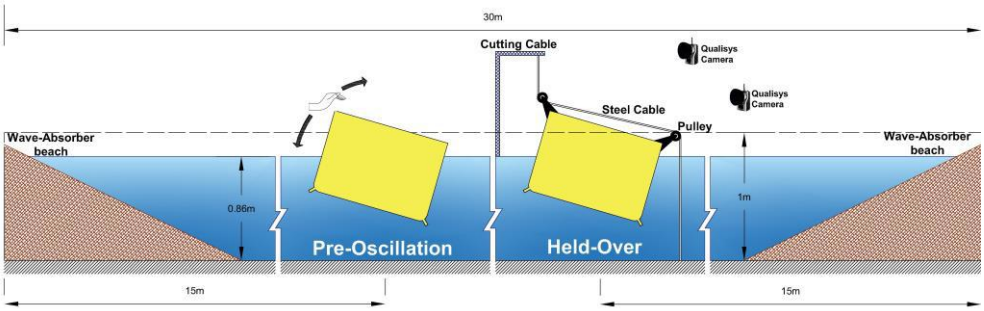

Figure 3.13– Experiment set-up for the held-over and pre-oscillation techniques.

In the experiments, the model of the ship was set at the middle of the tank in condition of calm water. The held-over technique (Fernandes, 2018) was adopted to perform free roll decay. By this technique a static pure couple is applied to the hull up to the point it reaches the specified initial angle. When the water is considered calm and the instrumentation is ready, the model is released by cutting the holding line. This nylon line is set at the end of the steel cable to avoid any unwanted displacement at the releasing time (Qualisys, 2006). illustrates a general view of the set-up and how the pure moment is applied through a kit of steel cable and pulleys. Basically, in held-over technique, the flow separation is undistributed when the model is released, therefore the first cycle does not participate in the roll damping calculation. However, in order to achieve larger mean angles the model is brought to its maximum roll angle through a series of pre-oscillation. In the pre-oscillation method, as Figure 3.14 shows the flow field is fully developed at the releasing moment (Van't Veer, 2011).

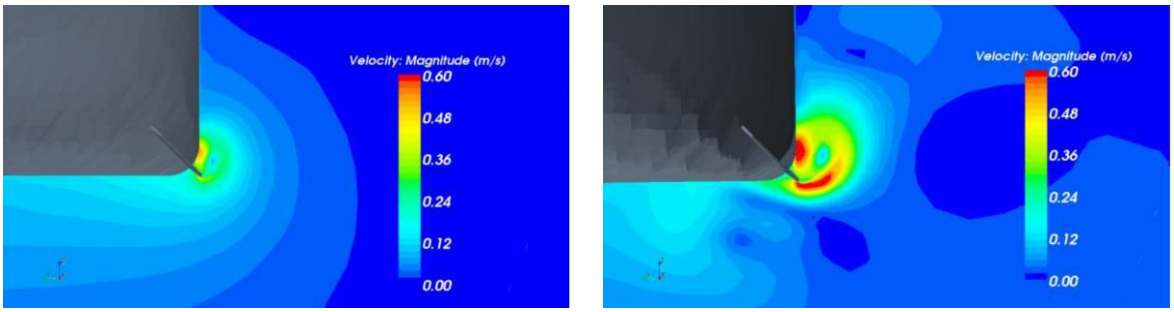

(a)Held-Over (b)Pre-Oscillation

Figure 3.14– Velocity field around the bilge keel at the middle of the first half cycle (t=T/4); (Van't Veer, 2011).

As it shown in Figure 3.13, the pre-oscillation is imposed by hand (avoiding any unwanted sway) and released when it is in desired angle. Due to the coupling terms, displacement of sway is unavoidable in any free decay test (held-over, pre-oscillation) Figure 3.15 illustrates sway for both free roll decay tests.

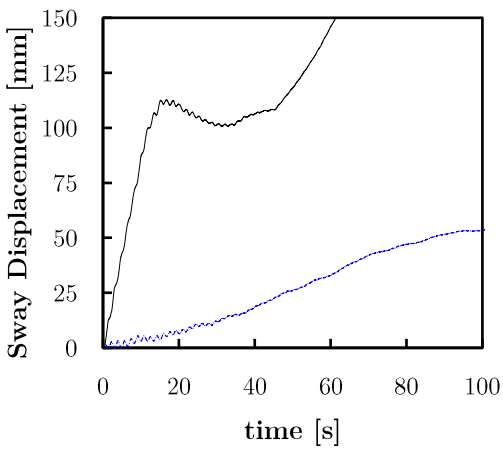

Figure 3.15– Comparison of sway displacement for held-over and pre-oscillation techniques; HO-NH: _._._. blue dotted line, PO-NH: _____ solid line.

The motions during the test were tracked by Qualisys's cameras (Qualisys, 2006). A rigid body can be defined by attached reference markers on the model while the

variation of the markers can be detected by two cameras using software QTM Qualisys Track Manager. After calibration, the system registers the position (six degrees of freedom) and velocities; the signal acquisition rate used in these experiments was 50 Hz.

3.4.2 Results and Discussion

So far Chapter 3 has focus on application of 3rd order system identification. The following section will discuss estimation of roll damping via 3rd SI for the model in intermediate draft comparing results of held-over and pre-oscillation techniques. As shown in Table 3.5, two approaches were applied to the experimental results to obtain roll damping coefficients.

Table 3.5 – Second and third order system identification approaches.

2nd S.I.:	$\ddot{\eta}_4 + b_1^{idp}\dot{\eta}_4 + b_2^{idp}\left\|\dot{\eta}_4\right\|\dot{\eta}_4 + c_{44}^{idp}\eta_4 = 0$
3rd S.I.:	$\dddot{\eta}_4 + \left\{b_{22} + b_1^{idp}\right\}\ddot{\eta}_4 + 2\times b_2^{idp}\left\|\dot{\eta}_4\right\|\ddot{\eta}_4 + b_{22}b_2^{idp}\left\|\dot{\eta}_4\right\|\dot{\eta}_4 + \left\{b_{22}b_1^{idp} - b_{24}^{idp}b_{42}^{idp} + c_{44}^{idp}\right\}\dot{\eta}_4 + b_{22}c_{44}^{idp}\eta_4 = 0$

Two cases of naked hull and with bilge-keel BK2-(1.8m) are studied and non-dimensional roll damping coefficients obtained from 3rd and 2nd order (used in typical methods such Faltinsen and Froude approaches) system identifications are presented, respectively, in Figure 3.16 and Figure 3.17.

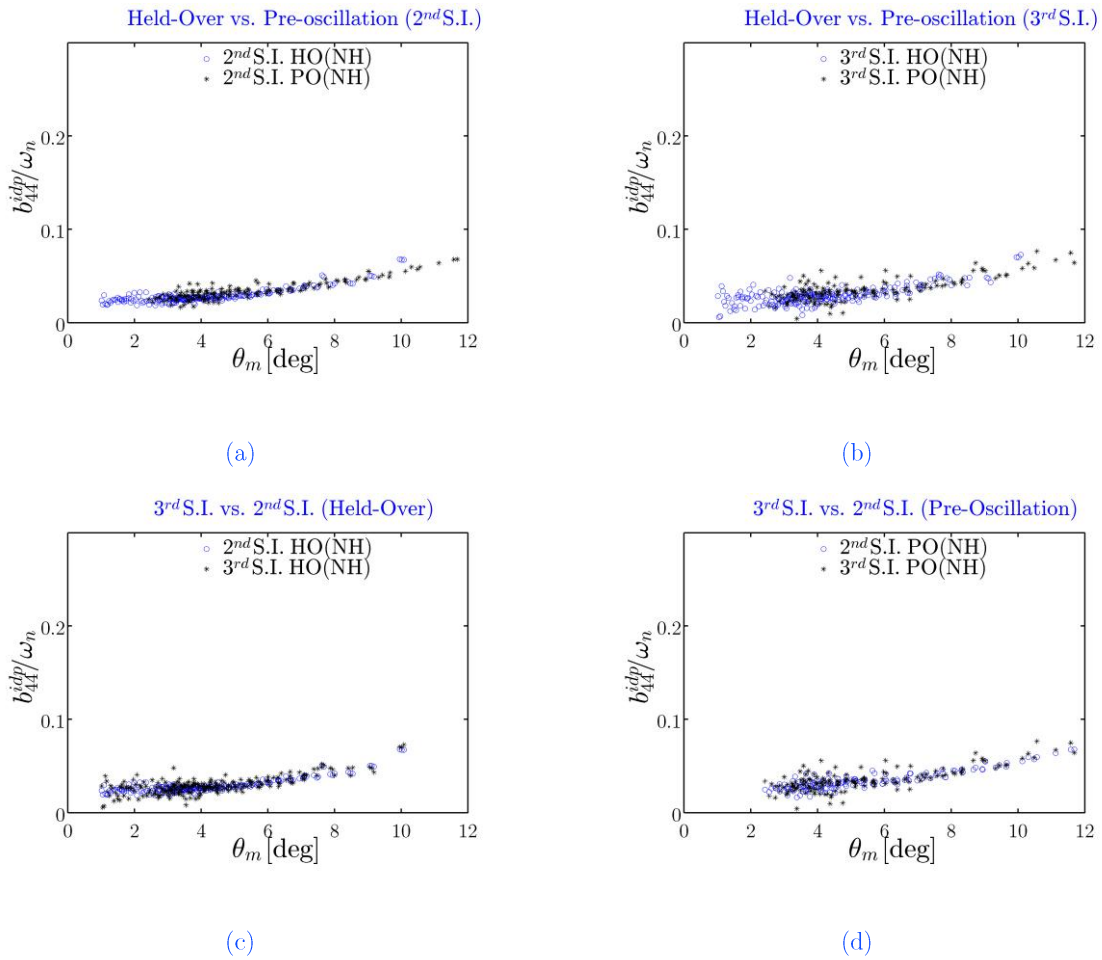

Figure 3.16– Comparison of non-dimensional equivalent roll damping of naked hull (NH) model for held-over and pre-oscillation tests applying 2nd and 3rd order approaches.

Figure 3.16(a,b) also compare damping between the held-over and pre-oscillation tests of the naked hull model obtained by both system identification. Surprisingly, the comparison showed good agreement between the different decay techniques independently of which system identification is used. Figure 3.16(c) compares 3rd and 2nd system identifications for the held-over technique and results showed good agreement for low nonlinearity. The same conclusion can be made from Figure 3.16(d) for the pre-oscillation technique.

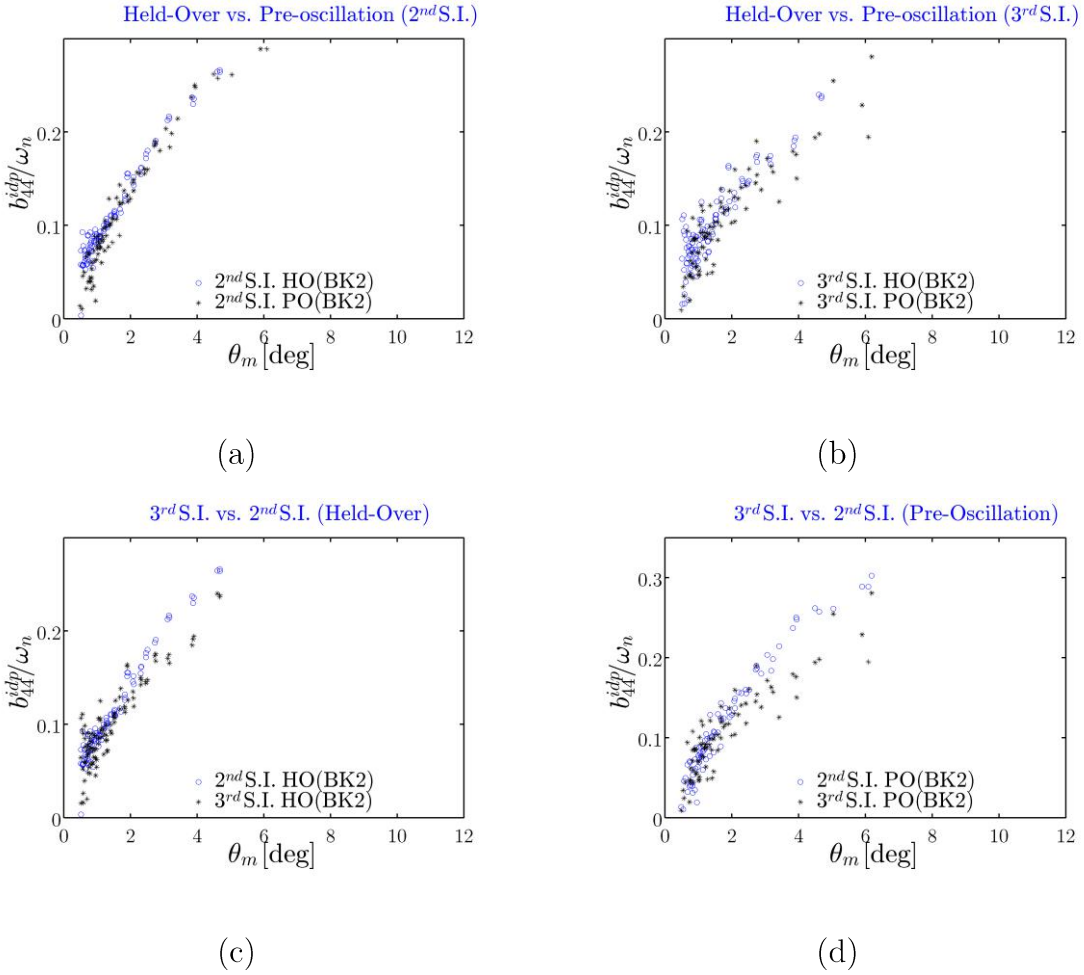

Figure 3.17– Comparison of non-dimensional equivalent roll damping of bilge-keel 1.8m (BK2) model for held-over and pre-oscillation tests applying 2nd and 3rd order approaches.

However, attaching the bilge-keel increases nonlinear damping and possible coupling terms effects on it. Figure 3.17(a) shows both techniques result in good agreement for the 2nd order approach, but in case of the 3rd order approach (Figure 3.17(b)) the results of held-over decay have smaller deviations where lower values of roll damping were observed in pre-oscillation technique, the lower values of roll damping in pre-oscillation technique may be interpreted as effects of sway and its coupling into roll

damping. The roll dampings obtained by 2nd and 3rd order approaches are compared in Figure 3.17(c, d) for both techniques, a significant difference can be observed from the approaches. By increasing the nonlinearity because of the bilge-keel, lower value of roll damping can be detected thanks to the 3rd order approach for larger mean angle. Based on the results obtained, it may be concluded that more realistic results are to be expected when taking into account the effects of the coupling terms. Figure 3.18 shows that a reduction in the quadratic terms of roll damping is observed with the linear-plus-quadratic approach for pre-oscillation tests.

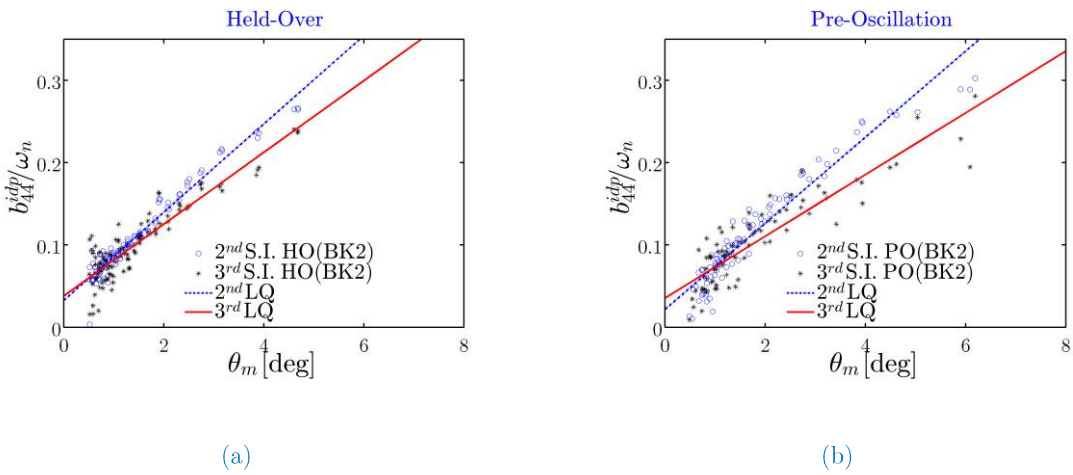

Figure 3.18– Comparison of non-dimensional linear-plus-quadratic damping of the model with BK2 for 2nd and 3rd order approaches; (a)held-over and (b)pre-oscillation.

The roll damping may divide the mean angle range into two intervals (q1 and q2) by a boundary angle θ_b where the regression lines have different slopes (see Figure 3.19).

$$b_{44}^{idp} = \begin{Bmatrix} b_1^{q1} + \frac{8\omega}{3} b_2^{q1}\theta_m, & if\,\theta_m \le \theta_b \\ b_1^{q2} + \frac{8\omega}{3} b_2^{q2}\theta_m, & if\,\theta_m > \theta_b \end{Bmatrix} \tag{3.15}$$

Furthermore, using a linear-plus-biquadratic (LBQ) form leads to a better nonlinear damping behaviour for larger angles as they are shown in Figure 3.19. should be noted that the results from pre-oscillation technique showed higher saturation, but in general, a significant different is observed in equivalent roll dampings for higher mean angles comparing with 2nd order method.

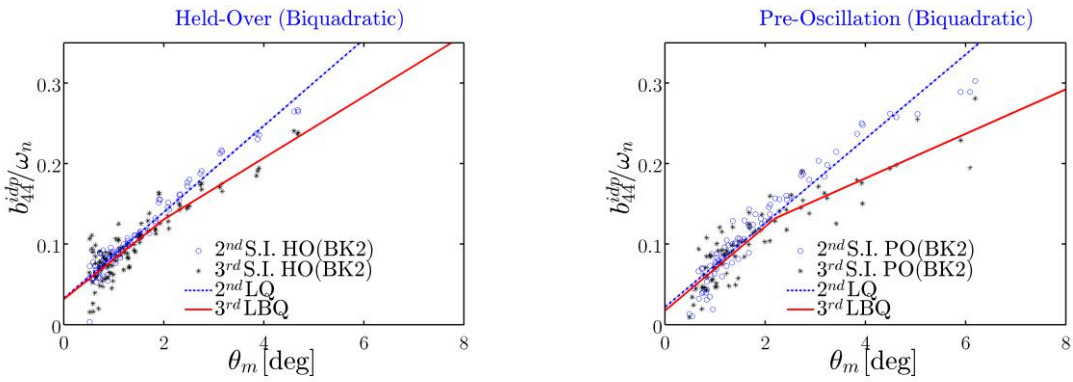

(a) (b)

Figure 3.19– Comparison of non-dimensional biquadratic damping of the model with BK2 for 3rd order approaches and quadratic damping 2nd order approach; (a)held-over and (b)pre-oscillation

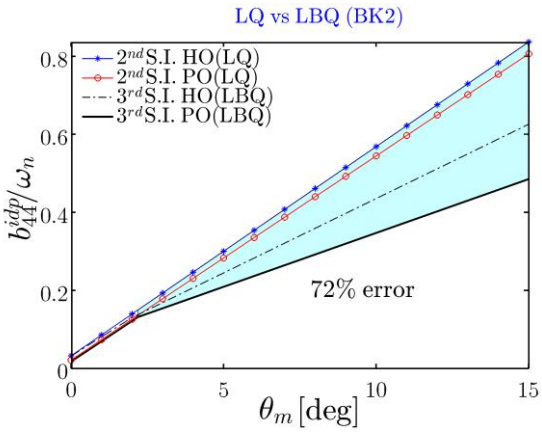

Figure 3.20– Direct comparison of the curves for biquadratic damping and linear-plus-quadratic damping for HO and PO.

Figure 3.20 may show how much the employing of the roll damping estimation approach can generate errors, where the roll angle is large. With traditional approaches, only the properties of roll damping can be obtained from the free roll decay test. Using the 3rd order SI approach, however, properties of the sway motion and its coupling with roll can also be well estimated (see (3.9)).

This is illustrated in Figure 3.21, which shows the estimated non-dimensional form of sway damping b_{22}^{idp} for tests on models with a naked hull (NH) and with a bilge keel (BK). b_{22}^{idp} showed linear behaviour for tests with a naked hull Figure 3.21(a), but increasing nonlinearity in tests with a bilge keel Figure 3.21(b).

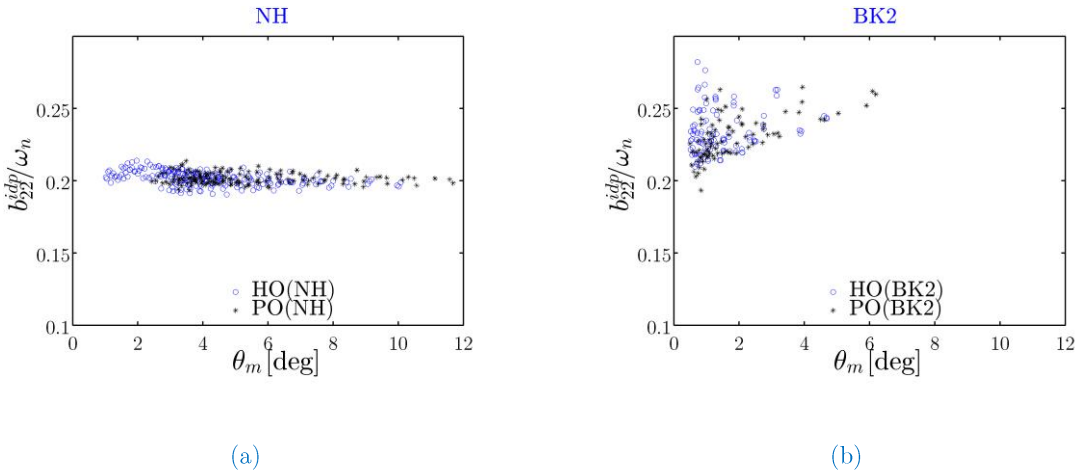

Figure 3.21– Estimation of b_{22}^{idp} via 3rd order approach for (a) NH and (b) BK2.

The product $b_{24}^{idp}b_{42}^{idp}$ may also be estimated using the 3rd order SI approach. Figure 3.22 illustrates the values of the product of damping coupling terms produced by applying this approach to models with a naked hull (NH) and with a bilge keel (BK2). The figure shows a clear trend of $b_{24}^{idp}b_{42}^{idp}$ deviating from constant values within a negligible region (i.e. near zero), especially for tests on a model with a bilge keel. It means that by increasing nonlinearity the effects of coupling term cannot be neglected anymore.

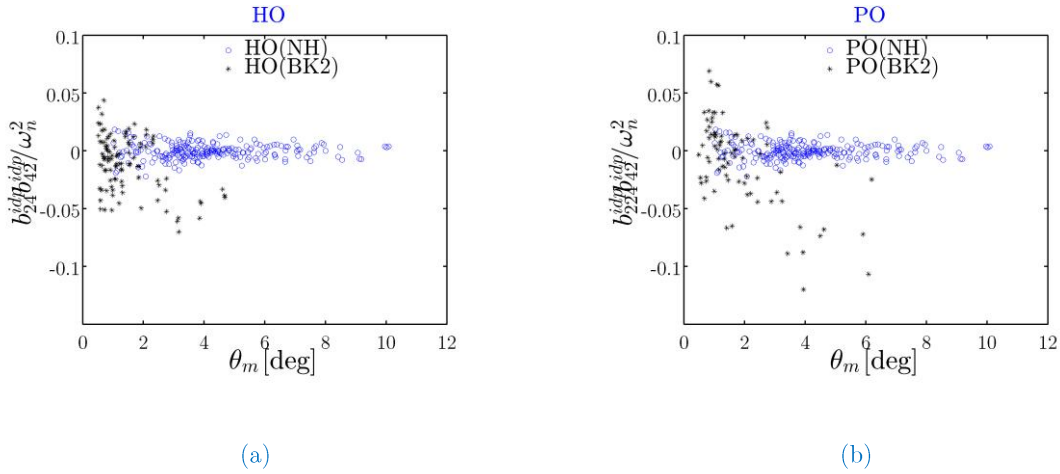

(a) (b)

Figure 3.22– Nondimensional form of coupled damping product term $b_{24}^{idp}b_{42}^{idp}/\omega^2$ for (a) NH and (b) BK2.

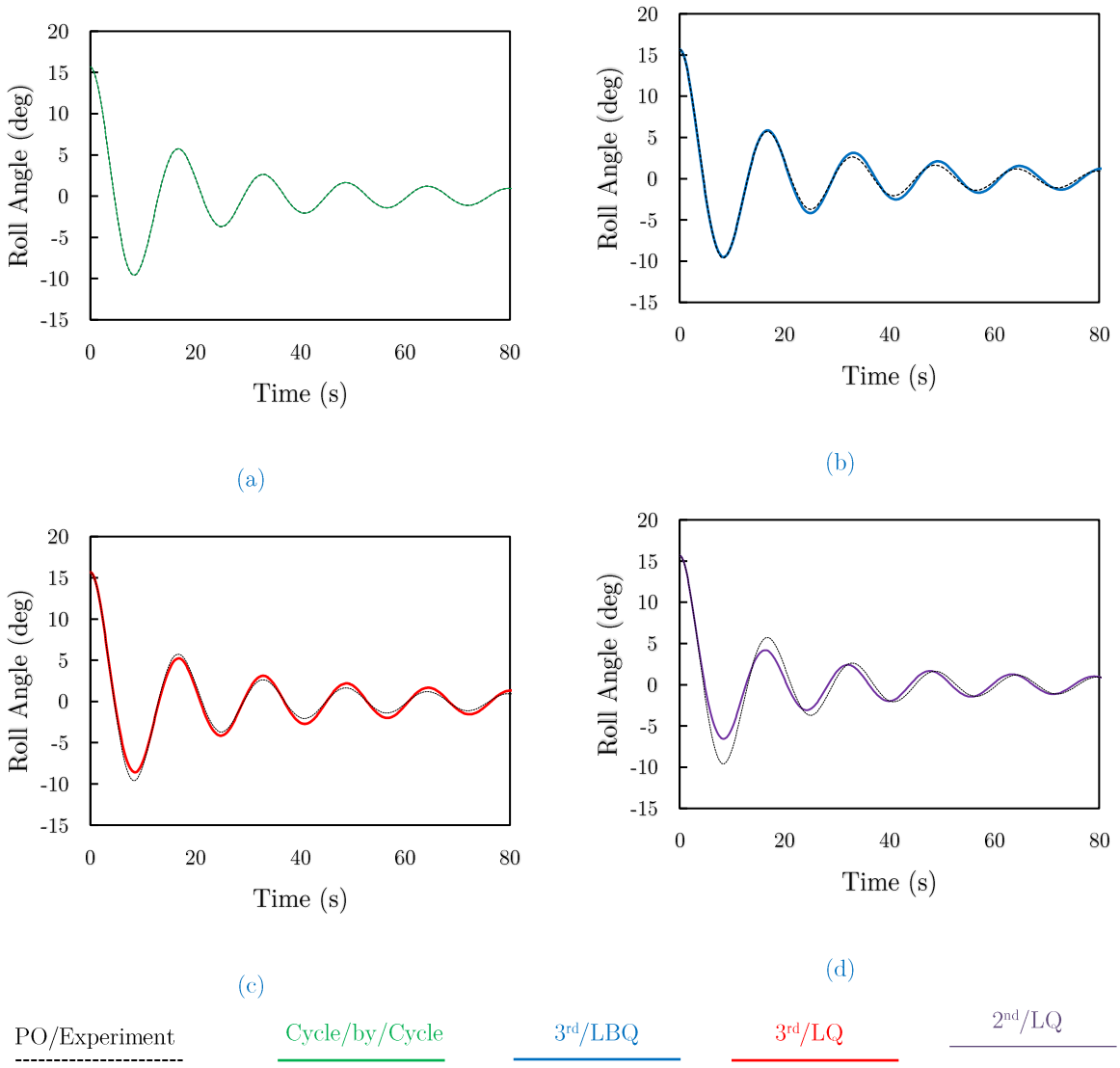

Figure 3.23– Roll time series for pre-oscillation product with different damping approaches.

Finally, time series of roll decay modelled with different methods are compared to each other and to experimental results in Figure 3.23. Figure 3.23(a) shows the time series generated by 3rd order approach with coefficients provided by the cycle-per-cycle analysis; Figure 3.23(b) shows the nonlinear roll damping represented in biquadratic

form; Figure 3.23(c) uses the traditional linear plus quadratic approach; finally, Figure 3.23(d) shows the time series for the traditional second-order system identification with a single degree of freedom. Note also that for high nonlinearity BK2, the roll restoring coefficient showed a higher nonlinear deviation.

The influence of coupling terms on the results has already been discussed numerically above; and results have shown in contrast with traditional methods that damping coupling terms are not negligible, especially when roll damping is nonlinear. The two 3rd order SIs shown in Table 3.5 have also been applied on experimental roll time series to obtain b_{44}^{idp}; the first included a damping coupling term $(b_{24}^{idp} b_{42}^{idp} \neq 0)$ while in the second the coupling term is neglected $(b_{24}^{idp} b_{42}^{idp} = 0)$. Figure 3.24 shows how neglecting coupling terms affects the estimation of b_{44}^{idp}. Comparing the results of both approaches for a model with a bilge keel (Figure 3.24 (b, d)), it can be seen that neglecting coupling terms causes overestimation of roll damping for large mean angles, similar to what is seen when applying a 2nd order SI. The main conclusion here is that the 3rd order SI approach seems to yield better, more robust results when nonlinearity is expected to be higher.

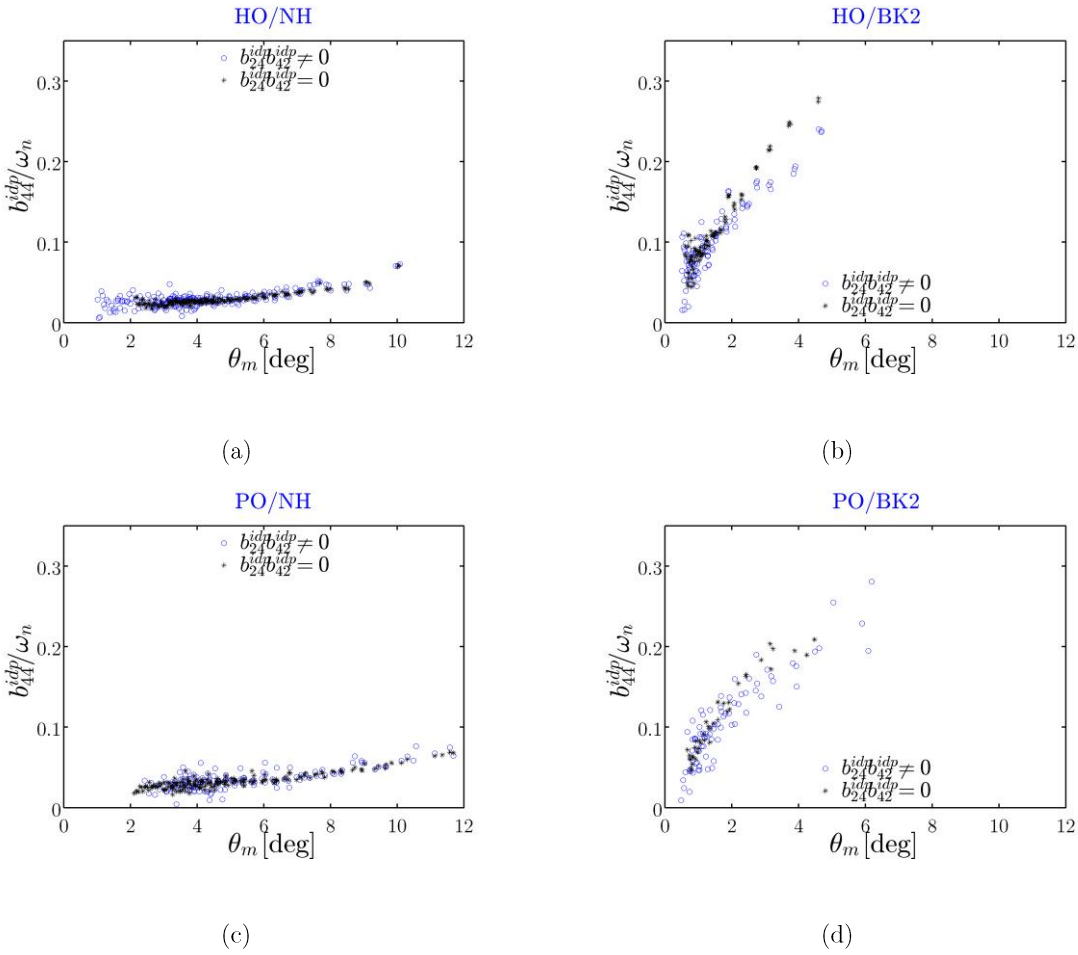

Figure 3.24– Equivalent roll dampings via 3rd order approach considering $b_{24}^{idp}b_{42}^{idp} \neq 0$, $b_{24}^{idp}b_{42}^{idp} = 0$.

In (2.36), the combination of damping terms is always grouped, that is, $b_{22}b_{44}^{idp} - b_{24}^{idp}b_{42}^{idp}$. This study therefore proposes that this grouped quantity be defined as a new term, the Coupled Damping Number – CDN, so that,

$$CDN = b_{22}b_{44}^{idp} - b_{24}^{idp}b_{42}^{idp} \tag{3.16}$$

One should immediately recognize that CDN = 0 (Fernandes, 1983) for the 2D case under analysis under a potential flow hypothesis, which is a result from the application of Green´s Theorem. In the presence of the viscosity the CDN's influence on the equation sway/roll has been investigated where two 3rd order system identifications were applied on experimental results. The first included the CDN, while the second system neglected it, as it shown in Table 3.6.

Table 3.6 – 3rd order system identifications in CDN aspect.

3rd S.I. $CDN \neq 0$:	$\dddot{\eta}_4 + \left\{b_{22} + b_{44}^{idp}\right\}\ddot{\eta}_4 + \left\{CDN\right\}\dot{\eta}_4 + \left\{c_{44}^{idp}\right\}\dot{\eta}_4 + \left\{b_{22}c_{44}^{idp}\right\}\eta_4 = 0$
3rd S.I. $CDN = 0$:	$\dddot{\eta}_4 + \left\{b_{22} + b_{44}^{idp}\right\}\ddot{\eta}_4 + \left\{c_{44}^{idp}\right\}\dot{\eta}_4 + \left\{b_{22}c_{44}^{idp}\right\}\eta_4 = 0$

shows that neglecting CDN does not have a large effect on roll damping estimation. This seems to be a remarkable indication that CDN is negligible even when viscous effects are present. It must be stressed that the possibility of neglecting the CDN does not mean that the effects of the coupling damping terms are negligible, but rather that the product of the main diagonal terms minus the product of the coupling terms could indeed be negligible (CDN≅0). This is probably the reason why the wrong assumption that the cross-damping term may be neglected has survived for so long!

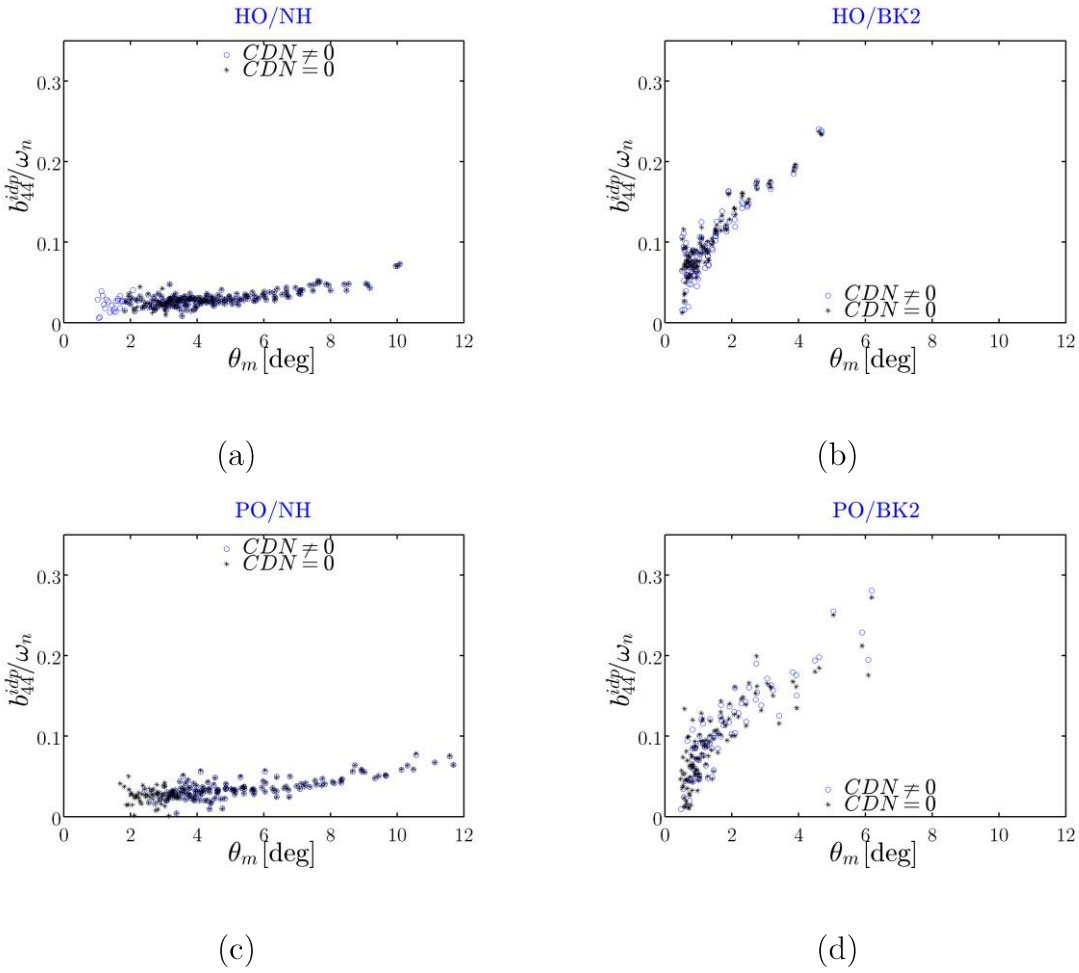

Figure 3.25– Comparison of estimated equivalent roll damping via system identification from Table 3.6 for HO and PO.

Chapter 3 points out conditions under which the conventional 2nd order equation considering only the roll degree of freedom may be used: based on (2.32), sway motion should be very small and, maybe most importantly, the pole should be the IDP (inertially decoupled point) for the 2nd order equation to work as a good approximation. This chapter has applied both numerical and experimental techniques. As a first step, it showed the importance of placing the pole at the IDP, which allows

a third order equation to be used for roll (2.36). The new approach using this third order equation has been validated and verified numerically. The 3rd order approach showed excellent results for the vast majority of nonlinearity ratios and initial angles in the numerical model, and is able to estimate not only roll properties, but also sway and sway/roll coupling properties.

The errors of this 3rd order SI compare favourably with those of the Froude and Faltinsen approaches. The results have shown that the 3rd order SI produces more efficient predictions of the linear-plus-quadratic damping coefficient when compared to Froude and Faltinsen approaches, especially when nonlinearity is high.

This study has shown that including damping coupling terms in 3rd order approach could improve the estimation of roll damping. Several free roll decay tests using the held-over (HO) and pre-oscillation (PO) techniques were carried out in the wave channel facility of the waves and currents laboratory (Laboratório de Ondas e Correntes - LOC) of the Federal University of Rio de Janeiro. The results obtained have shown good agreement of the new approach for different decay techniques. For experiments with a naked hull model, the 2nd order approach has shown similar results to the 3rd approach; however, in the presence of a bilge keel, the 2nd order approach produces higher roll damping values, while those estimated with the 3rd order approach are more realistic and less unsafe. It is worth mentioning that this approach has produced even better results for Held-Over tests (see Figure 3.24).

Finally, a new CDN (coupled damping number) term including all damping coefficients (3.16) is presented here. One of the most significant findings from 3.4.2 is that the CDN may be negligible even when viscous effects are present (non-potential). As mentioned above, it should be noted that neglecting the CDN does not mean that the

effects of the coupling damping term are negligible, but rather that the product of the main diagonal terms minus the product of the coupling terms could indeed be negligible (CDN≅0). This is probably the reason why the wrong assumption that the cross-damping term may be neglected has survived for so long!

Chapter 4 Free Roll Decay: Most Often Instantaneous Rotation Center – MOIRC

Previous chapter showed importance of the coupling terms to estimate the roll damping. This Chapter contributes to the understanding on how IRC behaves during free roll decay tests. Each IRC behaviour leads to a different damping value. This chapter initially describes and analyses free decay experiments to show the behaviour of the MOIRC for each cycle (and half cycle) and develops a linear analysis to observe the IRC behaviour. Finally, some interpretations of roll damping through MOIRC are presented to explain better influence of instantaneous rotation center on roll damping.

4.1 General

The Chapter 4 aims to clarify how IRC behaves during and its effect on damping estimation in free roll decay with different nonlinearity levels. The present paper could be considered the continuation of a previous chapter. The subsequent section presents and analyzes the results of the experiments. The surprising results include the level of damping for each half cycle and its relation with the IRC position motivated a linear theoretical analysis. The explanation of the data is confirmed in an innovative statistical analysis. The next session discusses the non-linear aspects. Finally, a

conclusion session at the end summarizes the achievements probably seen for the first time in the literature.

Different methods (Froude, 1955), (Roberts, 1985b), (de Oliveira, 2014), etc, have been proposed to assess roll damping as they were mentioned in 1.2, but the one used in this chapter is systematized by (Faltinsen, 1993) explained in 3.1.2 as 2nd order approach, by using a system identification technique and complete integration in each cycle (3rd order S.I.) explained in 3.2.4 as 3rd order approach.

4.2 Experimental Study

Chapter 3 aims to study the behaviour of the IRCs via held-over technique. The procedure of this technique and set-up are as same as 3.4.1.

4.2.1 Damping Results

Figure 4.1 compares the roll damping obtained from Faltinsen approach (2nd order approach) and 3rd order approach this time for two different bilge-keel lengths, where linear equivalent roll dampings are obtained using the full cycles. As conclusion of previous chapter, the most important, since unsafe, result of Figure 4.1 is that in the presence of nonlinearity the Faltinsen approach (generally 2nd order approach where the roll is studied in one degree of freedom) overestimates the damping for larger mean angles.

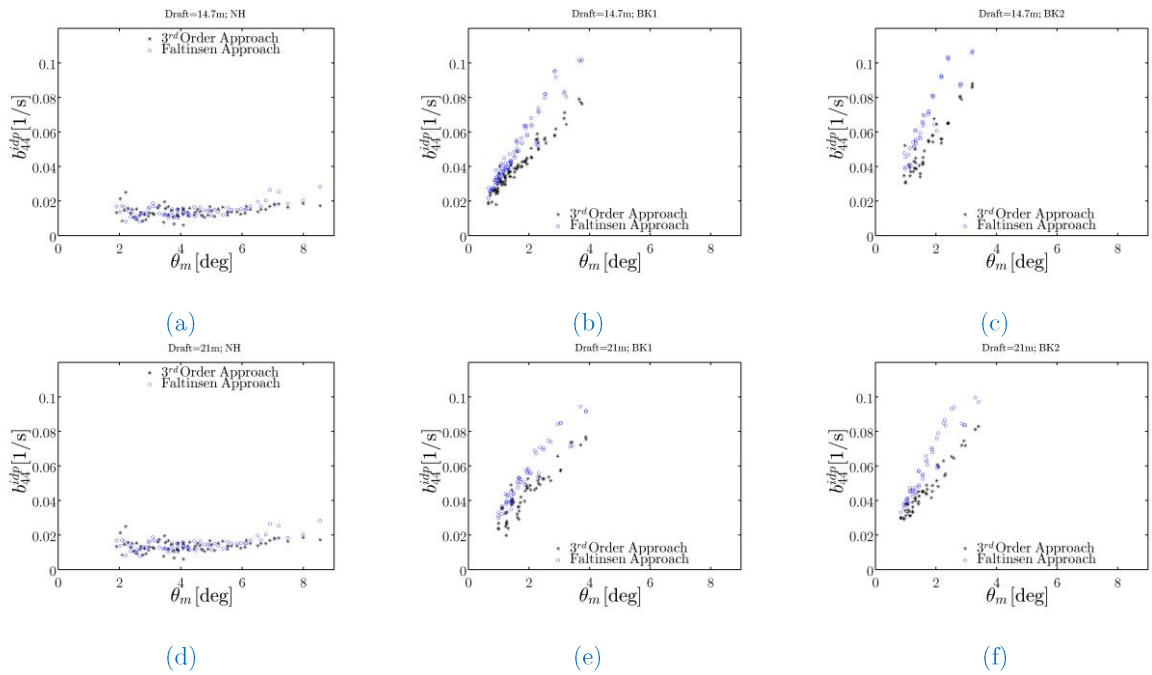

Figure 4.1– Comparison of linear equivalent roll damping obtained by 3rd order approach and Faltinsen (2nd order) approach; linear equivalent damping is obtained from full cycles.

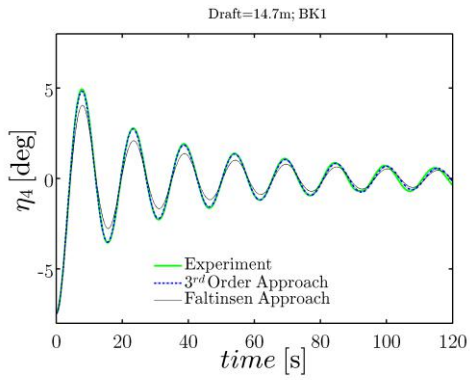

Figure 4.2– Comparison of roll decay time-history with 3rd order approach and Faltinsen (2nd order) approach; BK1; Draft 14.7m.

Figure 4.2 illustrates the time-history of roll for a model test with attached BK1 and compares with obtained roll time series of 2nd (Faltinsen) and 3rd order approaches using the quadratic damping model. The results from the 3rd order approach show good

agreement with the experimental. Note that the obtained coefficients are unique properties of the floating body for a given well defined pole such as the C_{idp} .

4.2.2 Instantaneous Rotation Center - IRC

Based on rigid body kinematics, the instantaneous rotation center – IRC (also called the instantaneous center of rotation) is the point in an extension of the body that has zero velocity at an instant of time. At this instant, the velocity vectors of the trajectories of the other points in the body generate an instantaneous circular field around this point.

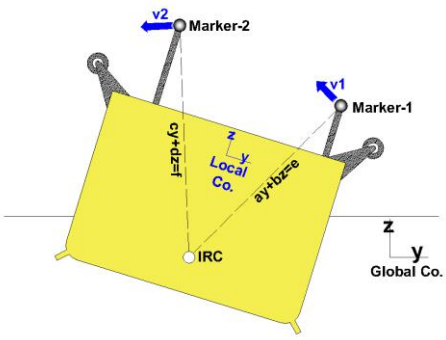

Figure 4.3– Methodology to obtain the Instantaneous Rotation Center – IRC by crossing two perpendiculars the simultaneous velocities of two markers of the body.

With Figure 4.3 in mind the velocities of the two markers can be recorded by the QTM optical system measurement during the decay test and their velocities v_1 and v_2 are transformed from global coordinate system into local fixed-body coordinate system with origin located at the center of gravity. Knowing the velocity vectors v_1 and v_2 in fixed-body (see Figure 4.3) coordinates, the perpendiculars of the velocity vectors can be expressed by (4.1) and (4.2), the intersection of two perpendiculars

yields the IRC at each instant. The position of the IRC in a fixed-body coordination system (y, z) can be obtained using (4.3).

$$ay + bz = e \tag{4.1}$$

$$cy + dz = f \tag{4.2}$$

$$\begin{bmatrix} Y_{irc}^{pole} \\ \mathbb{Z}_{irc}^{pole} \end{bmatrix} = \frac{1}{\det\begin{vmatrix} a & b \\ c & d \end{vmatrix}} \times \begin{bmatrix} d & -b \\ -c & a \end{bmatrix} \times \begin{bmatrix} e \\ f \end{bmatrix} \tag{4.3}$$

Figure 4.4 shows the variation of the vertical position of IRCs in relation to the center of gravity $\mathbb{Z}_{irc}^{pole}$ for different cases. For a NH Figure 4.4(a, d), the IRCs varies around a constant position most of the time; its locus has the behaviour of a tangent function coming from negative infinite and going to positive infinite in each half cycle. Note that the infinite cases correspond to pure translation, that is, they have a clear physical interpretation. With the introduction of the bilge keels there is an increase of roll damping (cases BK1 and BK2) and the variation of IRCs starts to change. Two regions can be observed, the first region still looks as a tangent in the first cycles but soon a second region starts where the IRC now has a double (one with upper concavity and other with lower concavity in a cycle) parabolic form and changes direction for each half cycle.

Now the minimum and maximum points of the approximate parabolas correspond to the MOIRCs at each cycle. Indeed, the IRC is around a specific point for low damping cases (NH), but, in contrast, by increasing damping with the use of bilge keels, (BK1 and BK2) the IRC is more scattered and changes its positions (maximum and minimum) for each half-cycle. See Figure 4.4 and the histograms in Figure 4.5.

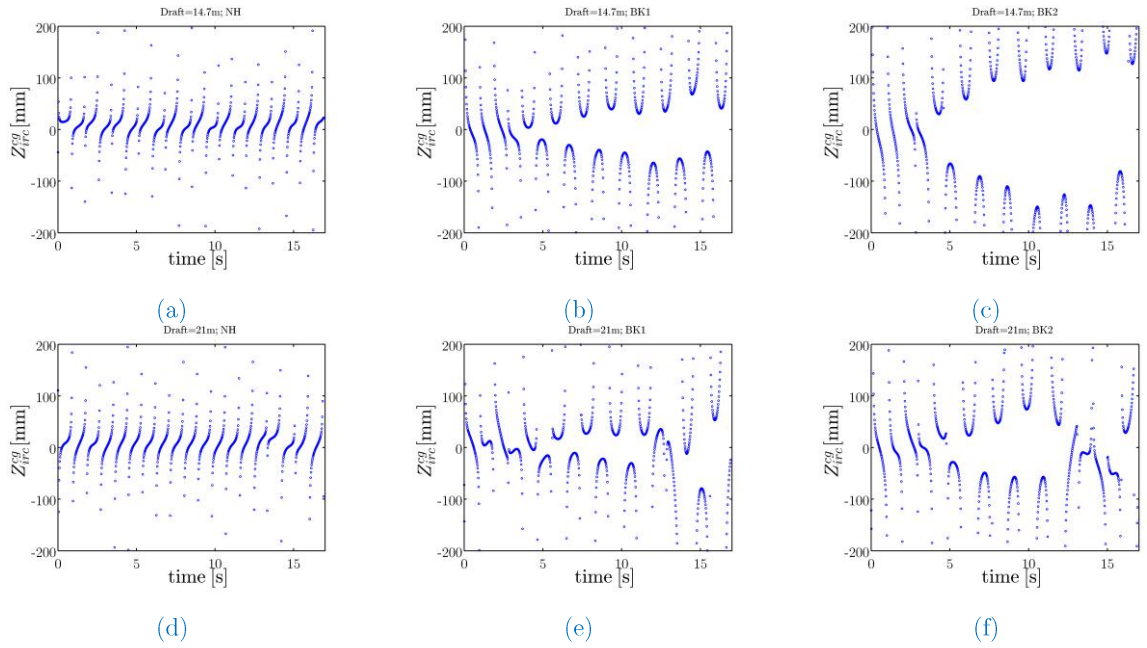

Figure 4.4– Variation of the vertical position of IRCs with time referring to the center of gravity

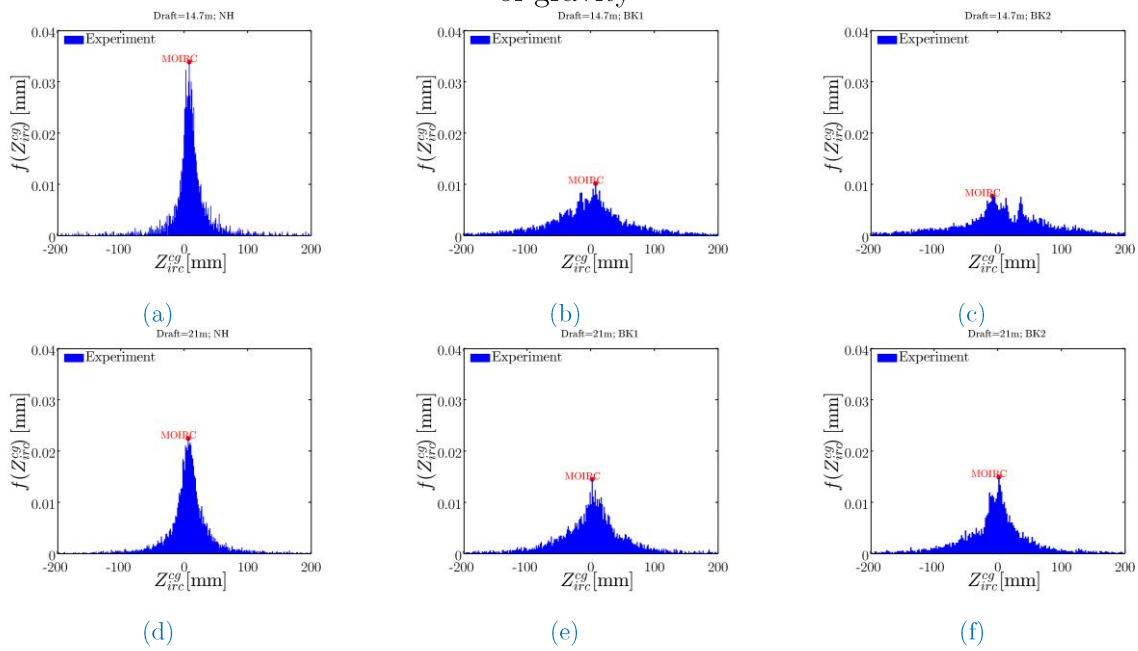

Figure 4.5– Experimental histogram for the vertical position of IRCs with time referring to the center of gravity.

The histograms presented in Figure 4.5 point to the practical probabilities of vertical position of the IRCs during the free roll decay corresponding to the time histories from

Figure 4.4. From the distribution functions in Figure 4.5(a, d), it is apparent that the IRCs stay most of the time near specific positions confirming the observation in the previous paragraph about the MOIRC in the tangent type of behaviour. However, by increasing the roll damping with the bilge keels, the distribution functions (See Figure 4.5(b, c, e and f)) have a more wide-band form and the MOIRCs are minimum or maximum of the parabolic forms.

As explained in the Introduction, previous studies showed that the roll damping is sensitive to the position of the fixed rotation center. Paying attention in Figure 4.4, it can be observed that the behaviour of the MOIRC changes in every half cycle. Therefore, for a full cycle the position of the MOIRC changes twice, which suggests that there are two different trends of roll damping. This is shown in Figure 4.1, that provides linear equivalent roll damping for each half cycle.

In decay experiments, the model goes counterclockwise in a given half cycle soon after releasing from initial angle and clockwise to complete a full cycle. Figure 4.6(a) illustrates this clearly. When the model goes counterclockwise, the MOIRCs have lower positions, but when the model goes clockwise in the second half cycle, the MOIRC value assumes an upper position (note that the graph starts from half-cycle(2) where the first cycle is omitted). Figure 4.6(b) shows the linear equivalent roll damping obtained by 3rd order approach applied for each half-cycle (counter-clockwise half-cycles and clockwise half-cycles). Comparing with Figure 4.6 (a) one can find that for lower MOIRCs in counter-clockwise half-cycles the linear equivalent roll dampings have lower values and for upper MOIRCs in the clockwise half-cycles the equivalent dampings are larger. This concurs with earlier observations of researchers such as (Haddara, 1990) (Bass, 1991) (Park, 2000) and (Chun, 2001). The position of MOIRCs

can affect the relative velocity of bilge keels, therefore, flow separations and, consequently, dissipated energies will be different for MOIRCs in clockwise and counterclockwise half cycles.

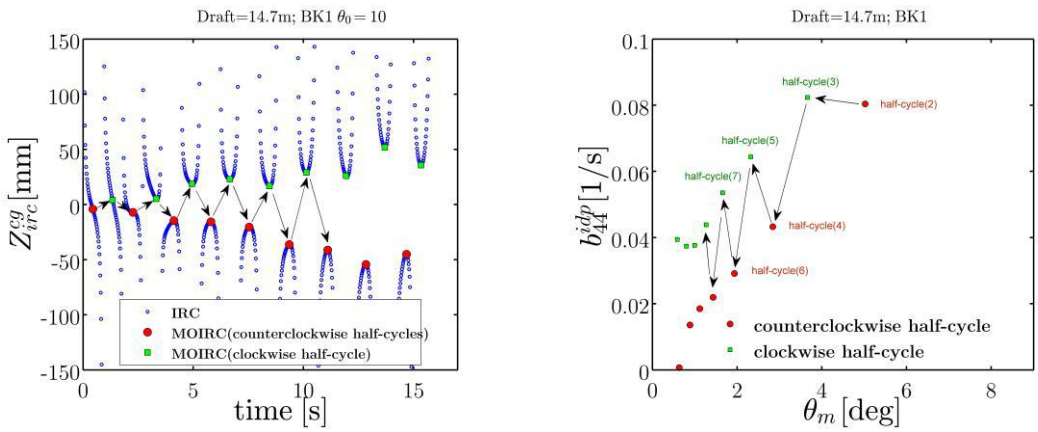

(a) (b)

Figure 4.6– (a) Variation of the vertical position of IRCs with time referring to the center of gravity, red and green points show MOIRC for each half-cycle; (b) linear equivalent roll damping obtained by 3rd order approach applying on each half-cycle.

As shown in Figure 4.6(b) the obtained linear equivalent damping varies for each half-cycle, thus the estimated roll damping for a full cycle may not accurately represent the true phenomena. Figure 4.7 compares linear equivalent roll dampings provided by 3rd order approach applied on each full-cycle and then on each half-cycle. From this data, again it can be seen that the 3rd order approach for a half-cycle resulted in lower values of roll damping regarding to counterclockwise half-cycles. This is very important for operation safety considerations (for instance see Figure 4.7(b)).

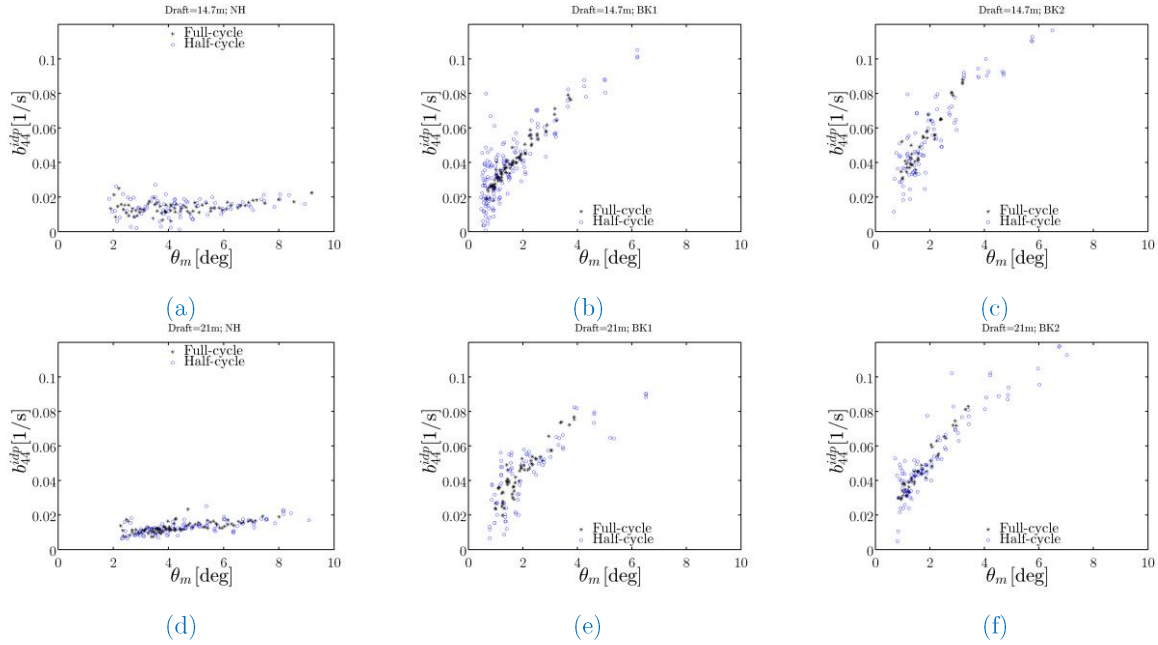

Figure 4.7– Comparison of linear equivalent roll dampings obtained by 3rd order approach for full-cycles and half-cycles

This finding suggests that to improve the safety of FPSOs operations, the lower boundary of linear equivalent roll damping (dotted line in Figure 4.8) should be considered.

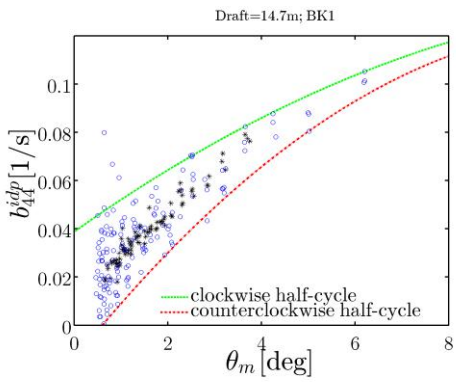

Figure 4.8– Lower and higher levels boundary lines for linear equivalent roll dampings from a decay test; The blue circles are damping obtained from half-cycles and black asterisks are the damping obtained from fullcycles.

It is noteworthy that all these somewhat clear observations were obtained experimentally. What seems to be new is the correlation of the position of the MORIC and the value of the equivalent damping for the cases with bilge keels. What is needed now is a theoretical analysis, which is performed next.

4.3 Analytical Study

To achieve the general solution for sway/roll equation of motion, the characteristic equation of (3.6) can be rewritten in general form as (4.4) for an arbitrary pole.

$$U_3\lambda^3 + U_2\lambda^2 + U_1\lambda + U_0 = 0 \tag{4.4}$$

Where,

$$U_3 = 1 - m_{24}^{pole} m_{42}^{pole}$$
$$U_2 = b_{44}^{pole} + b_{22}^{pole} - m_{24}^{pole} b_{24}^{pole} - m_{42}^{pole} b_{42}^{pole}$$
$$U_1 = c_{44} + b_{22}^{pole} b_{44}^{pole} - b_{24}^{pole} b_{42}^{pole}$$
$$U_0 = b_{22}^{pole} c_{44}$$

The particular-solution of form $\eta_2^{pole} = ke^{\lambda t}$ and $\eta_4^{pole} = rke^{\lambda t}$ can be shown as below:

$$(k_0, 0)$$
$$(k_s e^{\beta_s t}, r_s k_s e^{\beta_s t})$$
$$((k_{\mathrm{Re}} - ik_{\mathrm{Im}})e^{(\beta_r + i\omega)t}, r_r^+ (k_{\mathrm{Re}} - ik_{\mathrm{Im}})e^{(\beta_r + i\omega)t})$$
$$((k_{\mathrm{Re}} + ik_{\mathrm{Im}})e^{(\beta_r - i\omega)t}, r_r^- (k_{\mathrm{Re}} + ik_{\mathrm{Im}})e^{(\beta_r - i\omega)t})$$

where,

$$
\begin{aligned}
r_s &= \frac{-(\beta_s + b_{22})}{(\beta_s m_{24} + b_{24})} \\
r_r^+ &= \frac{-(\beta_r + i\omega + b_{22})}{(m_{24}\beta_r + i\omega m_{24} + b_{24})} \\
r_r^- &= \frac{-(\beta_r - i\omega + b_{22})}{(m_{24}\beta_r - i\omega m_{24} + b_{24})}
\end{aligned}
\tag{4.5}
$$

The general solution would be expressed as (4.6) to (4.9).

$$\eta_2^{pole}(t) = k_0 + k_s e^{\beta_s t} + \left(k_{\mathrm{Re}} - ik_{\mathrm{Im}}\right)e^{(\beta_r + i\omega)t} + \left(k_{\mathrm{Re}} + ik_{\mathrm{Im}}\right)e^{(\beta_r - i\omega)t} \tag{4.6}$$

$$\eta_4^{pole}(t) = r_s k_s e^{\beta_s t} + r_r^+\left(k_{\mathrm{Re}} - ik_{\mathrm{Im}}\right)e^{(\beta_r + i\omega)t} + r_r^-\left(k_{\mathrm{Re}} + ik_{\mathrm{Im}}\right)e^{(\beta_r - i\omega)t} \tag{4.7}$$

$$\dot{\eta}_2^{pole}(t) = \beta_s k_s e^{\beta_s t} + (\beta_r + i\omega)\left(k_{\mathrm{Re}} - ik_{\mathrm{Im}}\right)e^{(\beta_r + i\omega)t} + (\beta_r - i\omega)\left(k_{\mathrm{Re}} + ik_{\mathrm{Im}}\right)e^{(\beta_r - i\omega)t} \tag{4.8}$$

$$\dot{\eta}_4^{pole}(t) = \beta_s r_s k_s e^{\beta_s t} + (\beta_r + i\omega)r_r^+\left(k_{\mathrm{Re}} - ik_{\mathrm{Im}}\right)e^{(\beta_r + i\omega)t} + (\beta_r - i\omega)r_r^-\left(k_{\mathrm{Re}} + ik_{\mathrm{Im}}\right)e^{(\beta_r - i\omega)t} \tag{4.9}$$

The coefficients k_s, k_{Re} and k_{Im} can be obtained by taking account of the initial conditions. Since the held-over technique is employed to perform the free roll decay, the only initial condition is an imposed initial roll displacement ($\eta_4^p(0) = \theta_0$) on the floating body while the other initial conditions such as sway displacement, initial roll and sway velocity are equal to zero.

4.3.1 Vertical Position of Instantaneous Rotation Center

(Fernandes, 2016) et al studied the behaviour of the instantaneous rotation center (IRC) position (vertical and horizontal), Their results show that the IRC is frequency-dependent (the more detail can be found in Chapter 5). According to (Fernandes, 2016), the analytical form of the vertical position of IRCs with respect to the vertical

position of the pole for free roll decay with natural roll frequency of ω can be rewritten as:

$$\mathbb{Z}_{irc}^{pole}(t,\omega)=\frac{\dot{\eta}_2^{pole}(t,\omega)}{\dot{\eta}_4^{pole}(t,\omega)} \tag{4.10}$$

Considering general solution (4.8) and (4.9) and relation of $\mathbb{Z}_{irc}^{p}$, following expression can be obtained:

$$\mathbb{Z}_{irc}^{pole}(t,\omega)=\frac{\beta_s k_s e^{\beta_s t}+(\beta_r+i\omega)\left(k_{\mathrm{Re}}-ik_{\mathrm{Im}}\right)e^{(\beta_r+i\omega)t}+(\beta_r-i\omega)\left(k_{\mathrm{Re}}+ik_{\mathrm{Im}}\right)e^{(\beta_r-i\omega)t}}{\beta_s r_s k_s e^{\beta_s t}+(\beta_r+i\omega)r_r^{+}\left(k_{\mathrm{Re}}-ik_{\mathrm{Im}}\right)e^{(\beta_r+i\omega)t}+(\beta_r-i\omega)r_r^{-}\left(k_{\mathrm{Re}}+ik_{\mathrm{Im}}\right)e^{(\beta_r-i\omega)t}} \tag{4.11}$$

Exponential functions $e^{(\beta_r+i\omega)t}$ and $e^{(\beta_r-i\omega)t}$ in (4.11) can be written as a combination of *sin* and *cos*.

$$e^{(\beta_r+i\omega)t}=e^{\beta_r t}\left(\cos(\omega t)+i\sin(\omega t)\right) \tag{4.12}$$

$$e^{(\beta_r-i\omega)t}=e^{\beta_r t}\left(\cos(\omega t)-i\sin(\omega t)\right) \tag{4.13}$$

Substituting (4.12) and (4.13) into (4.11),

$$\mathbb{Z}_{irc}^{pole}(t,\omega)=\frac{\beta_s k_s e^{\beta_s t}+l_1+l_2}{\beta_s r_s k_s e^{\beta_s t}+q_1+q_2} \tag{4.14}$$

For,

$$l_1=\left(2\beta_r k_{\mathrm{Re}}+2\omega k_{\mathrm{Im}}\right)\cos(\omega t);$$
$$l_2=-\left(2\omega k_{\mathrm{Re}}-2k_{\mathrm{Im}}\beta_r\right)\sin(\omega t);$$
$$q_1=\left(\left(i\omega k_{\mathrm{Re}}-ik_{\mathrm{Im}}\beta_r\right)\left(r_r^{+}-r_r^{-}\right)+\left(\omega k_{\mathrm{Im}}+\beta_r k_{\mathrm{Re}}\right)\left(r_r^{+}+r_r^{-}\right)\right)\cos(\omega t)$$
$$q_2=\left(\left(i\beta_r k_{\mathrm{Re}}+i\omega k_{\mathrm{Im}}\right)\left(r_r^{+}-r_r^{-}\right)+\left(k_{\mathrm{Im}}\beta_r-\omega k_{\mathrm{Re}}\right)\left(r_r^{+}+r_r^{-}\right)\right)\sin(\omega t)$$

assume $\Re_1 = \left(r_r^+ - r_r^-\right)$ and $\Re_2 = \left(r_r^+ - r_r^-\right)$, then the equation of ZIRC can be written as.

$$\mathbb{Z}_{irc}^{pole}(t,\omega) = \frac{\beta_s k_s e^{(\beta_s-\beta_r)t} + 2\left(k_{\mathrm{Re}}\beta_r + k_{\mathrm{Im}}\omega\right)\cos(\omega t) - 2\left(k_{\mathrm{Re}}\omega - k_{\mathrm{Im}}\beta_r\right)\sin(\omega t)}{\beta_s r_s k_s e^{(\beta_s-\beta_r)t} + \left(\Re_1 k_{\mathrm{Im}}\beta_r - \Re_2 k_{\mathrm{Re}}\beta_r - \Re_1 k_{\mathrm{Re}}\omega - \Re_2 k_{\mathrm{Im}}\omega\right)\cos(\omega t) - \left(\Re_1 k_{\mathrm{Im}}\omega - \Re_2 k_{\mathrm{Re}}\omega + \Re_1 k_{\mathrm{Re}}\beta_r + \Re_2 k_{\mathrm{Im}}\beta_r\right)\sin(\omega t)}$$

or (4.15)

$$\mathbb{Z}_{irc}^{pole}(t,\omega) = \frac{\beta_s k_s e^{(\beta_s-\beta_r)t} - 2\left(k_{\mathrm{Re}}\beta_r + k_{\mathrm{Im}}\omega\right)\sin(\omega t - \frac{\pi}{2}) - 2\left(k_{\mathrm{Re}}\omega - k_{\mathrm{Im}}\beta_r\right)\cos(\omega t - \frac{\pi}{2})}{\beta_s r_s k_s e^{(\beta_s-\beta_r)t} - \left(\Re_1 k_{\mathrm{Im}}\beta_r - \Re_2 k_{\mathrm{Re}}\beta_r - \Re_1 k_{\mathrm{Re}}\omega - \Re_2 k_{\mathrm{Im}}\omega\right)\sin(\omega t - \frac{\pi}{2}) - \left(\Re_1 k_{\mathrm{Im}}\omega - \Re_2 k_{\mathrm{Re}}\omega + \Re_1 k_{\mathrm{Re}}\beta_r + \Re_2 k_{\mathrm{Im}}\beta_r\right)\cos(\omega t - \frac{\pi}{2})}$$

$\Re_1$ and $\Re_2$ also can be expressed as function of hydrodynamic properties.

$$\Re_1 = \frac{2\left(\omega m_{24}^{pole} b_{22}^{pole} - \omega b_{24}^{pole}\right)}{(m_{24}^{pole}\beta_r + b_{24}^{pole})^2 + (\omega m_{24}^{pole})^2} \tag{4.16}$$

$$\Re_2 = \frac{2\left(b_{24}^{pole} b_{22}^{pole} + b_{22}^{pole} m_{24}^{pole}\beta_r + m_{24}^{p}\omega^2 + \beta_r b_{24} + m_{24}^{pole}\beta_r^2\right)}{(m_{24}^{pole}\beta_r + b_{24}^{pole})^2 + (\omega m_{24}^{pole})^2} \tag{4.17}$$

The term $\beta_s - \beta_r$ plays an important role in (4.15). The behaviour of the IRC can vary depending on $\beta_s - \beta_r$. It is well known that for a typical free roll decay of a floating body both β_r and β_s have negative values, hence we have two categories:

- $|\beta_r| < |\beta_s|$: roll damping factor smaller than sway damping factor; this happens for floating bodies without anti-roll systems and eventually floating bodies with low extra roll damping (such as with a small conventional bilge keel).
- $|\beta_r| \geq |\beta_s|$: roll damping factor larger than sway damping factor; this happens for floating bodies with higher extra roll damping (such as unconventional large bilge keel).

4.3.1.1 Roll damping factor $|\beta_r|$ smaller than sway damping factor $|\beta_s|$

Under the assumption of $|\beta_r| < |\beta_s|$, the term $\beta_s - \beta_r$ would have a negative value. Hence, in (4.15) term $e^{(\beta_s - \beta_r)t}$ eventually goes to zero with time. As an example, Figure 4.9 shows the variation of $\mathbb{Z}_{irc}^{cg}(t)$ with time with respect to the center of gravity. A transient region (shown as Region-I) is observed in the system before being stationary (see (4.15)). In Region-II the effect of the exponential terms is negligible, and the periodic terms prevail, that is, there is a stationary behaviour.

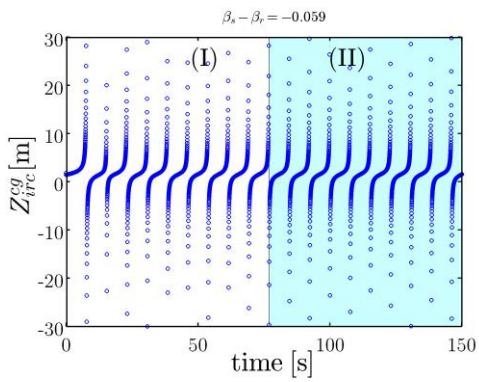

Figure 4.9 – Variation of ZIRCs in time with respect to the center of gravity, where $|\beta_r| < |\beta_s|$; Draft=14.7m; $b_{44}^{cg} = 0.0564$ and $b_{22}^{cg} = 0.0861$; (I) Transient region and (II) Stationary region.

As soon as the system can be considered stationary the form of a tangent function shows up, that is, we have (4.18). This will be shown next:

$$\mathbb{Z}_{irc}^{p}(t,\omega) = z_0 + \gamma \tan(\omega t - \frac{\pi}{2}) \tag{4.18}$$

According to (4.14), using the periodicity and the existence of a necessary inflection point, the analytical forms of z_0 and γ can be shown as (4.19) and (4.20).

$$z_0(n)=\frac{\beta_s k_s e^{(\beta_s-\beta_r)\frac{(2n+1)\pi}{2\omega}}-2\left(k_{\mathrm{Re}}\omega-k_{\mathrm{Im}}\beta_r\right)\cos(n\pi)}{\beta_s r_s k_s e^{(\beta_s-\beta_r)\frac{(2n+1)\pi}{2\omega}}-\left(\Re_1 k_{\mathrm{Im}}\omega-\Re_2 k_{\mathrm{Re}}\omega+\Re_1 k_{\mathrm{Re}}\beta_r+\Re_2 k_{\mathrm{Im}}\beta_r\right)\cos(n\pi)} \tag{4.19}$$

$$\gamma(n)=z_0(n)-\frac{\beta_s k_s e^{(\beta_s-\beta_r)\frac{\pi(1+4n)}{4\omega}}-2\left(k_{\mathrm{Re}}\beta_r+k_{\mathrm{Im}}\omega\right)\sin\left(\frac{\pi}{4}(4n-1)\right)-2\left(k_{\mathrm{Re}}\omega-k_{\mathrm{Im}}\beta_r\right)\cos\left(\frac{\pi}{4}(4n-1)\right)}{\beta_s r_s k_s e^{(\beta_s-\beta_r)\frac{\pi(1+4n)}{4\omega}}-\left(\Re_1 k_{\mathrm{Im}}\beta_r-\Re_2 k_{\mathrm{Re}}\beta_r-\Re_1 k_{\mathrm{Re}}\omega-\Re_2 k_{\mathrm{Im}}\omega\right)\sin\left(\frac{\pi}{4}(4n-1)\right)-\left(\Re_1 k_{\mathrm{Im}}\omega-\Re_2 k_{\mathrm{Re}}\omega+\Re_1 k_{\mathrm{Re}}\beta_r+\Re_2 k_{\mathrm{Im}}\beta_r\right)\cos\left(\frac{\pi}{4}(4n-1)\right)} \tag{4.20}$$

Knowing that, the terms $e^{(\beta_s-\beta_r)t}$ tend to zero in time, (4.15) for the stationary region can be rewritten as (4.21) or (4.22).

$$\mathbb{Z}_{irc}^{p}(t,\omega)=\frac{2\left(k_{\mathrm{Re}}\beta_r+k_{\mathrm{Im}}\omega\right)\sin(\omega t-\frac{\pi}{2})+2\left(k_{\mathrm{Re}}\omega-k_{\mathrm{Im}}\beta_r\right)\cos(\omega t-\frac{\pi}{2})}{\left(\Re_1 k_{\mathrm{Im}}\beta_r-\Re_2 k_{\mathrm{Re}}\beta_r-\Re_1 k_{\mathrm{Re}}\omega-\Re_2 k_{\mathrm{Im}}\omega\right)\sin(\omega t-\frac{\pi}{2})+\left(\Re_1 k_{\mathrm{Im}}\omega-\Re_2 k_{\mathrm{Re}}\omega+\Re_1 k_{\mathrm{Re}}\beta_r+\Re_2 k_{\mathrm{Im}}\beta_r\right)\cos(\omega t-\frac{\pi}{2})} \tag{4.21}$$

$$\mathbb{Z}_{irc}^{p}(t,\omega)=\frac{A_1\sin(\omega t-\frac{\pi}{2})+B_1\cos(\omega t-\frac{\pi}{2})}{A_2\sin(\omega t-\frac{\pi}{2})+B_2\cos(\omega t-\frac{\pi}{2})} \tag{4.22}$$

Where A_1, B_1, A_2 and B_2 are obtained by identification. (4.22) can be used to investigate the extreme of each half cycle, when $\omega t=n\pi$; for each half-cycle, the extremes are either minus infinite or plus infinite when the rotation is null. At these extremes, (4.22) reduces to,

$$\mathbb{Z}_{irc}^{p}(n\pi)=\frac{A_1\sin(n\pi-\frac{\pi}{2})}{A_2\sin(n\pi-\frac{\pi}{2})}=\frac{A_1}{A_2}=\pm\infty \tag{4.23}$$

Since A_1 and A_2 are constant, the only possibility for the ratio $\frac{A_1}{A_2}$ from (4.23) going to either plus or minus infinity, is to have $A_2 \approx 0$. The distinction between plus and minus infinite is necessary since it corresponds to pure translation at the extremes of each half-cycle. With $A_2 = 0$, (4.22) assumes a tangent function as in (4.24).

$$\mathbb{Z}_{irc}^{p}(t,\omega) = \frac{A_1 \sin(\omega t - \frac{\pi}{2}) + B_1 \cos(\omega t - \frac{\pi}{2})}{B_2 \cos(\omega t - \frac{\pi}{2})} = \gamma_\infty \tan\left(\omega t - \frac{\pi}{2}\right) + z_0^\infty \tag{4.24}$$

Comparing (4.24) with (4.18), following conclusion may be made.

$$z_0^\infty = \frac{B_1}{B_2} = \frac{2\left(k_{\mathrm{Re}}\omega - k_{\mathrm{Im}}\beta_r\right)}{\Re_1 k_{\mathrm{Im}}\omega - \Re_2 k_{\mathrm{Re}}\omega + \Re_1 k_{\mathrm{Re}}\beta_r + \Re_2 k_{\mathrm{Im}}\beta_r} \tag{4.25}$$

$$\gamma_\infty = \frac{A_1}{B_2} = \frac{2\left(k_{\mathrm{Re}}\beta_r + k_{\mathrm{Im}}\omega\right)}{\Re_1 k_{\mathrm{Im}}\omega - \Re_2 k_{\mathrm{Re}}\omega + \Re_1 k_{\mathrm{Re}}\beta_r + \Re_2 k_{\mathrm{Im}}\beta_r} \tag{4.26}$$

With $A_2 = 0$, the ZIRC for transient region would be written as (4.27).

$$\mathbb{Z}_{irc}^{p}(t,\omega) = \frac{ce^{(\beta_s - \beta_r)t} + A_1 \sin(\omega t - \frac{\pi}{2}) + B_1 \cos(\omega t - \frac{\pi}{2})}{cr_s e^{(\beta_s - \beta_r)t} + B_2 \cos(\omega t - \frac{\pi}{2})} \tag{4.27}$$

A numerical confirmation is possible. The results obtained from the preliminary analysis of z_0 and γ provided by the complete equations (4.19) and (4.20) are shown in Figure 4.10 (for two drafts) in the category of $|\beta_r| < |\beta_s|$. For the first few half-

cycles the values of z_0 and γ oscillate, but soon converge to stationary values. The convergence values will be called z_0^∞ and γ_∞ that are predicted in (4.25) and (4.26) respectively.

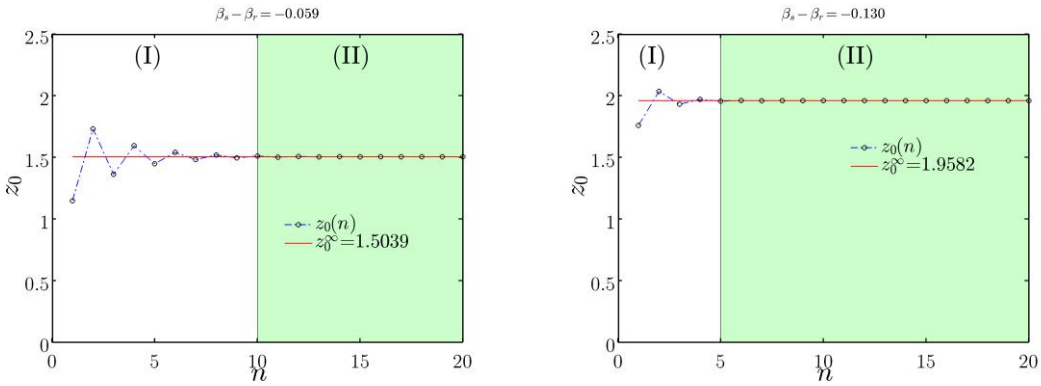

(a) Draft 14.7

(b) Draft 21m

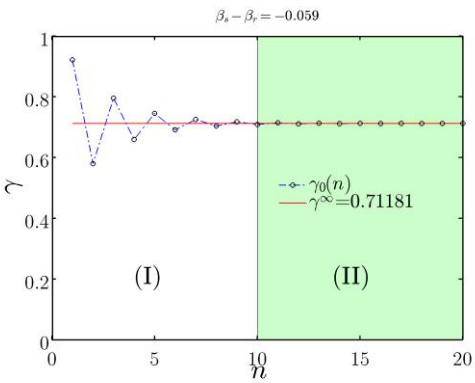

(c) Draft 14.7

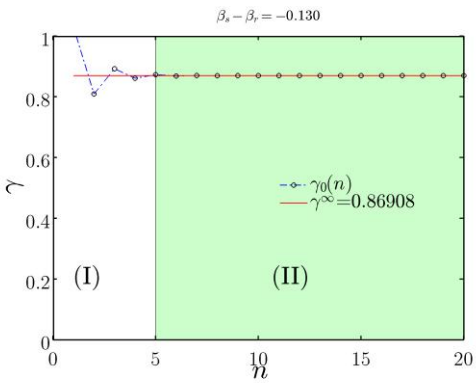

(d) Draft 21m

Figure 4.10 – Variation of z_0 and γ for each half-cycle (n), in the category $|\beta_r| < |\beta_s|$ and comparison with z_0^∞ and γ_∞ of (4.25) and (4.26); (a, c) $b_{44}^{cg} = 0.0564$ and $b_{22}^{cg} = 0.0861$ (b, d) $b_{44}^{cg} = 0.0651$ and $b_{22}^{cg} = 0.1584$.

As a matter of interpretation, Figure 4.11 illustrates the behaviour of $z_0(n)$ for each half cycle. In the first half cycle where the body moves from an initial condition of θ_1 to θ_2, $z_0(n=i)$ is below the position of z_0^∞ while in the second half cycle by changing the direction of rotation the $z_0(n=i+1)$ changes its position and goes to above z_0^∞, this oscillation lasts for several half cycles and finally the $z_0(n\to\infty)=z_0^\infty$.

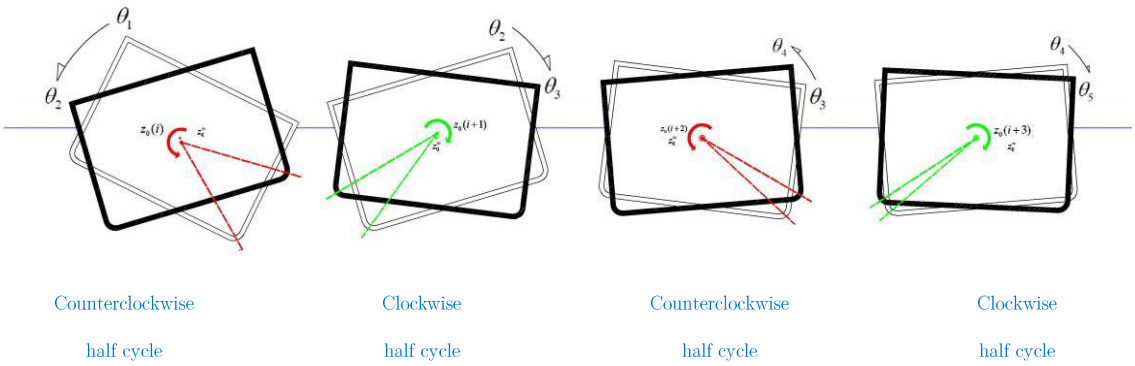

Figure 4.11 – Schematic of free roll decay and position of $z_0(n)$ and z_0^∞ for each half cycle; in this category the convergence with time leads to a MOIRC (z_0^∞) inside the hull.

4.3.1.1.1 Analytical Probability Density Function of the ZIRC

In the following analysis, consider a half cycle, in which case the $\mathbb{Z}_{irc}^p$ is a monotonic function of *t*. According to the probability theory, the probability density function (pdf) of $\mathbb{Z}_{irc}^p$, denoted as $f(\mathbb{Z}_{irc}^p)$, within the half-cycle can be expressed as:

$$f(\mathbb{Z}_{irc}^{p}) = \frac{f(t)}{\left|\frac{d\mathbb{Z}_{irc}^{p}}{dt}\right|} \tag{4.28}$$

where $f(t)$ is the pdf of t, which is assumed to follow a uniform distribution; if $t = 0$ to $\frac{T}{2}$, then $f(t) = \frac{2}{T}$.

Transient Region – The relation of the $\mathbb{Z}_{irc}^{p}$ for a transient region is defined by (4.27), and the derivative $\frac{d\mathbb{Z}_{irc}^{p}}{dt}$ could be derived as (4.29). (4.29) needs to be in terms of the $\mathbb{Z}_{irc}^{p}$, assuming $t = g^{-1}(\mathbb{Z}_{irc}^{p})$ however, the inverse function needs to be numerically evaluated, which is not the focus of this work.

$$\frac{d\mathbb{Z}_{irc}^{p}}{dx} = \frac{A_1\left(B_2\omega\left(\sin^2(\omega t)+\cos^2(\omega t)\right)+cr_s e^{(\beta_s-\beta_r)t}\left((\beta_s-\beta_r)\cos(\omega t)+\omega\sin(\omega t)\right)\right)+c\left(r_s B_1 - B_2\right)e^{(\beta_s-\beta_r)t}\left(\omega\cos(\omega t)-(\beta_s-\beta_r)\sin(\omega t)\right)}{\left(cr_s e^{(\beta_s-\beta_r)t}+B_2\cos(\omega t-\frac{\pi}{2})\right)^2} \tag{4.29}$$

Stationary Region – in the last part it was shown that the ZIRC function can be written as tangent function (4.24) for a stationary region. The derivative for the stationary region can be expressed as,

$$\frac{d\mathbb{Z}_{irc}^{p}}{dt} = \omega\gamma_{\infty}\sec^2\left(\omega t - \frac{\pi}{2}\right) \tag{4.30}$$

Substituting (4.30) into (4.28), the analytical pdf of $\mathbb{Z}_{irc}^{p}$ in the stationary region would be as (4.31) which is a Cauchy distribution.

$$f(\mathbb{Z}_{irc}^{p}) = \frac{\frac{\omega}{\pi}}{\left|\omega\gamma_{\infty}\sec^{2}\left(\omega t - \frac{\pi}{2}\right)\right|} \text{ or } \frac{1}{\pi\gamma_{\infty}\left|1-\left(\frac{\mathbb{Z}_{irc}^{p} - z_{0}^{\infty}}{\gamma_{\infty}}\right)^{2}\right|} \tag{4.31}$$

4.3.1.1.2 Cauchy Distribution (for Stationary Region) (based on (Low, Y.M. 2018)

The *Cauchy Distribution* also called the Lorentzian distribution or Lorentz distribution, is a continuous distribution describing resonance behaviour. Besides, in Cauchy distribution the moments (i.e. mean, variance, etc) are undefined since the improper integrals diverge. The general formula for the probability and cumulative density function of the Cauchy distribution is shown in (4.32) and (4.33), respectively.

$$f(\mathbb{Z}; z_0, \gamma) = \frac{1}{\pi\gamma\left[1+\left(\frac{\mathbb{Z}-z_0}{\gamma}\right)^{2}\right]} \tag{4.32}$$

$$F(\mathbb{Z}; z_0, \gamma) = \frac{1}{\pi}\tan^{-1}\left(\frac{\mathbb{Z}-z_0}{\gamma}\right) + \frac{1}{2} \tag{4.33}$$

According to the probability theory, if $\mathbb{Q} = F(\mathbb{Z}; z_0, \gamma)$ is a uniform distribution, then (4.33) can be written as,

$$\mathbb{Q} = \frac{1}{\pi}\tan^{-1}\left(\frac{\mathbb{Z}-z_0}{\gamma}\right) + \frac{1}{2} \tag{4.34}$$

Hence,

$$\mathbb{Z} = \gamma \tan\left[\pi\left(\mathbb{Q} - \frac{1}{2}\right)\right] + z_0 \tag{4.35}$$

(4.35) shows that the ZIRC has a tangent form, Figure 4.12 compares the results of (4.15) and (4.35), which show an excellent agreement. In the Cauchy distribution (4.32), z_0 is the location parameter, specifying the location of the distribution's mode (called here the most often value) and 2γ is the full width at half maximum. A clearer understanding of the instantaneous rotation center (IRC) distribution can be matched through the Cauchy distribution since the IRC is not a fixed point but changes continuously. However, most of the time it stays near to z_0^{∞} which is the mode of the distribution and called here the '*Most Often Instantaneous Rotation Center – MOIRC*'. Figure 4.13 compares analytical and numerical probability functions for two drafts. The analytical result shows a good agreement with numerical results, where the modes of both distributions match very well.

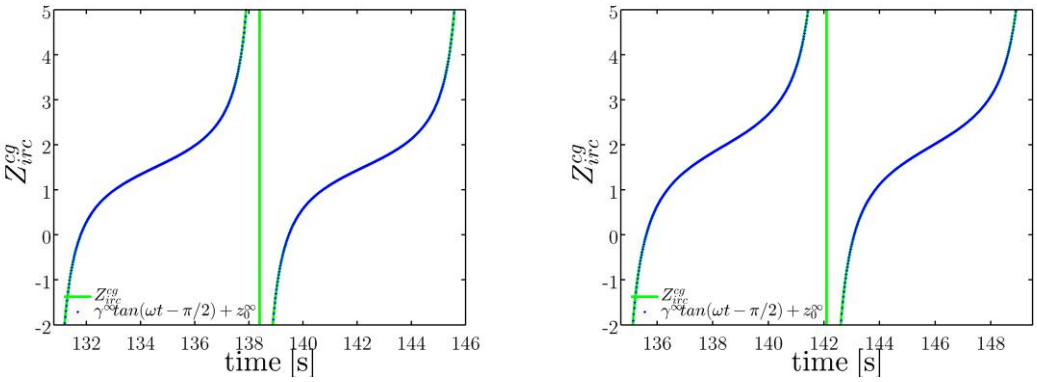

(a) Draft 14.7m (b) Draft 21m

Figure 4.12 – Comparison of analytical (solid-line) and statistical (dotted-line) variation of ZIRCs in time.

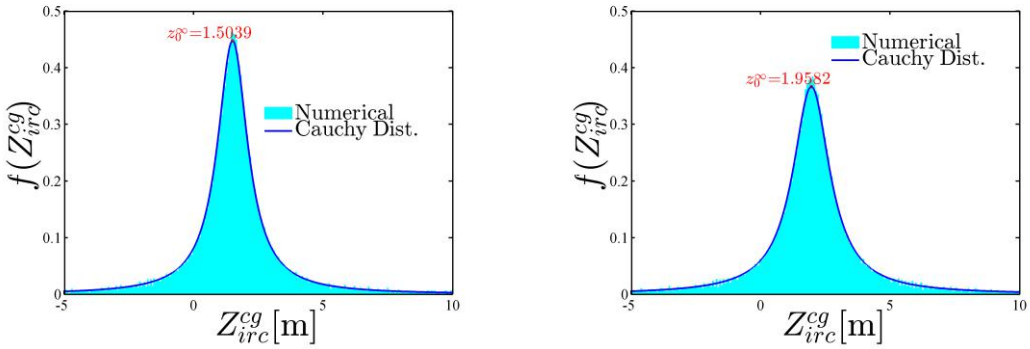

(a) Draft 14.7m (b) Draft 21m

Figure 4.13 – Numerical probability function versus analytical probability function (Cauchy Distribution)

4.3.1.2 Roll damping factor $|\beta_r|$ larger than sway damping factor $|\beta_s|$

Following the same assumption for the signs of β_r and β_s, the term $\beta_s - \beta_r$ would have a positive value. Hence, in (4.15) term $e^{(\beta_s-\beta_r)t}$ now grows with time but goes to a constant value. Figure 4.14 shows variation of the $\mathbb{Z}_{irc}^{cg}(t)$ with time with respect to the center of gravity. The behavior of ZIRCs could be divided into three regions. In

Region-I the motion is pure rotation, while in Region-II it is mostly a combination of translation and rotation motions. Finally, in Region-III, the motion turns to be pure translation motion. See Figure 4.14.

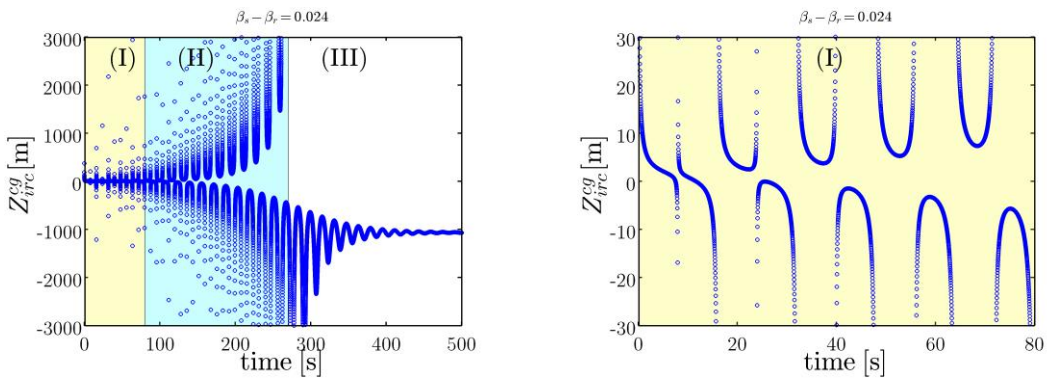

(a) All parts (b) Rotationally part

Figure 4.14 – Variation of ZIRCs with time with respect to the center of gravity where $|\beta_r| \geq |\beta_s|$; Draft=14.7m; (I) Pure rotation motion (II) Translation and rotation motion (III) Pure translation motion; $b_{44}^{cg} = 0.2255$ and $b_{22}^{cg} = 0.0861$.

At the beginning of the decay, the MOIRC stays near to z_0^{∞} and oscillates about it, but soon the MOIRCs stay far from the body, by increasing the rotation arm the motion tends to the translatory motion. Figure 4.15 illustrates how MOIRCs oscillate about z_0^{∞} for each half cycle.

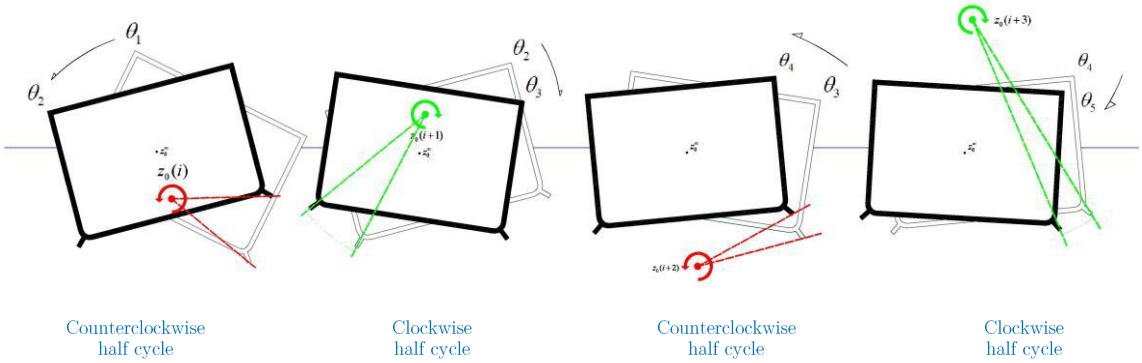

Figure 4.15 – Schematic variation of the position $z_0(n)$ in each half cycle. In this category there is no convergence; MOIRC position is oscillatory usually outside the hull; here the MOIRC is different from z_0^{∞}; eventually will converge to $1/r_s$ (See Figure 4.16).

The results obtained from the preliminary analysis of z_0 and γ provided by (4.19) and (4.20) are shown in Figure 4.16 in the case of $|\beta_r| \geq |\beta_s|$, and compared with values from (4.25) and (4.26). The results for z_0 show that for initial cycles the value of z_0 is near to z_0^{∞} and by increasing cycle number, z_0 goes to $1/r_s$ as shown by (4.19).

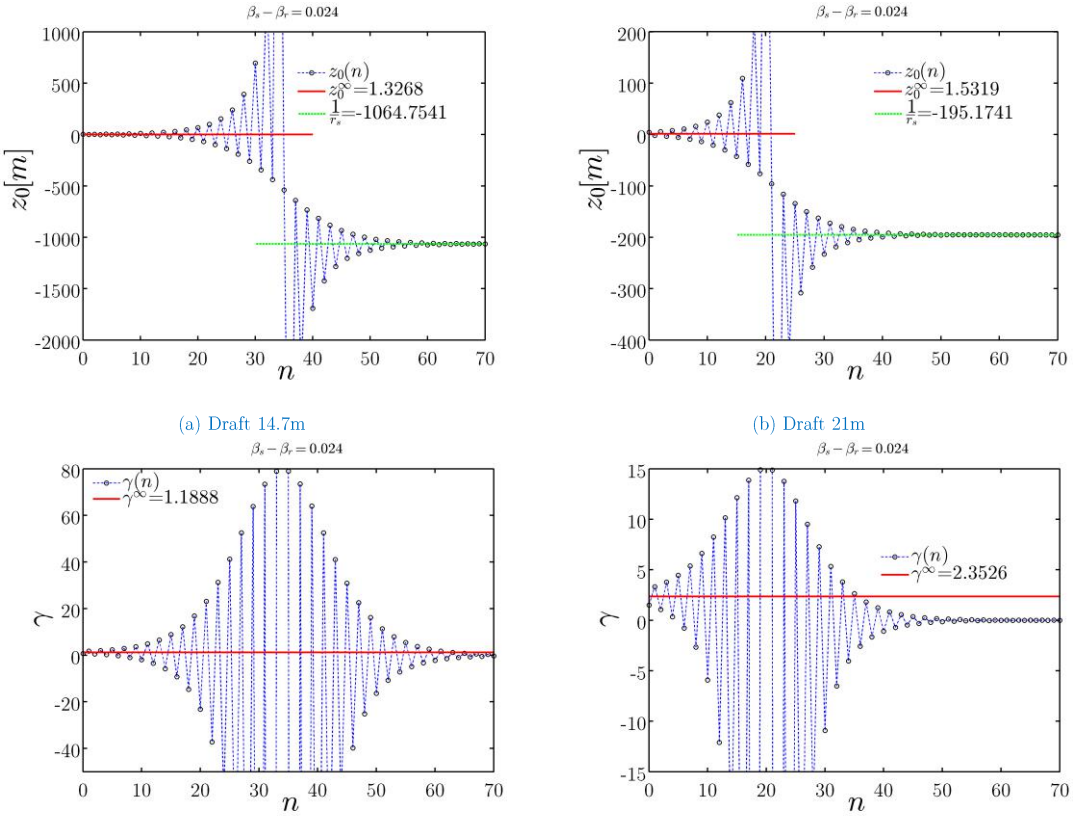

(a) Draft 14.7m (b) Draft 21m

(c) Draft 14.7m (d) Draft 21m

Figure 4.16 – Variation of z_0 and γ for each half cycle, in condition of $|\beta_r| \geq |\beta_s|$ and comparison with z_0^∞ and γ^∞ ((4.25) and (4.26)); (a, c) $b_{44}^{cg} = 0.2255$ and $b_{22}^{cg} = 0.0861$ (b, d) $b_{44}^{cg} = 0.3905$ and $b_{22}^{cg} = 0.1584$.

Figure 4.17 illustrates how the position of the MOIRC can affect the damping efficiency of the bilge keels by changing the motion behavior. For three conditions, the models have the same displacement from the initial angle of θ_1 to θ_2 in half cycle but different positions of the MOIRC. Figure 4.17(a) shows roll displacement generally for the first category (where normally MOIRC nears or lays on z_0^∞), in this category the bilge keel system has been expected to have its optimum efficiency since mostly

designed for cases such as when the body has roll around a fixed roll center to achieve higher flow separation in bilge keel's tip. However, in accordance with the experimental and analytical results, it can be concluded that most floating bodies such as FPSOs with attached bilge keels are included in the second category, thus the assumption of a rotation body having roll around a fixed roll center in each half cycle would be not valid anymore.

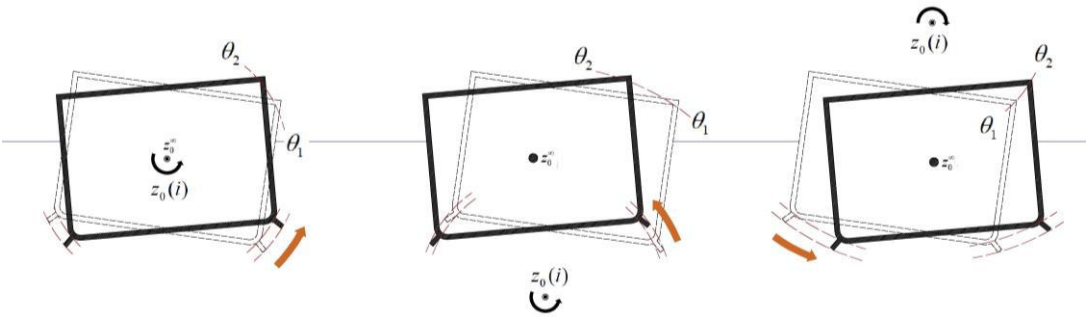

(a) (lays on z_0^∞) $|\beta_r| < |\beta_s|$

(b) (below z_0^∞) $|\beta_r| \geq |\beta_s|$

(c) (above z_0^∞) $|\beta_r| \geq |\beta_s|$

Figure 4.17 – Schematic of rotation of a body from θ_1 to θ_2 in half cycle for different positions of MOIRC with respect to z_0^∞.

In Figure 4.17(b), the same displacement occurs but in this time the MOIRC is placed below z_0^∞, normally this happens when the oscillation is in forth half cycles for free roll decay of bodies with bilge keel (second category). In this situation, the efficiency of the bilge keel falls down, by changing the nature of rotation as can be seen clearly in Figure 4.17(b). By decreasing the relative velocity of bilge keel's tip, flow separation and vortex generation decrease significantly.

In contrast, the efficiency of the bilge keel would increase when the MOIRC is placed above z_0^{∞} (See Figure 4.17 (c)), normally this happens when the oscillation is in back half cycles for free roll decay of bodies with bilge keel (second category). By increasing the height of the MOIRC, the rotation arm also increases, thus higher relative velocities may appear on bilge keels which leads to increasing the efficiency of the bilge keel system.

It should be said that the linear analysis has qualitatively confirmed the observations from the experimental analysis. It confirmed the existence of the MOIRC. It explained the change from tangent time histories to parabolic time histories depending on the relative value of the sway damping to the roll damping. The tangent behavior is getting an excellent correlation with the Cauchy distribution.

4.3.2 Numerical (Linear-plus-Quadratic Damping)

Looking back to analytical ZIRCs in Figure 4.14 and the experimental evidence on ZIRCs in Figure 4.4 and comparing both results, it can be seen that the analytical ZIRC diverges and finally tends to value $1/r_s$ (which does not have physical meaning) while in experiments by decreasing mean angles the ZIRCs go back to z_0^{∞} (See Figure 4.4). This is so because in the linear analytical analysis the roll damping is constant. However, it is well-known as a roll damping nonlinear phenomenon particularly for floating bodies with anti-roll systems, that the mean roll angle varies in subsequent cycles. To demonstrate this, a non-linear numerical approach was used considering the linear plus quadratic roll damping proposal. A 1652 panel model was used as model test representation in real scale to provide equivalent experimental results in this part. The 3rd order homogeneous equation of roll motion with consideration of sway-into-roll

damping term effect with coordinate system in C_{idp} is expressed in (4.36). The 3rd order sway motion forced by roll can be expressed as (4.37) where roll damping is non-linear. Based on roll damping experimental results provided by the 3rd order approach, the numerical linear b_1 plus quadratic b_2 damping model is proposed as (2.38) and the values for the numerical naked hull (NH), numerical with bilge keel length 1.2m (BK1) and 1.8m (BK2) models are shown in Table 4.1.

$$\dddot{\eta}_4^{idp} + \left(b_{22} + b_{44}^{idp}(\dot{\eta}_4)\right)\ddot{\eta}_4^{idp} + \left(b_{22}b_{44}^{idp}(\dot{\eta}_4) - b_{24}^{idp}b_{42}^{idp} + c_{44}\right)\dot{\eta}_4^{idp} + \left(b_{22}c_{44}\right)\eta_4^{idp} = 0 \tag{4.36}$$

$$\dddot{\eta}_2^{idp} + \left(b_{22} + b_{44}^{idp}(\dot{\eta}_4)\right)\ddot{\eta}_2^{idp} + \left(b_{22}b_{44}^{idp}(\dot{\eta}_4) - b_{24}^{idp}b_{42}^{idp}\right)\dot{\eta}_2^{idp} = \left(b_{24}^{idp}c_{44}\right)\eta_4^{idp} \tag{4.37}$$

Table 4.1 – Linear and quadratic terms for numerical models.

	$b_{44}^{idp}(\dot{\eta}_{44}^{idp}) = b_1 + b_2\left\lvert\dot{\eta}_{44}^{idp}\right\rvert$	
Numerical Models	$b_1\,[1/s]$	$b_2\,[-]$
BK2	0.012	0.060
BK1	0.010	0.045
NH	0.007	0.004

The numerical linear-plus-quadratic roll dampings in C_{idp} pole are shown in Figure 4.18 for NH, BK1 and BK2 based on experimental results for draft = 14.7m with consideration of coupling damping terms effects into the roll damping.

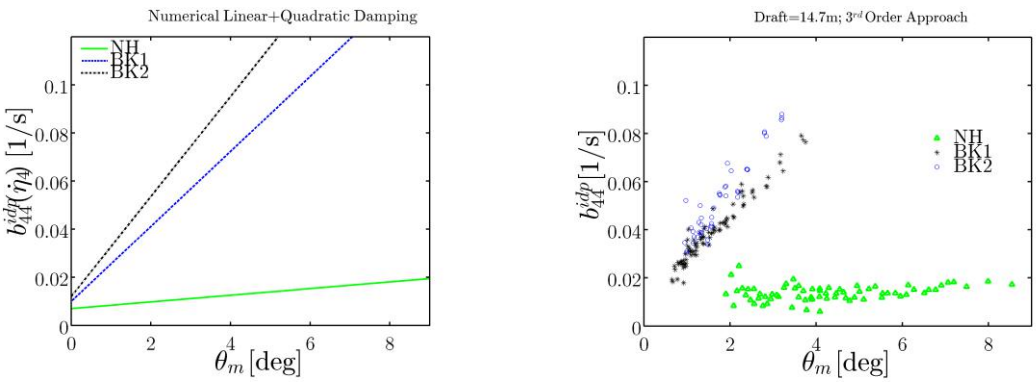

(a) Proposed LQ damping

(b) LQ damping from Experiment

Figure 4.18 – Numerical linear plus quadratic dampings for NH, BK1 and BK2.

The solution of ODEs in (4.36) and (4.37), can be approximated with high accuracy using Runge-Kutta 4th order method. Numerical time histories for each numerical model are shown in Figure 4.19, the time histories have good agreement with the experimental results as already shown in Figure 4.2.

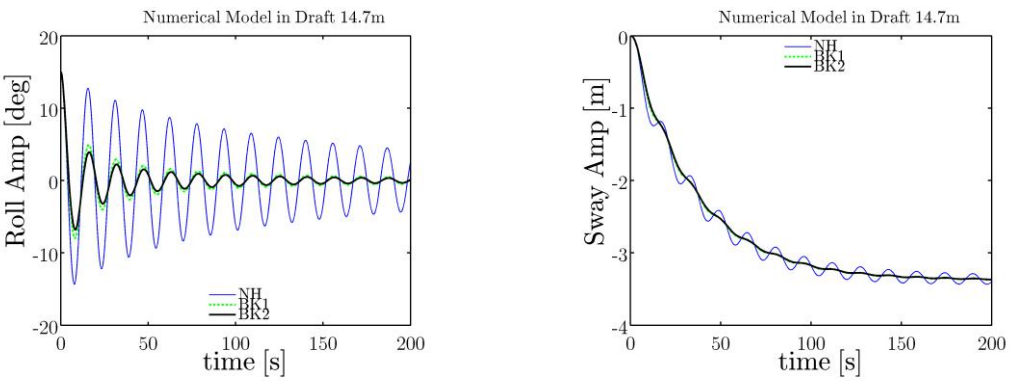

(a) (b)

Figure 4.19 – (a) Roll time history (b) Sway time history; draft 14.7m.

After solving the motion equation, the sway and roll velocities can be obtained, therefore the ZIRC can be obtained from (4.10), here with respect to the C_{idp}. Figure 4.20 shows the ZIRCs obtained numerically for NH, BK1 and BK2.

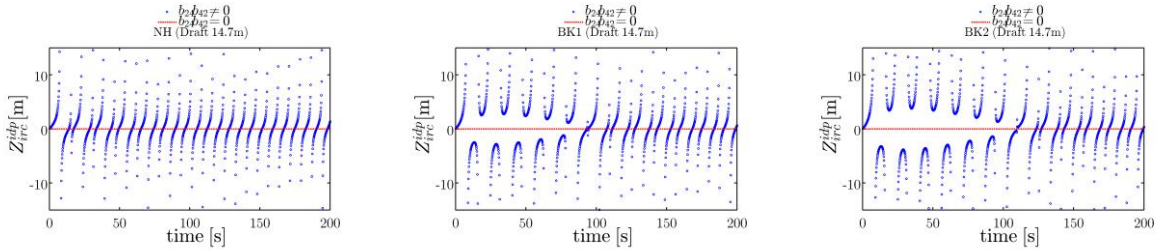

(a) NH (b) BK1 (c)BK2

Figure 4.20 – Vertical position of IRCs obtained from numerical model with respect to C_{idp}.

Figure 4.20(a) shows ZIRCs for the numerical NH with effects of coupled damping. The system is considered as Category-I, consequently the IRC function has tangent form and stays most of the time near the z_0^{∞}. The analytical result showed that sway-into-roll damping has a great influence on the position of MOIRC and its position by varying of sway-into-roll damping. It is apparent from Figure 4.20 that neglecting coupling terms ($b_{24}^{idp} b_{42}^{idp} = 0$) led to a fake constant MOIRC (red dotted line in Figure 4.20) which consequently can cause not accurate estimation of the roll damping. Neglecting coupling terms may not affect significantly for cases that have very low roll damping, but by increasing damping (adding bilge keel) the differences were significant.

In fact, from Figure 4.20(a) it can be observed that the MOIRC stays essentially constant with the tangent behavior (for low dampings) or has the double parabolic behavior for higher dampings (Figure 4.20(b), (d). As it is shown in Figure 4.20(b, c) for BK1 and BK2, in larger mean angles the roll damping has larger values and the system is considered as category-II where the ZIRC stays far from the z_0^{∞} and MOIRC

changes its direction in each full half cycle. However, by decreasing the mean angle in decay the damping also decreases until the system category-II converts into category-I. Similarly, to the NH model, also the ZIRC is calculated for BK1 in condition of $b_{24}^{idp} = 0$ and results are significant for larger angles comparing with results when $b_{24}^{idp} \neq 0$.

Figure 4.15 illustrates how the position of the MOIRC can affect the efficiency of the bilge keels. For instance, when the sway-into-roll damping is neglected the rotation of the body would be around a fixed (constant) MOIRC which can increase efficiency of the bilge keel by increasing flow separation and vortex consequently causing higher roll dampings. Therefore, neglecting coupled damping terms would lead to an overestimation of the roll damping. The coupled damping terms such as sway-into-roll damping always exist, then real rotation never would be around a fixed roll center in the roll decay. This is an alert on the effectiveness of the forced oscillation tests.

The damping obtained from the free roll decay test is in principle different from the one from forced oscillation test (with fixed rotation axis). This is so because the roll damping is non-linear. The same could be said about the damping in regular waves, irregular waves and roll decay with a fixed rotation axis. In a free decay test the IRC lays on the body center-line and varies vertically with time, while for forced oscillation and roll decay with a fixed rotation axis, the rotation center is assumed fixed during the test.

The present research, when analyzing the ZIRCs (or the vertical position of the IRC) time histories has determined two very different categories of geometrical forms. As shown by the linear analysis, the determinant parameters for these two behaviors are

related with β_r and β_s, which are the roll and sway damping coefficients. The two categories are described next.

Category-I $|\beta_r| < |\beta_s|$: Normally, ZIRC variation has tangent form (See Figure 4.9) and MOIRC uses to be near the C_{idp}. For Category-I, the present investigation proved that the Cauchy Distribution is very adherent to the histogram for the ZIRC within the linear analysis. It in fact provides a direct way to estimate the MOIRC as shown in Figure 4.13.

Category-II $|\beta_r| \leq |\beta_s|$: In this case the MOIRC oscillates within the same half cycle alternating the upper position with the lower position, as shown in Figure 4.14. The MOIRC position alternates from an upper position to a lower position. The tangent form becomes a double parabolic form. When the MOIRC is in the upper position, the bilge keel receives the flow almost perpendicular, generates stronger vortex and dissipates more energy. When the MOIRC is in the lower position, the bilge keel is more tangent to the trajectory, produces vortices not so strong and dissipates less energy. This is an observation that improves the safety of the results in the decay test.

These perhaps interesting conclusions were possible because of the analysis of ZIRC, which was never reported in the literature to the authors' best knowledge. These observations when seen from the linear analysis have a qualitative approach. One pitfall in the linear analysis is that the sequence of the MOIRC diverges as shown in Figure 4.14 (a).

For this reason, the work returns to the non-linear case within the linear plus quadratic type that yields adequate results. The type of non-linearity discussion is out

of the scope here. In fact, Chapter 4, by the use of Runge Kutta integration has arrived to the same behavior observed in the experiments with remarkable adherence.

Chapter 5 Regular Waves: Most Often Instantaneous Center of Rotation – MOIRC

In this chapter, the experiments of the body in condition of the regular beam waves are presented and investigated in the aspect of the instantaneous rotation center. Also, numerical study is provided to support the experiments. A concept of the locus straight line is presented which shows the variation of the IRCs in transversal section of the body. The analytical part presented probability function and confirmed the MOIRC for the condition of the beam waves and compared with the experiments.

5.1 Experimental Study

The same tank of the Laboratory of Waves and Currents at COPPE-Federal University of Rio de Janeiro (Laboratório de Ondas e Correntes COPPE-UFRJ) and the same models were used to investigate interaction of floating body with the incident beam waves, but this time and hydraulic wave-maker is placed one side and a wave-absorber beaches is laid on end of the tank. The depth of the was kept in 86cm for all cases. The model with different drafts and bilge-keels which are detailed in Table 3.4 have roll natural frequency between 1.7s~1.8s in scale of model, hence a range of the waves with periods 1.5s up to 2s are considered to study of the roll. However,

considering constant depth of the tank, the waves are all in intermediate water ($0.04 > h / L_w > 0.5$).

One limitation of the test would be the reflection. The model is positioned in the possible far position from the wave-maker to avoid any reflection interferences on the recorded data (see Figure 5.1).

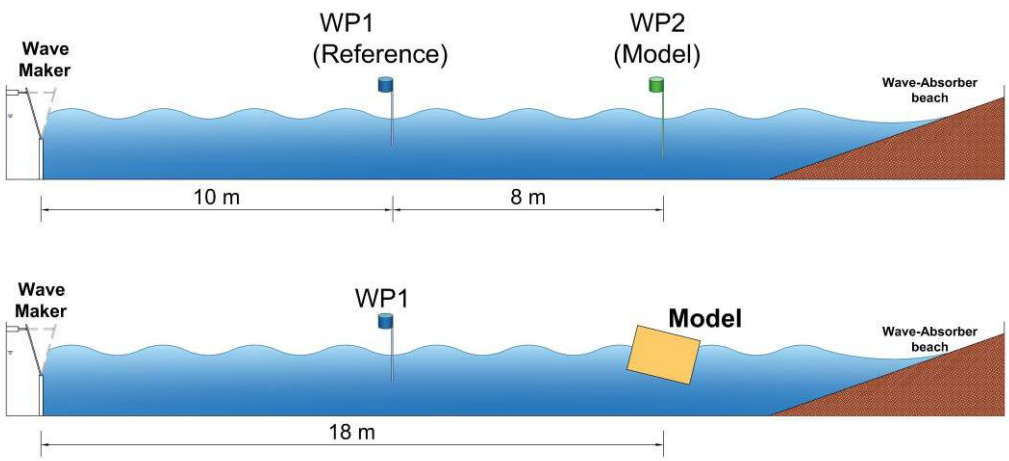

Figure 5.1 – Test set-up for the regular beam waves experiments.

Two wave probes are considered to calibrate the regular waves, the WP1 is used as reference and WP2 shows wave elevation in position of the model test. Each wave has minimum three repetitions and results showed excellent agreement between them, thus definition of each wave (W) with different amplitudes (A) are listed in Table 5.1.

Table 5.1 – Experimental regular wave's specification

	k	T_w [s]	A_w [mm]	H_w / L_w
W1A1	0.001925	1.5000	4.9050	0.0030
W1A2	0.001925	1.5000	7.3450	0.0045
W1A3	0.001925	1.5000	9.9750	0.0061
W2A1	0.001588	1.7000	4.8900	0.0025
W2A2	0.001588	1.7000	8.6850	0.0044
W2A3	0.001588	1.7000	12.4900	0.0063
W3A1	0.001406	1.8500	4.1350	0.0019
W3A2	0.001406	1.8500	7.7000	0.0034
W3A3	0.001406	1.8500	11.2600	0.0050
W4A1	0.001265	2.0000	6.5700	0.0026
W4A2	0.001265	2.0000	7.8150	0.0031
W4A3	0.001265	2.0000	13.4850	0.0054

According to the ITTC (ITTC, 2011), the ratio of wave height to wave-length H_w / L_w should be maintained constant around recommended value 0.02. As it mentioned before the waves are in intermediate depth and the wave length definition can be presented as (5.1), where T_w is wave period, g is gravity acceleration (9.806 m/s2) and h is water depth.

$$L_w = \frac{g}{2\pi} T_w^2 \tanh(2\pi \frac{h}{L_w}) \tag{5.1}$$

Some limitations should be noted, since the waves are in the intermediate depth then keeping the ratio around 0.02 could be challenging task because of increasing wave height H_w the wave profile does not have more sinus form and not be considered linear according to the limitation of the tank, however the tank was not able to generate desired high wave-length. Therefore, three wave heights were considered in range of ratio 0.002 ~ 0.006 to study nonlinearity (see Table 5.1).

5.1.1 Response Amplitude Operators - RAOs

The model is exposed to the beam seas and the motions of sway, heave and roll are all measured as an example of Figure 5.2.

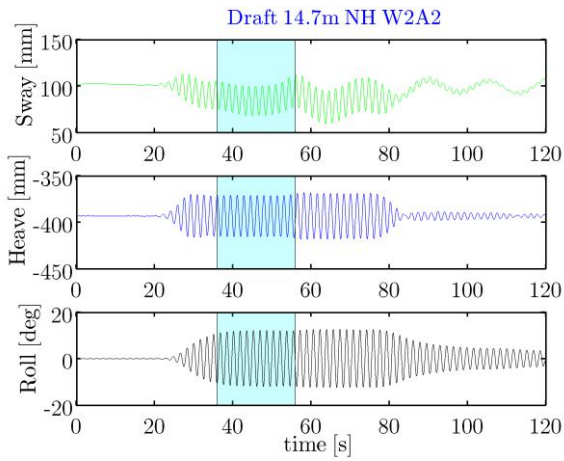

Figure 5.2 – 3-DoF motions for the naked hull model in draft 14.7m exposed to the W2A2.

After the transient, the model gets stable, but it should be noted that recording must be in short window (shown as green box in Figure 5.2) before any reflection perturbation. Depending on the wave period, the windows can be last about 10 to 20 seconds. The response amplitude operator for the model with different bilge keels obtained and shown in Figure 5.3. it must be noted that for the periods of W1=1.5s the beating phenomena was happening, more detail is provided about this period in Appendix A.

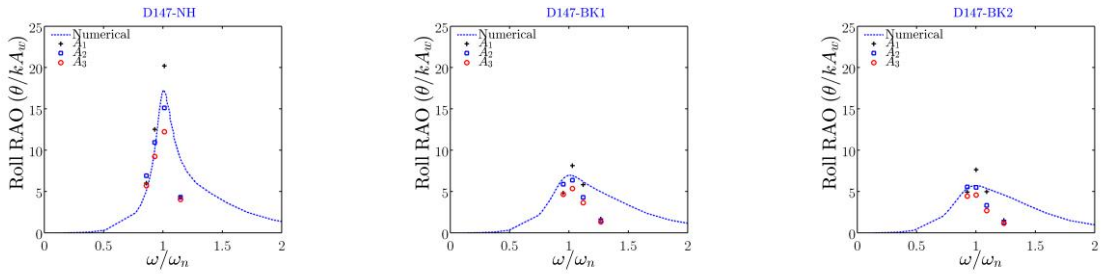

(a) (b) (c)

Figure 5.3 – Comparison of numerical RAOs with experiments for (a) NH, (b) BK1 and (c) BK2.

The results showed that roll response in nonlinear with respect to the wave amplitude where for higher wave heights the dampings are larger and consequently lower responses are expected. In this part the author adjusted a linear numerical model on intermediate wave amplitude (A2). A remarkable observation would be the low response of the roll for $\omega/\omega_n > 1$, where the response is significantly lower than predicted value from the numerical model or on the other word, the roll damping for this region is higher than the prediction. The explanation will be provided at the end of this part.

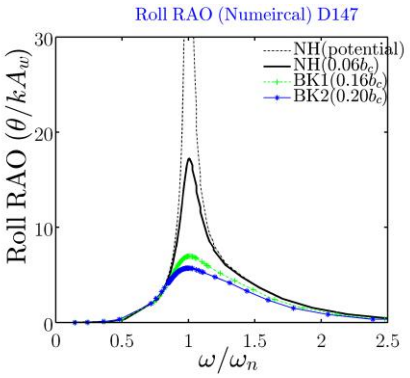

Figure 5.4 – Numerical roll RAOs.

Finally, three numerical model represent our model test, since the calculation of the hydrodynamic coefficients is based on potential theory (diffraction/radiation), viscose

dampings are not included. Therefore, the viscose and bilge-keel dampings are added to the system as an extra damping which is percentage of the critical damping (6% for NH, 16% for BK1 and 20% for BK2). The roll RAOs of the numerical model are shown in Figure 5.4.

5.1.2 IRCs

The position of the instantaneous rotation centers – IRCs can be obtained using (4.3), by crossing two perpendiculars the simultaneous velocities of two markers of the body shown in Figure 4.3 (the methodology is explained in 4.2.2). The variation of vertical position of instantaneous rotation center ZIRC is shown experimentally in Figure 5.5 for different wave periods and amplitudes. As can be seen from the graphs, the ZIRCs in beam seas continue to have the tangents form. Closer inspection of the graphs shows that the ZIRCs height increase by increasing the wave period independently of the wave amplitude.

Figure 5.6 also, is showing variation of the horizontal position of instantaneous rotation center YIRC. Another important finding was that by increasing the roll damping the YIRCs tends to stay far from the center-line on lee-side. It is important to state that this shifting of the YIRCs lead an asymmetric rotation which can affect the efficiency of the bilge-keels.

The present study was designed to determine the effect of the rotation center on roll damping estimation. Chapter 4 studied the effect of rotation center in case of the free roll decay and showed how the roll damping can be influenced by the position of the rotation center.

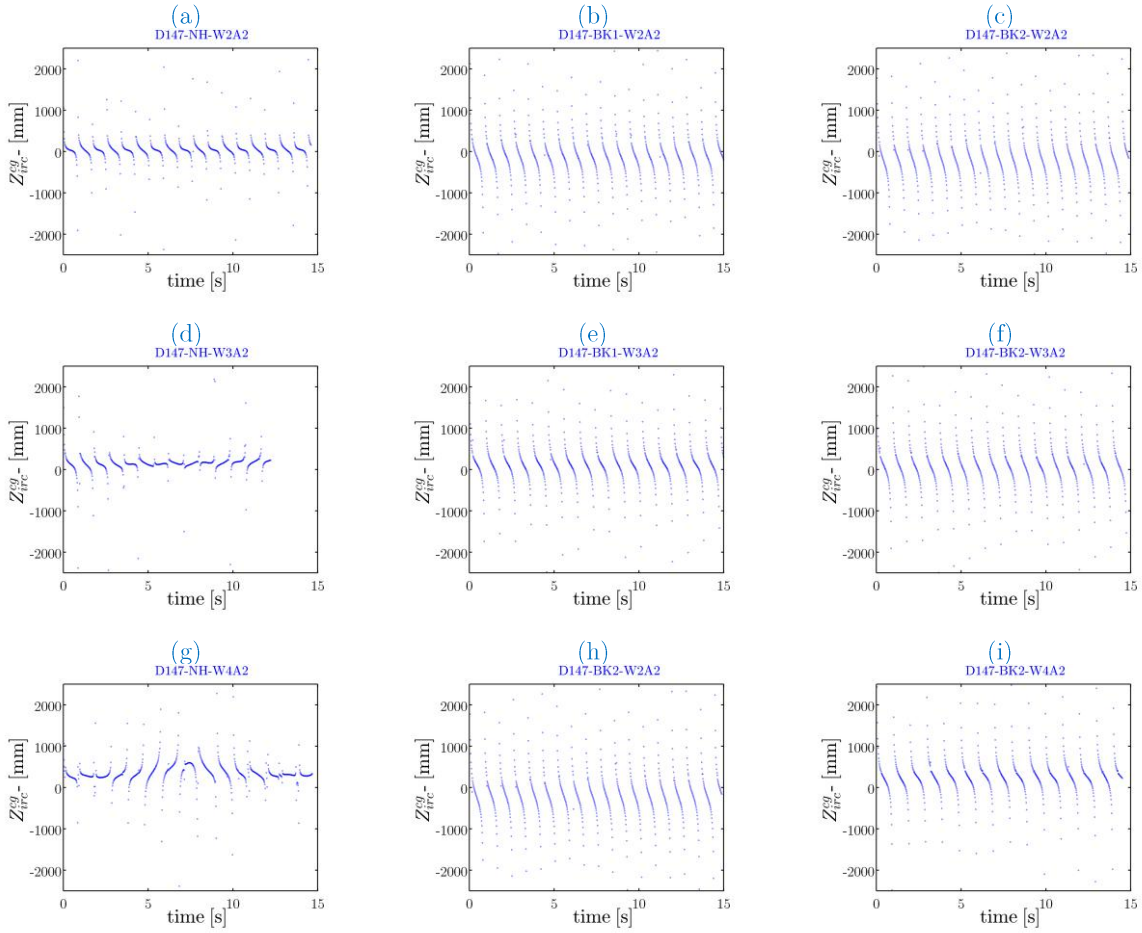

Figure 5.5 – Vertical position of the instantaneous rotation center - ZIRCs for the experiments.

Figure 5.5 and Figure 5.6 showed the variation of IRCs in time when the body is exposed to the beam wave, one of the main difference in result comparing with results obtained from free decay roll in Chapter 4 is that the IRCs laid on the center line during the decay, but in contrast, in presence of the wave the position of the YIRCs does not stay on the center line anymore. Therefore, the obtained roll damping from free decay roll and in wave condition would not be necessarily the same since the rotation is not the same.

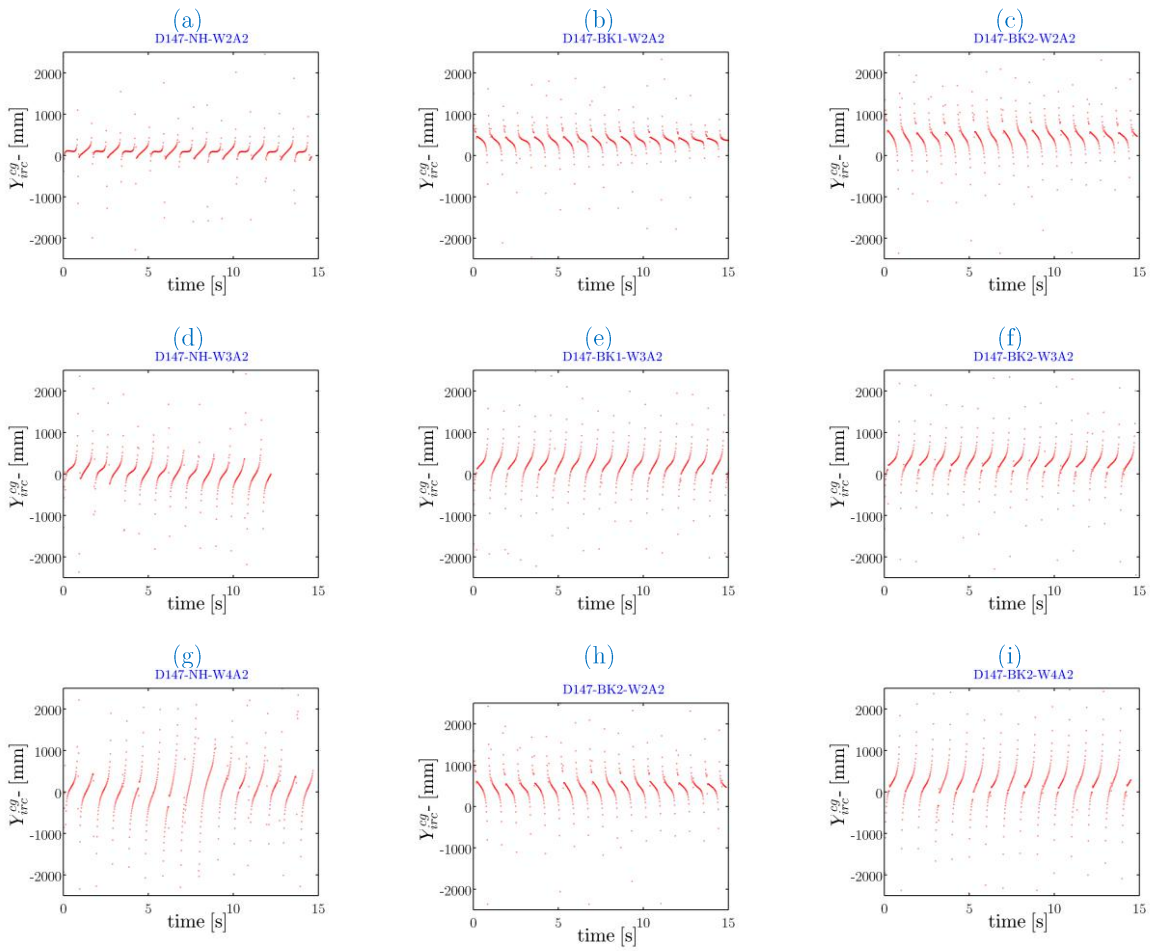

Figure 5.6 – Horizontal position of the instantaneous rotation center - YIRCs for the experiments.

5.2 Numerical

To have an independent result, the investigation has processed an FPSO hull with the same mid-ship section using the software WAMITs as detailed in 3.2.2. For the numerical calculations, however, since we have the roll angular velocity

instantaneously, the present work uses the basic equations of the rigid body kinematics that only requires a point to estimate the IRC. See Figure 5.7.

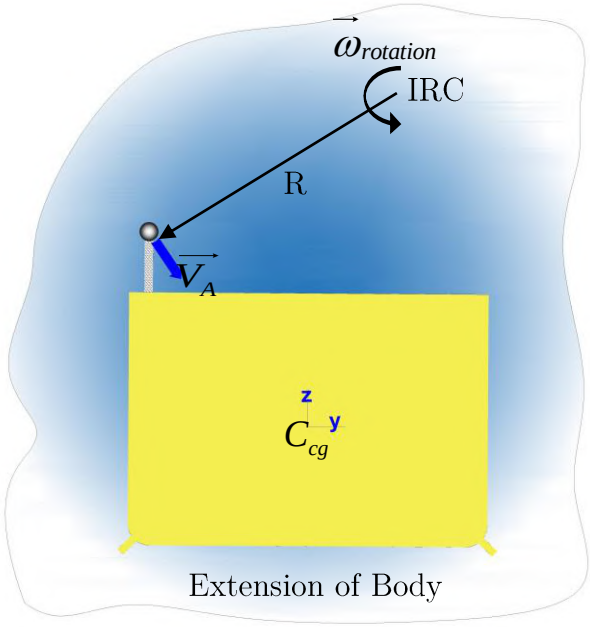

Figure 5.7 – schematic view of the extension body kinematic for mid-section of the vessel.

The motions are analysed in plane YZ, that is, considering sway, heave and roll Figure 5.7. (5.2) shows the general equation that relates the velocity at any point with the correspondent angular velocity.

$$\vec{V}_A = \vec{\omega}_{rotation} \times \vec{R} \tag{5.2}$$

Where $\vec{V}_A$ is velocity of point A, $\vec{R}$ is arm with respect to the IRC and $\vec{\omega}_{rotation}$ is angular velocity. In Figure 5.7, the origin of the coordinate system is an arbitrary pole.

$$\overrightarrow{V_A} = \omega_{rotation}(t)\hat{i} \times \left\{ \left(y_A^{pole} - y_{irc}^{pole}(t) \right) j + \left(z_A^{pole} - z_{irc}^{pole}(t) \right) k \right\} \tag{5.3}$$

$$\overrightarrow{V_A} = \omega_{rotation}(t)\left(y_A^{pole} - y_{irc}^{pole}(t) \right) k - \omega_{rotation}(t)\left(z_A^{pole} - z_{irc}^{pole}(t) \right) j \tag{5.4}$$

Velocity of the point A (5.4) can be written as normal and tangent component as (5.5) and (5.6).

$$V_y^A(t) = -\omega_{rotation}(t)\left(z_A^{pole} - z_{irc}^{pole}(t) \right) j \tag{5.5}$$

$$V_z^A(t) = \omega_{rotation}(t)\left(y_A^{pole} - y_{irc}^{pole}(t) \right) k \tag{5.6}$$

Thus, the unknowns $z_{irc}^{pole}(t)$ and $y_{irc}^{pole}(t)$ can be obtained for any pole using (5.7) and (5.8).

$$z_{irc}^{pole}(t) = \frac{V_y^A(t)}{\omega_{rotation}(t)} + z_A^{pole} \tag{5.7}$$

$$y_{irc}^{pole}(t) = -\frac{V_z^A(t)}{\omega_{rotation}(t)} + y_A^{pole} \tag{5.8}$$

To simplify, assume that the point A and pole are located on the center of gravity. Thereby, $y_{A=cg}^{cg} = z_{A=cg}^{cg} = 0$ and following equations shows instantaneous position of the IRCs.

$$z_{irc}^{cg}(t) = \frac{\dot{\eta}_2^{cg}(t)}{\dot{\eta}_4^{cg}(t)} \tag{5.9}$$

$$y_{irc}^{cg}(t) = -\frac{\dot{\eta}_3^{cg}(t)}{\dot{\eta}_4^{cg}(t)} \tag{5.10}$$

Figure 5.8 compares time history of vertical and horizontal position of instantaneous rotation centers obtained from (5.9) and (5.10) with the experiments results for the model BK1 in wave condition W3A2 for draft 14.7m. the results showed pretty good agreement between numerical and experimental.

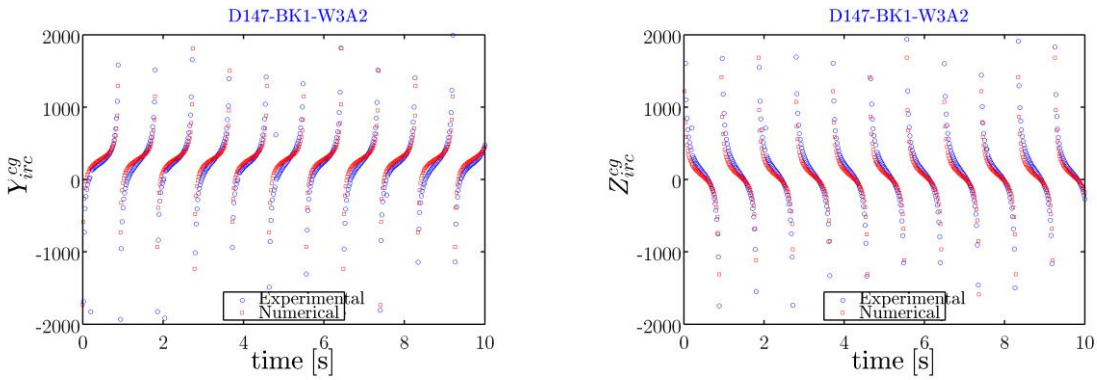

(a) (b)

Figure 5.8 – Comparison of the experiment and numerical results for (a) horizontal position of instantaneous rotation center and (b) vertical position of instantaneous rotation center.

5.3 Analytical

The analytical part 5.3 is based on private communication with professor Low Ying Min[1]. The motion of the 2-DoF section of FPSO can be written in vertical plan as superposition of sway, heave and roll motion for regular wave. The harmonic motion of each mode of motion are:

$$\eta_2^{pole}(t) = \eta_{2_0}^{pole} \sin(\omega t + \phi_s) \tag{5.11}$$

$$\eta_3^{pole}(t) = \eta_{3_0}^{pole} \sin(\omega t + \phi_h) \tag{5.12}$$

$$\eta_4^{pole}(t) = \eta_{4_0}^{pole} \sin(\omega t + \phi_r) \tag{5.13}$$

[1] Associate Professor, Department of Civil and Environmental Engineering National University of Singapore 1 Engineering Drive 2, E1A 07-03, Singapore 117576
Tel:(65)6516 4127
Email: ceelowym@nus.edu.sg

Where $\eta_{2_0}^{pole}$, $\eta_{3_0}^{pole}$ and $\eta_{4_0}^{pole}$ are amplitudes of sway, heave and roll respectively. From 5.2, the vertical and horizontal position of instantaneous rotation center in coordinate of center of gravity can be shown as:

$$z_{irc}^{cg}(t) = \frac{\dot{\eta}_2^{cg}(t)}{\dot{\eta}_4^{cg}(t)} = \frac{\eta_{2_0}^{cg}\omega\cos(\omega t+\phi_s)}{\eta_{4_0}^{cg}\omega\cos(\omega t+\phi_r)} = \frac{\eta_{2_0}^{cg}\cos(\Theta+\phi_s)}{\eta_{4_0}^{cg}\cos(\Theta+\phi_r)} \quad \text{Where, } \Theta = \omega t \tag{5.14}$$

Similarly,

$$y_{irc}^{cg}(t) = \frac{-\dot{\eta}_3^{cg}(t)}{\dot{\eta}_4^{cg}(t)} = \frac{-\eta_{3_0}^{cg}\omega\cos(\omega t+\phi_h)}{\eta_{4_0}^{cg}\omega\cos(\omega t+\phi_r)} = \frac{-\eta_{3_0}^{cg}\cos(\Theta+\phi_h)}{\eta_{4_0}^{cg}\cos(\Theta+\phi_r)} \tag{5.15}$$

It is convenient to make a transformation so that roll motion has zero phase, i.e.

$$\varphi = \Theta + \phi \tag{5.16}$$

Hence,

$$z_{irc}^{cg}(t) = \frac{\eta_{2_0}^{cg}\cos(\varphi+\psi_s)}{\eta_{4_0}^{cg}\cos(\varphi)} = \frac{\eta_{2_0}^{cg}(\cos\varphi\cos\psi_s - \sin\varphi\sin\psi_s)}{\eta_{4_0}^{cg}\cos(\varphi)} \tag{5.17}$$

$$\therefore z_{irc}^{cg}(t) = \frac{\eta_{2_0}^{cg}\cos\psi_s}{\eta_{4_0}^{cg}} - \frac{\eta_{2_0}^{cg}\sin\psi_s}{\eta_{4_0}^{cg}}\tan\varphi \tag{5.18}$$

$$\therefore \tan\varphi = \frac{\eta_{4_0}^{cg} z_{irc}^{cg}(t) - \eta_{2_0}^{cg}\cos\psi_s}{-\eta_{2_0}^{cg}\cos\psi_s} \tag{5.19}$$

Likewise, where $\psi_s = \phi_s - \phi_r$ and $\psi_h = \phi_h - \phi_r$.

$$y_{irc}^{cg}(t) = \frac{-\eta_{3_0}^{cg}\cos(\varphi+\psi_h)}{\eta_{4_0}^{cg}\cos(\varphi)} = \frac{-\eta_{3_0}^{cg}(\cos\varphi\cos\psi_h - \sin\varphi\sin\psi_h)}{\eta_{4_0}^{cg}\cos\varphi} \tag{5.20}$$

$$\therefore y_{irc}^{cg}(t) = \frac{-\eta_{3_0}^{cg}\cos\psi_h}{\eta_{4_0}^{cg}} + \frac{\eta_{3_0}^{cg}\sin\psi_h}{\eta_{4_0}^{cg}}\tan\varphi \tag{5.21}$$

$$\therefore \tan\varphi = \frac{y_{irc}^{cg}(t)\eta_{4_0}^{cg} + \eta_{3_0}^{cg}\cos\psi_h}{\eta_{3_0}^{cg}\sin\psi_h} \tag{5.22}$$

Equation (5.18) emphases on previous form equated as (4.24) in 4.3.1.1 which variation of instantaneous rotation center can be represented by a tangent form function.

Another important observation from Figure 5.9 is that the roll center locus apparently is a straight line, although at this point of the investigation this was not certain till is was proved analytically as shown see below. It is also noticeable that the locus is not symmetric. The waves are coming from starboard but the roll center for this frequency stays on the portside, away from the hull plan of symmetry. But to effectively prove this one needs further steps has shown by (Low, 2018).

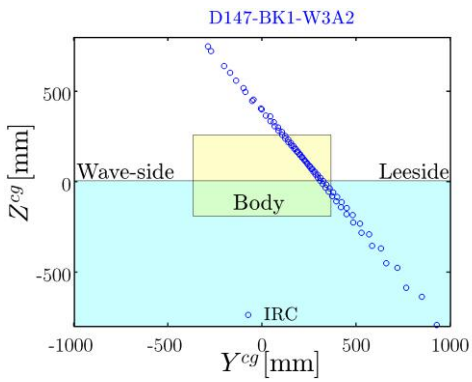

Figure 5.9 – Coordination of IRCs in pane of YZ for the experimental wave W3A2 with respect to the center of gravity.

Considering equations (5.19) and (5.21),

$$\frac{\eta_{4_0}^{cg} z_{irc}^{cg}(t) - \eta_{2_0}^{cg} \cos\psi_s}{-\eta_{2_0}^{cg} \cos\psi_s} = \frac{y_{irc}^{cg}(t)\eta_{4_0}^{cg} + \eta_{3_0}^{cg} \cos\psi_h}{\eta_{3_0}^{cg} \sin\psi_h} \tag{5.23}$$

$$\eta_{4_0}^{cg}\eta_{3_0}^{cg} z_{irc}^{cg}(t)\sin\psi_h - \eta_{2_0}^{cg} y_{irc}^{cg}(t)\eta_{4_0}^{cg} \cos\psi_s = \eta_{2_0}^{cg}\eta_{3_0}^{cg}(\cos\psi_s \sin\psi_h - \cos\psi_h \cos\psi_s) \tag{5.24}$$

And finally,

$$\left\{\eta_{4_0}^{cg}\eta_{3_0}^{cg} \sin(\varphi_h - \varphi_r)\right\} z_{irc}^{cg}(t) - \left\{\eta_{4_0}^{cg}\eta_{2_0}^{cg} \cos(\varphi_s - \varphi_r)\right\} y_{irc}^{cg}(t) = \eta_{2_0}^{cg}\eta_{3_0}^{cg} \sin(\varphi_h - \varphi_s) \tag{5.25}$$

Which is a typical straight line with constants such:

$$C_1 z_{irc}^{cg} - C_2 y_{irc}^{cg} = C_3 \tag{5.26}$$

The experimental locus are shown in Figure 5.10 and compared with numerical and analytical results for various wave periods and amplitudes for model in draft 14.7m. the locus line for a random beam waves is discussed in Appendix B analytically.

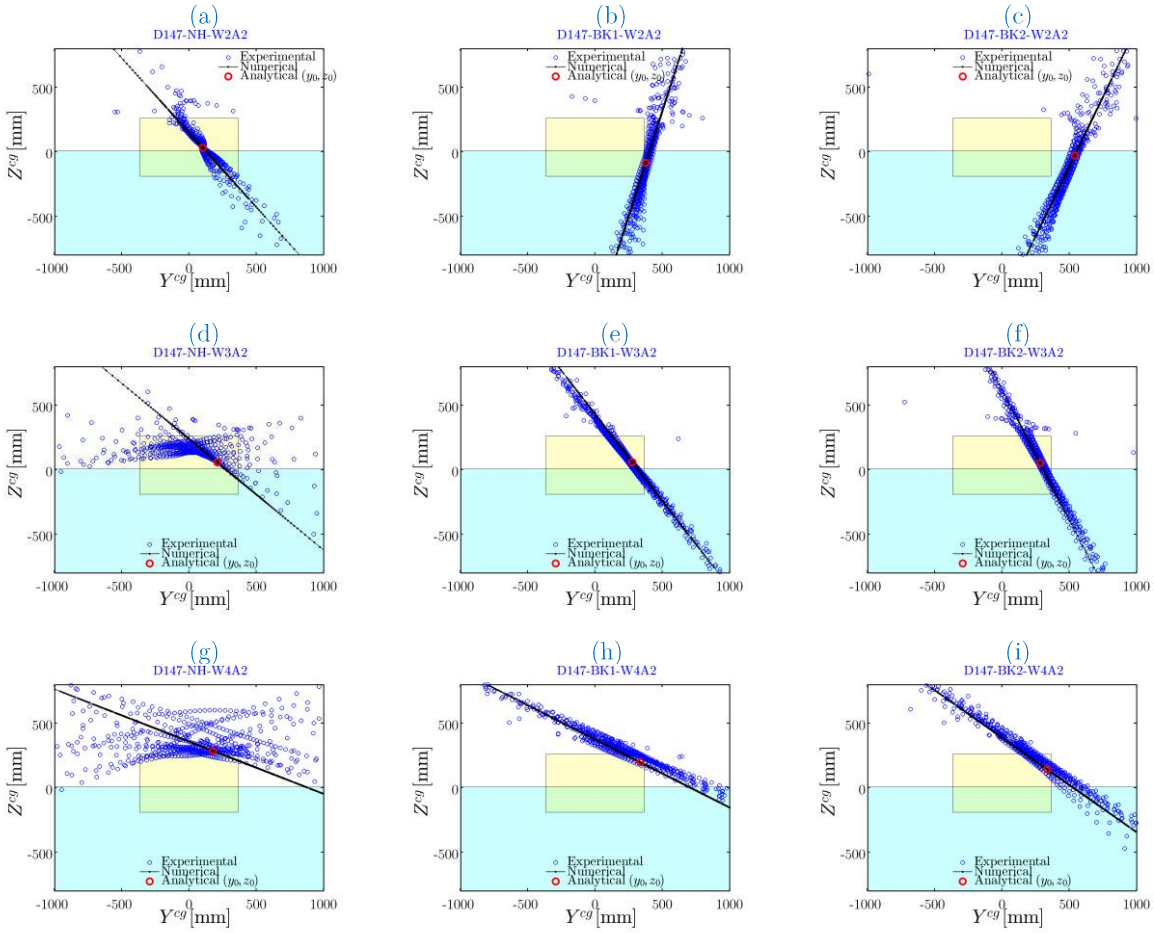

Figure 5.10 – Rotation center locus obtained experimentally, numerically and analytical for the model in draft 14.7m shows IRCs position with the constant time interval 50Hz.

The numerical locus line is laid on the analytical, the red cycle point in Figure 5.10 shown the point which has the most often occurrence of IRC analytically.

It was observed that the IRCs stay most of the time on the leeside most of the time, this is also is a function of the roll damping, by attaching the BK1 and BK2 consequently increasing the damping, the IRCs tend to stay far from the body on the leeside. Depending on how far the IRCs and vertical positions of them are the efficiency of the bilge-keels will change. For instance, if the IRCs stay next to the

bilge-keel in leeside the velocity on bilge keel may increase! But do not forget that the bilge-keel of leeside may lose the almost all its efficiency.

Closer inspection of the Figure 5.3(a) shows for NH where the roll damping is not large enough the IRCs are almost located on the centreline for the wave period next to the natural roll period. This confirms that it is valid if considering the roll center on the centreline but just for *very low roll damping* in condition of wave periods next to the *roll natural period*. As soon as the roll damping increase this fact will not be valid anymore (see Figure 5.3(b, c)). So far, increasing the roll damping led to IRCs stay far from the body on leeside, the same behaviour also was observed for wave periods W3 and W4 as well.

From the data in Figure 5.3, it is apparent that vertical position of the IRCs increase by the wave periods. It means for lower wave periods the IRCs are normally in below the body but by increasing the wave periods they stay above the body. Regarding to the 1.2, investigations showed that larger dampings are expected for higher center of rotation, consequently when the wave periods increase the higher roll dampings is expected, this was discussed in 4.3.1 and illustrated schematically in Figure 4.17(c) where the efficiency of the bilge keel would increase in case of MOIRC is placed above the body. Now it make sense why the values of roll response in Figure 5.3 are significantly lower than the numerical values for higher periods ($\omega/\omega_n > 1$) because of the position of IRCs.

Finally, the behaviour of the roll center was studied numerically for different frequency ratios ω/ω_n. The results were shown in Figure 5.10, equation (5.25) shows that the

straight locus of the IRCs is a frequency dependent function which the phases are important. It is again clear that roll center tends to infinity at the pure translation instants. Note that there is a concentration of the IRCs on the body region. This concentration is coarser for lower and higher periods but very concentrated at periods near natural period. To make this clearer, the work presents histograms indicating the frequency, $f(z_{irc}^{cg})$ and $f(y_{irc}^{cg})$.

5.3.1 Probability Function of IRCs

In 4.3.1.1.2, Cauchy distribution, probability density function - PDF (4.32) and cumulative distribution function – CDF (4.33) were presented as well. Also, previous part 5.3, showed that the vertical and horizontal position of the IRCs can be presented as tangent function, while equations (5.18) and (5.21) remind us the equation (4.35). Thus, the Cauchy distributions for (5.18) and (5.21) can be introduced as following:

$$f(\mathbb{Z}_{irc}^{cg}; z_0, \gamma) = \frac{1}{\pi\gamma\left[1+\left(\frac{\mathbb{Z}_{irc}^{cg} - z_0}{\gamma}\right)^2\right]} \tag{5.27}$$

Where,

$$(z_0, \gamma) = \left(\frac{\eta_{2_0}^{cg}\cos(\varphi_s - \varphi_r)}{\eta_{4_0}^{cg}}, -\frac{\eta_{2_0}^{cg}\sin(\varphi_s - \varphi_r)}{\eta_{4_0}^{cg}}\right) \tag{5.28}$$

Similarly,

$$f(Y_{irc}^{cg};y_0,\alpha)=\frac{1}{\pi\alpha\left[1+\left(\frac{Y_{irc}^{cg}-y_0}{\alpha}\right)^2\right]} \tag{5.29}$$

Where,

$$(y_0,\alpha)=\left(\frac{-\eta_{3_0}^{cg}\cos(\varphi_h-\varphi_r)}{\eta_{4_0}^{cg}},\frac{\eta_{3_0}^{cg}\sin(\varphi_h-\varphi_r)}{\eta_{4_0}^{cg}}\right) \tag{5.30}$$

For Cauchy distribution, the moments (i.e. mean, variance, etc) are undefined. The mode (most often value) is z_0 for $f(\mathbb{Z}_{irc}^{cg};z_0,\gamma)$ and y_0 for $f(Y_{irc}^{cg};y_0,\alpha)$, therefore, the coordination of the Most Often Instantaneous Rotation Center – MOIRC can be defined as (5.31).

$$MOIRC=(y_0,z_0)=\left(\frac{-\eta_{3_0}^{cg}\cos(\varphi_h-\varphi_r)}{\eta_{4_0}^{cg}},\frac{\eta_{2_0}^{cg}\cos(\varphi_s-\varphi_r)}{\eta_{4_0}^{cg}}\right) \tag{5.31}$$

In Figure 5.11 the experimental histograms are compared with numerical and analytical probability density functions for vertical position of the IRCs and the same comparison is made for horizontal position of IRCs in Figure 5.12.

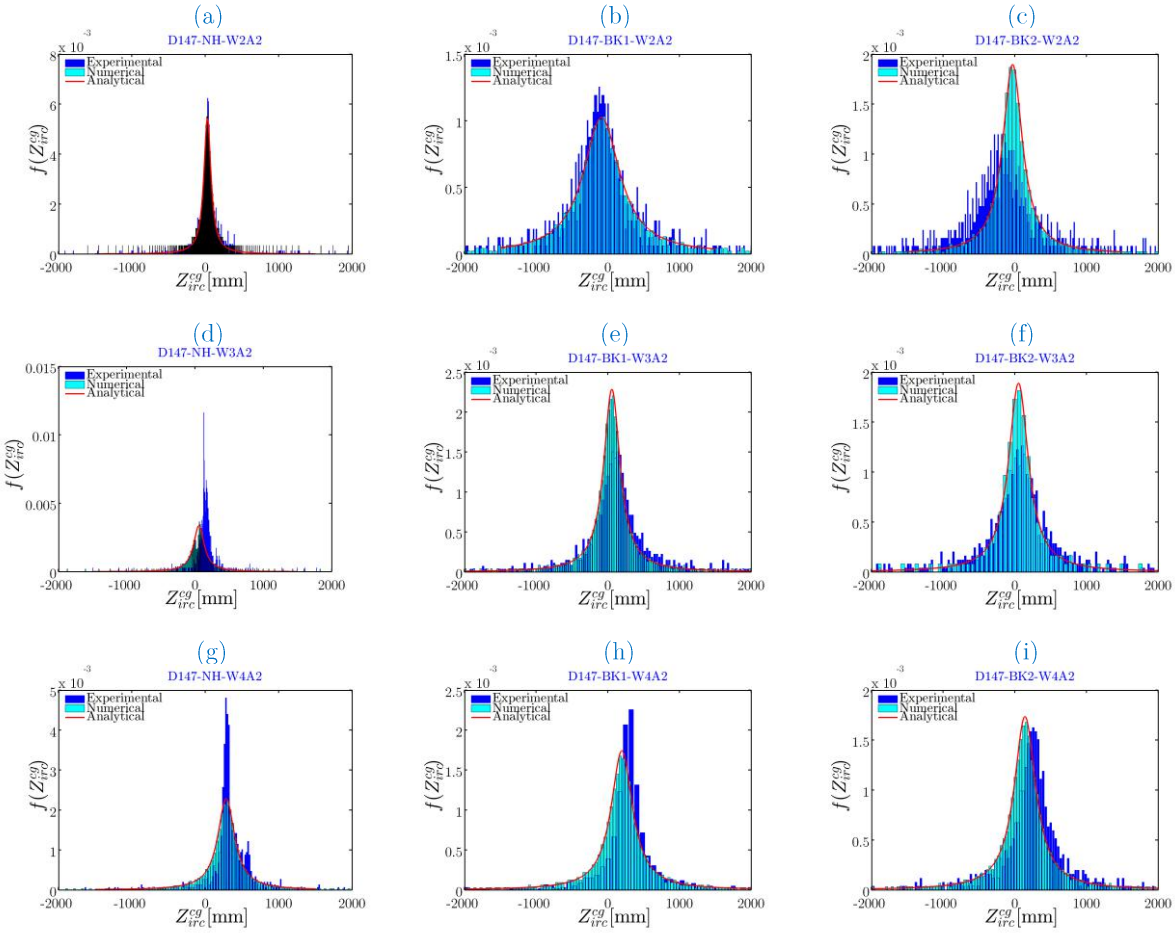

Figure 5.11 – Probability density function of vertical position of the instantaneous rotation center with respect to the center of gravity for experimental, numerical and analytical models; draft 14.7m.

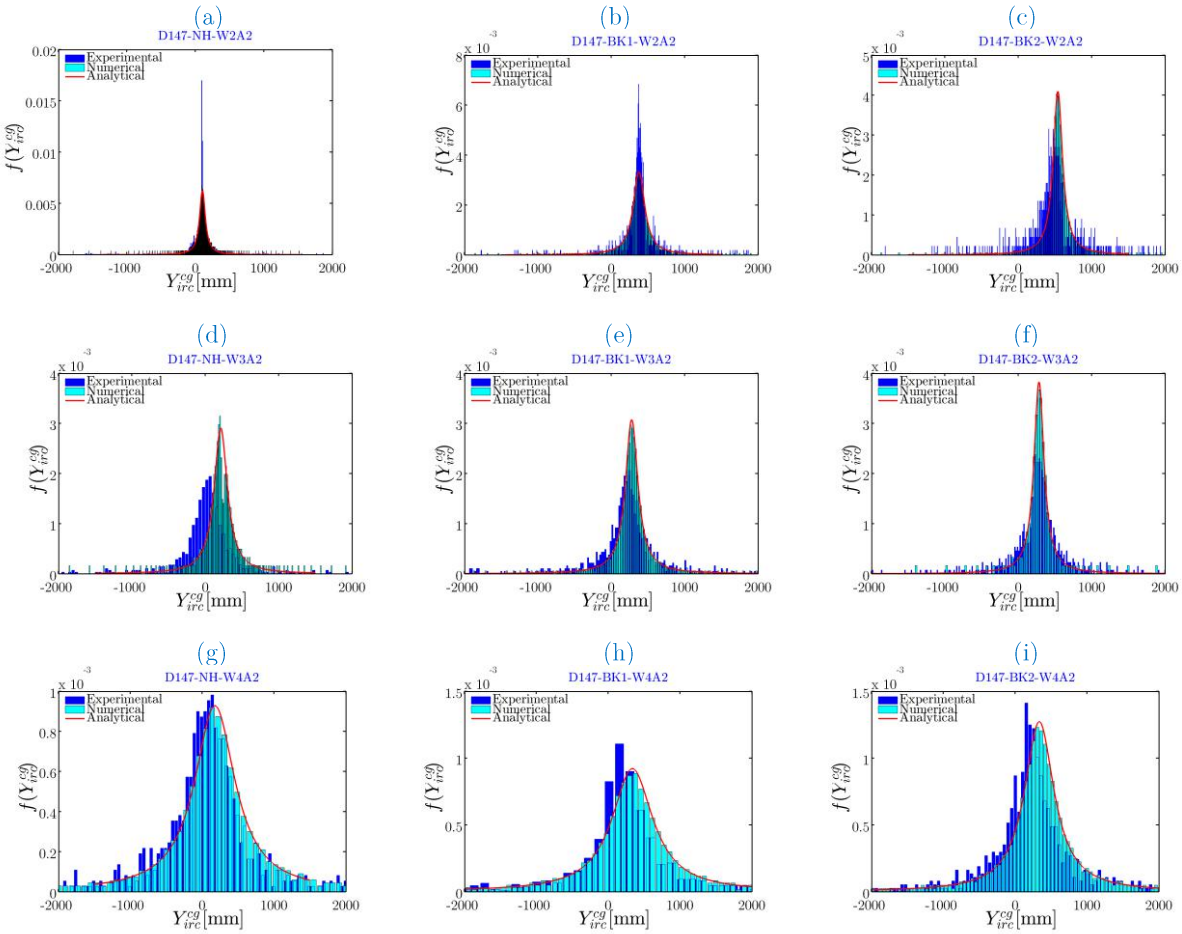

Figure 5.12 – Probability density function of horizontal position of the instantaneous rotation center with respect to the center of gravity for experimental, numerical and analytical models; draft 14.7m.

The summary of Figure 5.11 and Figure 5.12 may be found in following figures.

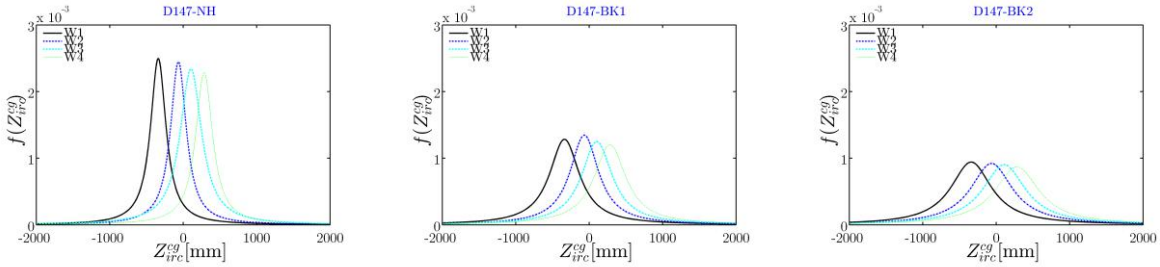

(a) (b) (c)

Figure 5.13 – Analytical probability density function of ZIRCs for each model in different wave periods.

The increasing roll damping leads to lower concentration of IRCs and consequently larger γ for the vertical position of the IRCs. In wave periods the vertical position of the MOIRC is next to the center of gravity but for larger periods tends to stay above the center of gravity which means larger roll damping.

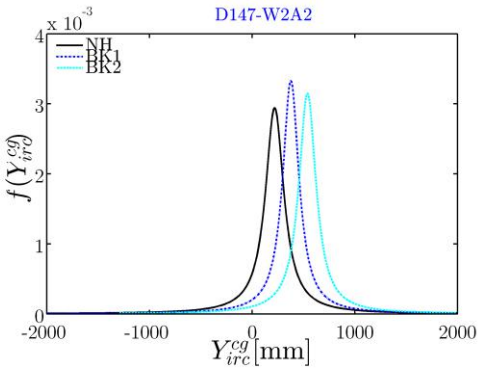

Figure 5.14 – Analytical probability density function of YIRCs for each model in different wave periods.

It can be concluded from Figure 5.14 that for the same incident wave period and amplitude, increasing the roll damping can shift the horizontal position of the MOIRC and causes asymmetric roll motion which can affect too much the efficiency of the bilge keel.

This chapter first presented the experimental results from the regular beam wave tests and analyzed the motion in aspect of the IRCS. The relation of the IRCs and waves

presented numerically and analytically as a straight locus in YZ-plane and concept of MOIRC confirmed for the body with interaction of the incident beam waves. The Cauchy distribution was verified to estimate the coordination of the MOIRC.

Chapter 6 Conclusions

The aim of this thesis is the investigation of the coupling terms and rotation center effects on the roll damping behaviour of a FPSO and development of a mathematical model for roll damping estimation. After an introduction to the thesis topic, introduction chapter gave a theoretical background and an overview state of the art of the roll. The methodology part is divided into four chapters: Development of the third order system identification approach procedure and analysis of the free decay roll experiments (Chapter 3), The numerical experimental and analytical analysis of the MOIRC for free decay roll (Chapter 4), MOIRC and IRCs behaviour in condition of the regular beam-waves (Chapter 5).

6.1 Contributions

- Due to lack of coupled damping term's effects on roll damping estimation in conventional 2nd order approaches, this work has derived a 3rd order equation of roll motion including the coupling terms, linearly and nonlinearly in Equation (2.36) and (2.41), respectively.

- This work presents a comprehensive review of the instantaneous rotation center and suggests the C_{idp} as pole where the hydrodynamic coefficients obtained from a roll decay.
- Based on the challenges described above, this work proposes an innovative, robust approach (3rd approach) to assess roll damping of FPSOs, taking into account a clear definition of the pole on which to center the motion equations as well as the influence of the coupled damping for sway and roll damping estimation, using both numerical and experimental techniques
- The errors of this 3rd order SI compare favourably with those of the Froude and Faltinsen approaches. The results have shown that the 3rd order SI produces more efficient predictions of the linear-plus-quadratic damping coefficient when compared to Froude and Faltinsen approaches, especially when nonlinearity is high.
- Comparing results from two different techniques held-over and pre-oscillation demonstrate that the pre-oscillation may provide lower roll damping values in comparison with the held over.
- This work shows that neglecting the coupling term significantly affect on roll damping estimation for larger angle when the roll damping is high (large bilge-keels), the work recommends strongly not to neglect the coupling terms.
- A new CND (Coupled Damping Number) term including all damping coefficients is proposed by this work. It may one of the significant findings from Chapter 3. CDN is negligible in the 3rd order equation even in presence of the viscosity, it should be noted that neglecting the CDN does not mean that the effects of the coupling damping term are negligible, but rather that the product

of the main diagonal terms minus the product of the coupling terms could indeed be negligible (CDN ≅ 0).

- A new MOIRC which is Most Often Instantaneous Rotation Center defined as mode of the histogram of IRCs (depending on situation could be defined as model of only a half cycle). The analysis of the ZIRC and the MOIRC, has never been reported in the literature to the author' best knowledge. Two categories have been recognized related with β_r and β_s which are the roll and sway damping coefficients. In fact, the study shows that the Cauchy distribution is very adherent to provide direct way to estimate the MOIRC where the case where β_r is smaller than β_s (normally naked hull without any Extra roll damping systems).
- When β_r gets larger than β_s, the MOIRC position alternates from an upper position to a lower position. The tangent form becomes a double parabolic form. When the MOIRC is in the upper position, the bilge keel receives the flow almost perpendicular, generates stronger vortex and dissipates more energy. When the MOIRC is in the lower position, the bilge keel is more tangent to the trajectory, produces vortices not so strong and dissipates less energy. This is an observation that improves the significance of the results in the decay test per se, however point that the decay test, due to clear different physics, may not be very representative of the real case. This is closer to regular and random wave incidence cases
- The investigation showed clearly that for a symmetric body in incident regular beam seas the roll response is not symmetrical and can be explained within linear wave potential flow, provided the correct average equivalent linear

viscose damping. Also, the work has shown quite satisfactory correlation between the experimental measurements and the results of a numerical and analytical and concluded that the locus of the instantaneous rotation center is a frequency depended straight line which confirmed in closed form by (5.25).

- The experiments in regular waves targeted four different incident wave periods. The results showed that the IRCs for periods smaller than natural period of roll tend to stay in lower position which leads into the lower dampings but in contrast, by increasing the wave periods the IRCs tend to stay in higher positions, consequently higher roll damping. These can be observed from (5.3).
- The significant observation of the Chapter 5 may be resumed in that by increasing roll dampings (using larger bilge-keels) the MOIRC tends stay far from the center line on lee-side, this shifting can be affect directly on functionality of the lee-side's bilge-keel. In the resonance cases it may lose almost all its efficiency and the body continue only with wave-side's bilge keel.
- An ellipse form of IRCs locus is proposed for theoretical future research for the body exposed to the random beam-wave.
- Based on provided information thanks to the IRCs and MOIRC, and loss functionality of the lee-side's bilge keel this work suggests using roll dampings estimated from the beam-wave tests (regular/random) instead of free decay roll.
- The contributions of the thesis have provided a deeper insight into roll motion and roll damping of FPSO (or box shape floating body) which instead of improving roll damping estimation may bring new aspects to the design of anti-roll systems with respect to riser fatigue analysis and extreme loads. A non-symmetric bilge keel arrangement then may be considered.

6.2 Future Works

In the end of present study, there are several details that would have been beneficial to continue in the future investigation of the two-dimensional FPSO section.

- Is recommended to conduct the roll tests for lightship draft. The weight of the naked hull model was one of the reasons to carry out the tests for draft 8.7m unfeasible.
- Conduct the random wave tests and comparing with theoretical results of the Appendix B.
- Analytical proof of $CDN \approx 0$ for viscous flow.
- Study on the correction function on roll damping obtained from free decay roll and regular/random waves tests, proposing to achieve on more realistic values of damping in the wave conditions
- Finding parametric relation between roll damping obtained from regular waves with random waves via MOIRC
-

References

Asgari P., Fernandes, A. C. Most Often Instantaneous Rotation Center (MOIRC) for Damping Interpretation in the Free Decay Test of a FPSO [Relatório]. - [s.l.] : Journal of Nonlinear Dynamics, 2019.

Barr R. A. A Review and Comparison of Ship Manoeuvring Simulation methods [Periódico]. - New York : SNAME, Centennial Meeting, 1993. - Vol. 18.

Bass D. W., & Haddara, M. R. Roll and sway-roll damping for three small fishing vessels [Conferência]. - 1991. - Vol. 38. - pp. 51-71.

Bishop R. E. D., & Price, W. G. Bishop, R. E. D., & Price, W. G. (1974). On the slowness of a small departure from steady flow [Conferência] // Noise, Shock and Vibration Conference. - Melbourne, Australia : [s.n.], 1974.

Bishop R.E.D., Parkinson, A.G., Price, W.G. On the nature of slow motion derivatives [Periódico]. - [s.l.] : Journal of Sound and Vibration, 1977. - 1 : Vol. 51.

Cardo A., Francescutto, A., & Nabergoj, R. On damping models in free and forced rolling motion [Periódico]. - [s.l.] : Ocean Engineering, 1982. - 2 : Vol. 9.

Chakrabarti S. Empirical calculation of roll damping for ships and barges [Periódico]. - [s.l.] : Ocean Engineering, 2001. - 7 : Vol. 28.

Chun H. H., Chun, S. H., & Kim, S. Y. Roll damping characteristics of a small fishing vessel with a central wing [Periódico] // Ocean Engineering. - 2001. - 12 : Vol. 28. - pp. 1601-1619.

Chun H. H., Chun, S. H., & Kim, S. Y. Roll damping characteristics of a small fishing vessel with a central wing [Periódico]. - [s.l.] : Ocean Engineering, 2001. - 12 : Vol. 28.

Clayton B. R., & Bishop, R. E. D. Mechanics of marine vehicles [Livro]. - [s.l.] : E. & FN Spon, 1982.

Clayton B. R., & Bishop, R. E. D. Mechanics of marine vehicles. E. & FN Spon. [Livro]. - [s.l.] : Gulf Pub Co; First American Edition edition (December 1, 1982), 1982.

Dalgarno A., Stewart, A. L. On the Perturbation Theory of Small Disturbances [Periódico] / ed. Society Royal. - [s.l.] : Proceedings of the Royal Society of London. Series A, Mathematical and Physical Sciences, 18 de Dec de 1956. - Vol. 238. - pp. 269-275.

Dalzell J. F. A Note on the Form of Ship Roll Damping [Periódico]. - [s.l.] : Journal of Ship Research, 1978. - 3 : Vol. 22. - pp. 178-185.

de Oliveira A. C., & Fernandes, A. C. The nonlinear roll damping of a FPSO hull [Periódico]. - [s.l.] : Journal of Offshore Mechanics and Arctic Engineering, 2014. - 1 : Vol. 136.

Esperança P. T., Sales, J. S., Liapis, S., Matsuura, J. P. J., & Schott, W. An experimental investigation of roll motions of an FPSO [Conferência] // ASME 2008 27th International Conference on Offshore Mechanics and Arctic Engineering. - [s.l.] : American Society of Mechanical Engineers, 2008.

Faltinsen O. M. Sea Loads on Ships and Offshore Structures [Livro]. - Cambridge, UK : Cambridge University, 1990.

Faltinsen O. Sea loads on ships and offshore structures [Livro]. - [s.l.] : Cambridge university press, 1993. - Vol. 1.

Faltinsen O.M. Hydrodynamics of High-Speed Marine Vehicles [Livro]. - UK : Cambridge University Press, 2005. - Vol. Ch.7.

Fernandes A. C. Analysis of an axisymmetric pneumatic buoy by reciprocity relations and a ring-source method [Livro]. - [s.l.] : Doctoral dissertation, Massachusetts Institute of Technology, 1983.

Fernandes A. C., Asgari, P., & Junior, J. S. S. Linear and non-linear roll damping of a FPSO via system identification of a third order equation with sway-roll coupled damping effects [Periódico] // Ocean Engineering. - 2018. - Vol. 166. - pp. 191-207.

Fernandes A. C., Asgari, P., & Seddigh, M. Roll Center of a FPSO in Regular Beam Seas for All Frequencies [Conferência] // ASME 2015 34th International Conference on Ocean, Offshore and Arctic Engineering. - [s.l.] : American Society of Mechanical Engineers, 2015.

Fernandes A. C., Asgari, P., Soares, A. R. Asymmetric roll center of symmetric body in beam waves [Periódico] // Ocean Engineering. - 2016. - Vol. 112. - pp. 66-75.

Fernandes A. C., Oliveira, A. C. The roll damping assessment via decay model testing (new ideas about an old subject) [Periódico]. - [s.l.] : Journal of Marine Science and Application, 2009. - 2 : Vol. 8.

Ferreira M. D. Hydrodynamic Aspects of the New Build FPSOBR2005 [Conferência] // 2nd International Workshop on Applied Offshore Hydrodynamics. - Rio de Janeiro : [s.n.], 2005.

Ferreira M. D., de Oliveira, M. C., Carvalho, R. C., & Sphaier, S. H. Asymmetric FPSO roll response due to the influence of lines arrangement. [Conferência] // ASME 2012 31st International Conference on Ocean, Offshore and Arctic Engineering. - [s.l.] : American Society of Mechanical Engineers, 2012.

Fossen T. I. Guidance and control of ocean vehicles (Vol. 199, No. 4). [Livro]. - New York : Wiley, 1994.

Fossen T. I. Handbook of Marine Craft Hydrodynamics and Motion Control [Livro]. - Newyork : Weily, 2011.

Fossen T. I. Kinematics of Ship Motion. Chapter 3 [Seção do Livro] // Ship Motion Control: Course Keeping and Roll Stabilisation using Rudder and Fins / A. do livro Perez T.. - [s.l.] : Springer, 2005.

Fossen T. I. The NEROV Autonomous Underwater Vehicle [Livro]. - Trondheim, Norway : The Norwegian Institute of Technology, 1991.

Froude W. On the rolling of ships [Periódico]. - [s.l.] : Trans INA, 1861. - Vol. 2.

Froude W., Abell, W., Gawn, R. W. L., & Duckworth, A. D. The Papers of William Froude [Livro]. - [s.l.] : Institution of Naval Architects, 1955.

Haddara M. R., & Bass, D. W. On the form of roll damping moment for small fishing vessels [Periódico] // Ocean Engineering. - 1990. - 6 : Vol. 17. - pp. 525-539.

Haddara M.R. On the stability o f ship motion in regular [Periódico]. - [s.l.] : International shipbuilding progress, 1971. - 207 : Vol. 18.

Hayes W.D., Probstein, R.F. Chapter II - Small-Disturbance Theory [Seção do Livro] // Applied Mathematics and Mechanics. - [s.l.] : Elsevier, 1959. - Vol. 5.

Himeno Y. Prediction of Ship Roll Damping - State of the Art [Relatório]. - [s.l.] : University of Michigan, 1981.

Ikeda Y. ,Fujiwara, T., & Katayama, T. Roll damping of a sharp-cornered barge and roll control by a new-type stabilizer [Conferência] // The Third International Offshore and Polar Engineering Conference. - [s.l.] : International Society of Offshore and Polar Engineers, 1993.

Ikeda Y., Himeno, Y. and Tanaka, N. A Prediction Method for Ship Roll Damping [Periódico]. - Osaka : [s.n.], 1978b.

Ikeda Y., Himeno, Y., & Tanaka, N. On eddy making component of roll damping force on naked hull [Periódico] // Journal of the Society of Naval Architects of Japan. - 1977a. - Vol. 142. - pp. 54-64.

Ikeda Y., Ishikawa, M., Tanaka, N. Viscous Effect on Damping Forces of Ship in Sway and Roll Coupled Motion [Periódico]. - [s.l.] : Naval architecture and ocean engineering, 1981. - Vol. 19.

Ikeda Y., Komatsu, K., Himeno, Y., & Tanaka, N. On roll damping force of ship-effect of hull surface pressure created by bilge keels [Periódico] // Journal of Kansai Society of Naval Architects. - 1977. - Vol. 165. - pp. 31-40.

Ikeda Y., Tanaka, N., Himeno, Y., Effect of Hull Form and Appendage on Roll Motion of Small Fishing Vessels [Conferência] // Proceedings of the 2nd International Conference on Stability of Ships and Ocean Vehicles. - Tokyo : British Maritime Technology, 1982.

ITTC Final Report and Recommendations to the 28th ITTC [Relatório]. - WUXI : The Ocean Engineering Committee, 2017.

ITTC ITTC – Recommended Procedures and Guidelines - Seakeeping Experiments 75-02-07-021 [Relatório]. - [s.l.] : 26th ITTC Seakeeping Committee, 2011.

Journée J. M. J., & Massie, W. W. Offshore Hydromechanics [Relatório]. - [s.l.] : Lecture notes on offshore hydromechanics for Offshore Technology students, code OT4620, 2001.

Kato H. On the frictional resistance to the rolling of ships [Periódico] // Journal of Zosen Kiokai. - 1957. - pp. 115-122.

Kato H. On the Frictional Resistance to the Rolling Ships [Periódico] // Journal of Zosen Kiokai. - (in Japanese) : Society of Naval Architects of Japan, 1958. - Vol. 102. - pp. 115-122.

Kato H., Effects of bilge keels on the rolling of ships [Periódico] // Journal of Zosen Kiokai. - 1965. - pp. 93-101.

Levenberg K. A method for the solution of certain non-linear problems in least squares [Periódico]. - [s.l.] : Quarterly of applied mathematics, 1944. - 2 : Vol. 2.

Lewis E. V. Principles of Naval Architecture [Seção do Livro] // Principles of Naval Architecture: Volume III-Motions in Waves and Controllability. - Jersey City : Society of Naval Architects and Marine Engineers, 1989.

Lewison G.R.G. Optimum design of passive roll [Periódico]. - [s.l.] : The Naval Architect, 1976.

Lewison G.R.G. Optimum design of passive roll stabilizer tanks [Periódico]. - [s.l.] : The Naval Architect, 1973.

Low Y. M, Private communication [Relatório]. - [s.l.] : NUS, 2018.

Marquardt D. W. An algorithm for least-squares estimation of nonlinear parameters [Periódico]. - [s.l.] : Journal of the society for Industrial and Applied Mathematics, 1963. - 2 : Vol. 11.

Molin B. Hydrodynamique des structures offshore [Livro]. - 2002. - Technip.

Moré J. J. The Levenberg-Marquardt algorithm: implementation and theory [Periódico]. - Berlin : In Numerical analysis, 1978.

Neves M. A. S. Analise de Testes de Decaimento (Decay Test Analysis) [Relatório]. - [s.l.] : LabOceano Internal Report, Rio de Janeiro, Brazil (in Portuguese), 2004.

Neves M.A.S. , Lenin M. Sobre a Dinâmica do Sistema Navio-Monobóia [Periódico]. - Rio de Janeiro : SOBENA, 2006.

Oliveira A. C., & Fernandes, A. C. The Nonlinear Roll Damping of a FPSO Hull [Periódico]. - [s.l.] : Journal of Offshore Mechanics and Arctic Engineering, 2014. - 1 : Vol. 136.

Oliveira A.C. NOVAS ABORDAGENS PARA A ANÁLISE DO AMORTECIMENTO NÃO LINEAR DO BALANÇO TRANSVERSAL DE FPSOS [Relatório]. - Rio de Janeiro : Doctoral Dissertation, 2011.

Ommani B., Kristiansen, T., & Firoozkoohi, R. Nonlinear roll damping, a numerical parameter study [Conferência]. - Kona, Big Island, Hawaii, USA : The Twenty-fifth International Ocean and Polar Engineering Conference, 2015.

Park I. K., Shin, H. S., Kim, J. W., & Cho, J. W. Effect of the Roll Center Position On the Roll Damping of FPSO [Conferência]. - Seattle, Washington, USA : he Tenth International Offshore and Polar Engineering Conference, 2000.

Qualisys A. B. Qualisys Track Manager User Manual [Relatório]. - [s.l.] : Gothenburg, 2006.

Rezende F. Non Linear Roll JIP. Technical report [Relatório]. - Rio de Janeiro : BV, 2012.

Roberts J. B. Estimation of Nonlinear Ship Roll Damping from Free-Decay Data [Periódico]. - [s.l.] : Journal of Ship Research, 1985b. - 2 : Vol. 29.

Roberts J. B., & Dacunha, N. M. C. Roll Motion of a Ship in Random Bea Waves: Comparison Between Theory and Experiment [Periódico]. - [s.l.] : Journal of Ship Research, 1985a. - 2 : Vol. 29.

Sasajima H. On the Action of Bilge keels in Ship Rolling [Periódico]. - (in Japanese) : Society of Naval Architects of Japan, 1954. - Vol. 86.

Standing R. G. Prediction of viscous roll damping and response of transportation barges in waves [Conferência] // The First International Offshore and Polar Engineering Conference. - [s.l.] : International Society of Offshore and Polar Engineers, 1991.

Standing R. G., Cozens, P. D., & Downie, M. J. Numerical prediction of roll damping and response of ships and barges, based on the discrete vortex method [Periódico] // Computer Modelling in Ocean Engrg / ed. Zienkiewicz B.A. Schrefler and O.C.. - Balkema : [s.n.], 1988.

Tanaka N. A Study on the Bilge Keel- Part 1-4 [Periódico]. - (in Japanese) : Society of Naval Architects of Japan, 1957. - Vol. 109.

Tanaka N. A study on the bilge keels [Periódico] // Journal of Zosen Kiokai. - 1961. - pp. 205-212.

Van't Veer R., Fathi, F., & Kherian, J. G. On Roll Hydrodynamics of FPSO's fitted with Bilge Keels and Riser Balcony [Conferência] // ASME 2011 30th International Conference on Ocean, Offshore and Arctic Engineering. - [s.l.] : American Society of Mechanical Engineers, 2011.

Veritas D. N. Classification Notes: CSA-Direct Analysis of Ship Structures [Relatório]. - [s.l.] : DNV, 2013.

Vugts J. H. The hydrodynamic coefficients for swaying, heaving and rolling cylinders in a free surface [Periódico]. - [s.l.] : International Shipbuilding Progress, 1968. - 167 : Vol. 15. - pp. 251-276.

.

Appendix A Beating for Wave period 1.5s

the graphs of Chapter 5 for the W1A2 are presented here:

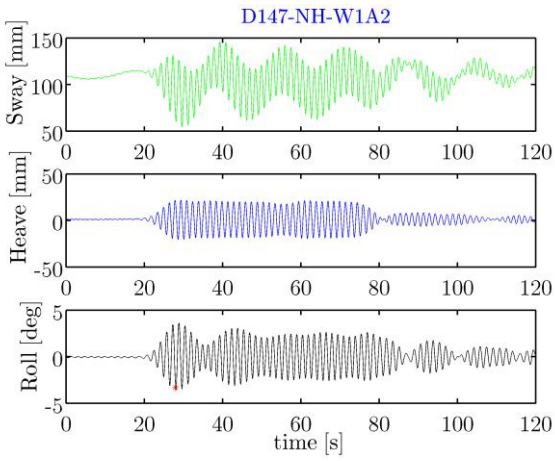

Fig. A.1 - 3-DoF motions for the naked hull model in draft 14.7m exposed to the W1A2.

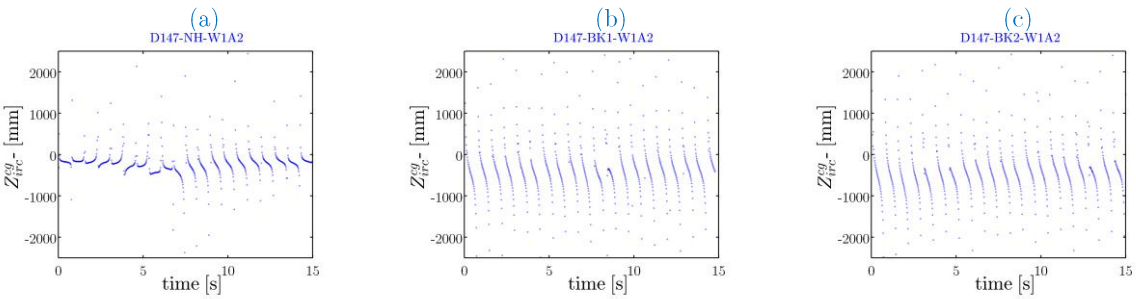

Fig. A.2 - Vertical position of the instantaneous rotation center - ZIRCs for the experiments for W1A2

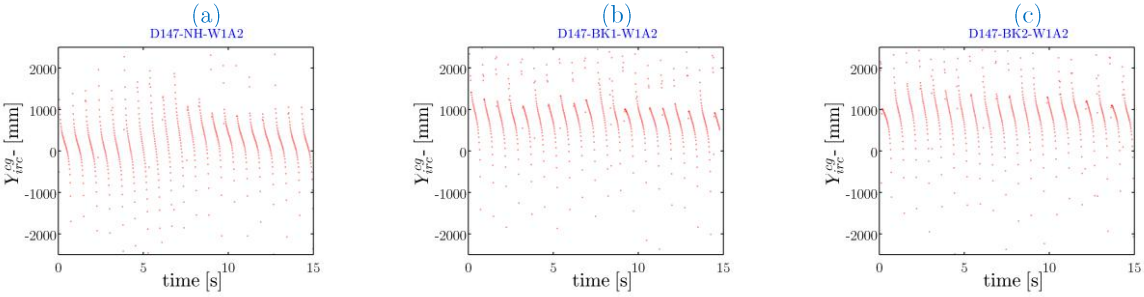

Fig. A.3 - Horizontal position of the instantaneous rotation center - YIRCs for the experiments for W1A2.

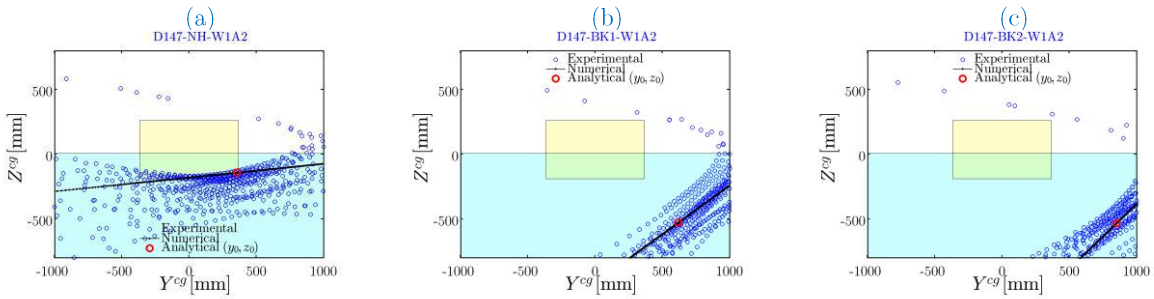

Fig. A.4 - Rotation center locus obtained experimentally, numerically and analytical for the model in draft 14.7m shows IRCs position with the constant time interval 50Hz for W1A2

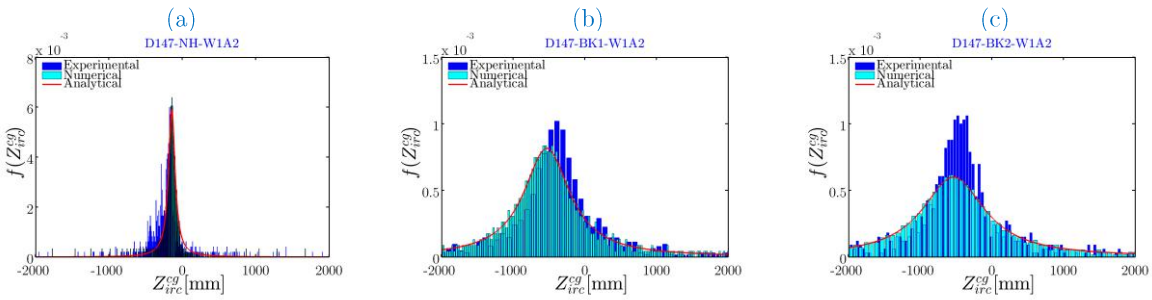

Fig. A.5 - Probability density function of vertical position of the instantaneous rotation center with respect to the center of gravity for experimental, numerical and analytical models; draft 14.7m for W1A2.

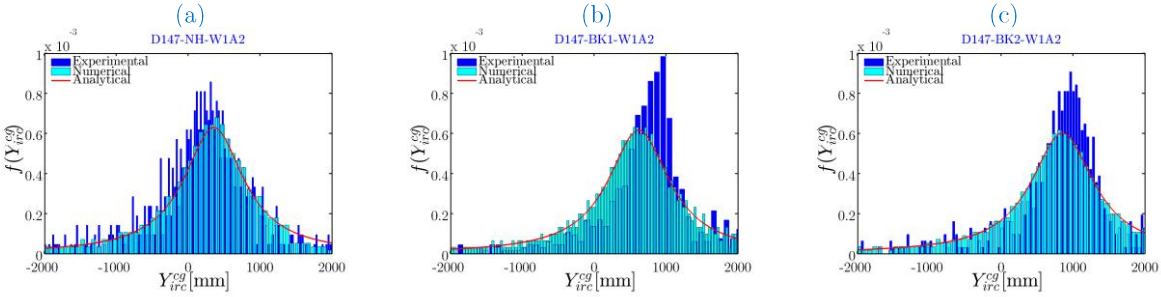

Fig. A.6 - Probability density function of horizontal position of the instantaneous rotation center with respect to the center of gravity for experimental, numerical and analytical models; draft 14.7m for W1A2

Appendix B Random Waves: Most Often Instantaneous Center of Rotation - MOIRC

B.1 Random Wave Response Spectra

Consider random beam-waves of which the energy distribution over the wave frequencies (the wave spectrum) is known. These random waves are input to a system that possesses linear characteristics. These frequency characteristics are known, for instance via model experiments or computations. The output of the system is the motion of the floating structure. This motion has an irregular behavior, just as the random beam-waves that causes the motion (Journée, 2001). (See Fig. B.1).

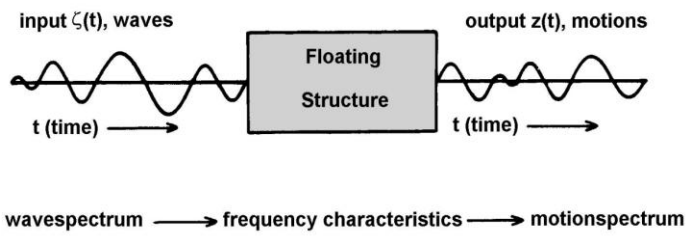

Fig. B.1 – Relation between motions and waves analytical; (Journée, 2001).

The response spectrum of the motion mode i (or response S_r) on the basis of encounter frequency ω_e, can be found from response amplitude operator (or transfer function) of the motion i and the wave spectrum (S_w) by:

$$S_r(\omega_e) = \left|RAO_i(\omega_e)\right|^2 .S_w(\omega_e) \tag{B.1}$$

It is well known that the displacements η_i and velocities $\dot{\eta}_i$ time histories can be obtained from response spectrum (for instance using Fast Fourier Transform).

B.2 MOIRC for the Body in Random Waves

In B.1, procedure to obtain the velocity of each mode was presented briefly. Let's define the velocities in transversal motion for a 2-D section as below:

$\dot{\eta}_2^{cg}$: Sway velocity;

$\dot{\eta}_3^{cg}$: Heave velocity;

$\dot{\eta}_4^{cg}$: Roll velocity.

and,

ρ_{ij}^2: Correlation coefficient between $\dot{\eta}_i^{cg}$ and $\dot{\eta}_j^{cg}$

σ_i^2: Variance of $\dot{\eta}_i^{cg}$

$\dot{\eta}_2^{cg}$, $\dot{\eta}_3^{cg}$ and $\dot{\eta}_4^{cg}$ follow a trivariate normal distribution:

$$f_{\dot{\eta}_2^{cg}\dot{\eta}_3^{cg}\dot{\eta}_4^{cg}}(\xi_2,\xi_3,\xi_4)=\frac{1}{2\sqrt{2}\pi^{3/2}\sqrt{1-\alpha}\sigma_2\sigma_3\sigma_4}\exp\left[\frac{-1}{2(1-\alpha)}\begin{pmatrix}c_{22}\xi_2^2+c_{33}\xi_3^2+c_{44}\xi_4^2+\ldots\\ \ldots+c_{32}\xi_3\xi_2+c_{24}\xi_2\xi_4+c_{34}\xi_3\xi_4\end{pmatrix}\right] \tag{B.2}$$

Where,

$$c_{22}=\frac{1-\rho_{34}^2}{\sigma_2^2},\ c_{33}=\frac{1-\rho_{24}^2}{\sigma_3^2},\ c_{44}=\frac{1-\rho_{32}^2}{\sigma_4^2}$$

$$c_{32}=\frac{2(\rho_{24}\rho_{34}-\rho_{32})}{\sigma_2\sigma_3},\ c_{34}=\frac{2(\rho_{32}\rho_{24}-\rho_{34})}{\sigma_3\sigma_4},\ c_{24}=\frac{2(\rho_{32}\rho_{34}-\rho_{24})}{\sigma_2\sigma_4}$$

$$\alpha=\rho_{32}^2+\rho_{24}^2+\rho_{34}^2-2\rho_{23}\rho_{24}\rho_{34}$$

According to Chapter 5, the vertical and horizontal position of the instantaneous rotation center can be obtained by dividing sway velocity and heave velocity over roll angular velocity as they are shown in (5.9) and (5.10), respectively. Therefore, the joint distribution of z_{irc}^{cg} and y_{irc}^{cg} can be written as:

$$f_{y_{irc}^{cg}z_{irc}^{cg}}(y,z)=\frac{1}{2\pi\sigma_2\sigma_3\sigma_4}\left(c_{33}y^2+c_{22}z^2+c_{44}-c_{32}yz-c_{34}y+c_{24}z\right)^{-3/2} \tag{B.3}$$

Marginal distribution for y_{irc}^{cg} can be expressed as (B.4).

$$f_{y_{irc}^{cg}}(y)=\frac{1}{\pi}\left[\frac{\left(\frac{\sigma_3}{\sigma_4}\right)\sqrt{1-\rho_{34}^2}}{\left(y+\left(\frac{\sigma_3}{\sigma_4}\right)\rho_{34}\right)^2+\left(\frac{\sigma_3}{\sigma_4}\right)^2\left(1-\rho_{34}^2\right)}\right] \tag{B.4}$$

The distribution (B.4) can be represented as Cauchy distribution with location parameter (mode) $\frac{-\sigma_3\rho_{34}}{\sigma_4}$ and scale parameter $\frac{\sigma_3\sqrt{1-\rho_{34}^2}}{\sigma_4}$. Likewise, for z_{irc}^{cg}:

$$f_{z_{irc}^{cg}}(z)=\frac{1}{\pi}\left[\frac{\left(\frac{\sigma_2}{\sigma_4}\right)\sqrt{1-\rho_{24}^2}}{\left(y-\left(\frac{\sigma_2}{\sigma_4}\right)\rho_{24}\right)^2+\left(\frac{\sigma_2}{\sigma_4}\right)^2\left(1-\rho_{24}^2\right)}\right] \tag{B.5}$$

Similarly, the distribution (B.5) can be represented as Cauchy distribution with location parameter (mode) $\frac{\sigma_2\rho_{24}}{\sigma_4}$ and scale parameter $\frac{\sigma_2\sqrt{1-\rho_{24}^2}}{\sigma_4}$. As the conclusion, The MOIRC is located on $\left(\frac{-\sigma_3\rho_{34}}{\sigma_4},\frac{\sigma_2\rho_{24}}{\sigma_4}\right)$.

In order to find region corresponding to some probability, let assume the probability (P) that the MOIRC does not exceed a prescribed region. In order to simplify the joint distribution of z_{irc}^{cg} and y_{irc}^{cg} (shown in (B.3)) rearranged under below simplifications:

$$P=\frac{1}{2\pi\sigma_2\sigma_3\sigma_4}\left(ay^2+2byz+cz^2+c_{44}+2dy+2fz\right)^{-3/2} \tag{B.6}$$

Where

$$a=c_{33},\quad b=-c_{32}/2,\quad c=c_{22},\quad d=-c_{34}/2,\quad f=c_{24}/2$$

The equation (B.6) can be written as:

$$P=\frac{\pi}{\sqrt{ac-b^2}}\left(\frac{p2\pi\sigma_2\sigma_3\sigma_4}{1-\alpha}\right)^{-2/3}\left(3M^{1/3}\right)+\frac{\pi M\left(af^2+cd^2-2bdf\right)}{\left(ac-b^2\right)^{3/2}}-\frac{\pi c_{44}M}{\sqrt{ac-b^2}} \tag{B.7}$$

It should be noted that:

$$0 \le M \le \frac{\sigma_4^2}{2\pi\sqrt{1-\alpha}\sigma_2\sigma_3}$$

When P=1, M is as below:

$$M = \frac{\sigma_4^2}{2\pi\sqrt{1-\alpha}\sigma_2\sigma_3}$$

Considering $g = c_{44} - \left(\frac{2\pi M\sigma_2\sigma_3\sigma_4}{1-\alpha}\right)^{-2/3}$, it can be proved that the region is an ellipse as shown in (B.8)

$$ay^2 + 2byz + cz^2 + 2dy + 2fz + g = 0 \tag{B.8}$$

Where the semi-axis lengths are:

$$a' = \sqrt{\frac{2\left(af^2 + cd^2 + gb^2 - 2bdf - acg\right)}{\left(b^2 - ac\right)\left(\sqrt{(a-c)^2 + 4b^2} - (a+c)\right)}} \tag{B.9}$$

$$b' = \sqrt{\frac{2\left(af^2 + cd^2 + gb^2 - 2bdf - acg\right)}{\left(b^2 - ac\right)\left(-\sqrt{(a-c)^2 + 4b^2} - (a+c)\right)}} \tag{B.10}$$

And the counter-clockwise angle of rotation Φ from the y-axis to the major axis of the ellipse is:

$$\Phi = \begin{cases} 0 & b = 0 \,\&\, a < c \\ \dfrac{\pi}{2} & b = 0 \,\&\, a > c \\ \dfrac{1}{2}\cot^{-1}\left(\dfrac{a-c}{2b}\right) & b \neq 0 \,\&\, a < c \\ \dfrac{\pi}{2} + \dfrac{1}{2}\cot^{-1}\left(\dfrac{a-c}{2b}\right) & b \neq 0 \,\&\, a > c \end{cases} \tag{B.11}$$

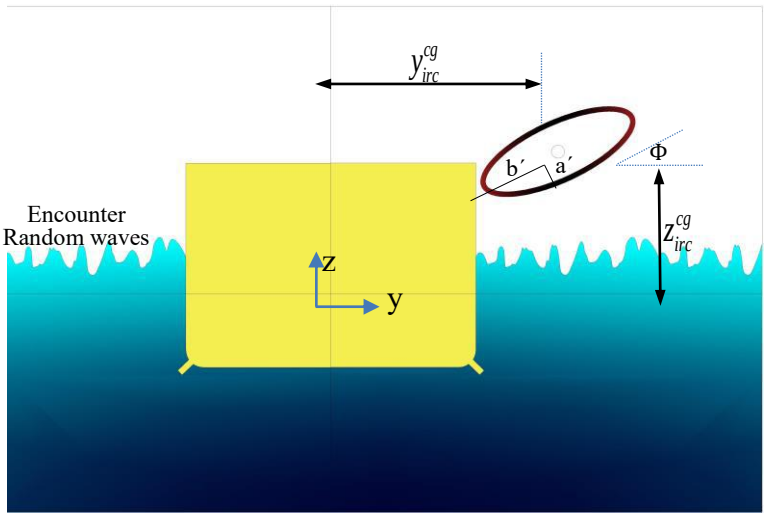

Fig. B.2 – Schematic of the MOIRC for a random beam-wave.

Fig. B.2 illustrates a schematic of the position of the MOIRC in condition of random beam-wave. In contrast with the regular beam wave the locus is not a straight line. What is significant and interesting from the theoretical and also schematic figure is that the IRCs vary in an ellipse form which the characteristics of this ellipse can be presented by analytical/statistical solution. In fact, the knowledge about the position of the rotation center/IRCs or MOIRC can be significantly improve our understanding about the roll and consequently efficiency of the anti-roll system. This chapter suggest

more investigation (numerically and experimentally) about the MOIRC in condition of the random seas and correlation of the position of the MOIRC with the roll damping.